INVESTIGATION OF ELECTROCHEMICAL CO$_2$ CAPTURE SYSTEM

A Thesis Submitted to
The Graduate School of Engineering and Sciences of
Izmir Institute of Technology
In Partial Fulfillment of the Requirements for the Degree of

MASTER OF SCIENCE

in Chemical Engineering

by
Cansu GÜLER

October 2022
İZMİR

ACKNOWLEDGEMENT

ABSTRACT

INVESTIGATION OF ELECTROCHEMICAL
CO$_2$ CAPTURE SYSTEM

Fossil fuels have been used as a primary energy source for many years to meet the increasing energy demand since the industrial revolution. Fossil fuels are an important source of carbon that triggers global warming and climate change. To reduce the accumulation of carbon dioxide in the atmosphere, carbon capture has become more important. Conventional carbon capture technology is a thermally regenerated amine-based capture based on monoethanolamine (MEA). In this process, carbon dioxide is captured in an absorption column with the amine solution, and CO$_2$-amine solution is sent to the stripping column, where the solution is heated to release the captured CO$_2$ and regenerate the amine solution. However, an important disadvantage of this process is that it requires high energy for the CO$_2$ release step. Recently, electrochemical CO$_2$ capture process is proposed in the literature to decrease the energy requirement.

The aim of this study is to investigate the electrochemical CO$_2$ capture process using homopiperazine (HPZ). Unlike the conventional CO$_2$ capture process, the CO$_2$ release step is performed using an electrochemical cell. In the anode compartment of this electrochemical cell, the formed CO$_2$-amine complexes are converted into amine-metal complexes from which the CO$_2$ is released. The amine-metal complexes are then sent to the cathode, where the complex decomposes and metal deposition occurs. Laboratory-scale studies of the electrochemical capture process using MEA and HPZ as solvent were carried out. In the obtained results, it was found that HPZ has higher CO$_2$ capture capacity and CO$_2$ release rate than MEA and a similar CO$_2$ absorption rate as MEA. In addition, UV-Vis spectra analyses showed that the reaction rate at the anode was much higher than the reaction rate at the cathode for both amines.

ÖZET

ELEKTROKİMYASAL CO_2 TUTMA
PROSESİNİN İNCELENMESİ

Fosil yakıtlar, sanayi devriminden bu yana artan enerji talebini karşılamak için uzun yıllardır birincil enerji kaynağı olarak kullanılmaktadır. Fosil yakıtlar, küresel ısınmayı ve iklim değişikliğini tetikleyen önemli bir karbon kaynağıdır. Atmosferdeki karbondioksit birikimini azaltmak için karbon yakalama daha önemli bir hale gelmiştir. Geleneksel karbon yakalama teknolojisi, monoetanolamin (MEA) kullanılan termal olarak rejenere-amin bazlı bir yakalama işlemidir. Bu işlemde, karbondioksit, amin solüsyonu ile bir absorpsiyon kolonunda tutulur ve CO_2-amin solüsyonu, yakalanan CO_2'yi serbest bırakmak ve amin solüsyonunu rejenere etmek için solüsyonun ısıtıldığı sıyırma (stripping) kolonuna gönderilir. Ancak bu işlemin önemli bir dezavantajı, CO_2 salma adımı için yüksek enerji gerektirmesidir. Son zamanlarda, enerji ihtiyacını azaltmak için literatürde elektrokimyasal CO_2 yakalama işlemi önerilmiştir.

Bu çalışmanın amacı, homopiperazin (HPZ) kullanılarak elektrokimyasal CO_2 yakalama sürecini araştırmaktır. Geleneksel CO_2 yakalama işleminin aksine, CO_2 salma adımı bir elektrokimyasal hücre kullanılarak gerçekleştirilir. Bu elektrokimyasal hücrenin anot bölmesinde oluşan CO_2-amin kompleksleri, CO_2'nin serbest bırakıldığı amin-metal komplekslerine dönüştürülür. Amin-metal kompleksleri daha sonra kompleksin ayrıştığı ve metal birikiminin meydana geldiği katoda gönderilir. Çözücü olarak MEA ve HPZ kullanılan elektrokimyasal yakalama işleminin laboratuvar ölçekli çalışmaları yapılmıştır. Elde edilen sonuçlarda, HPZ'nin MEA'ya göre daha yüksek CO_2 tutma kapasitesine ve CO_2 salma hızına, MEA ile benzer bir CO_2 absorpsiyon hızına sahip olduğu bulunmuştur. Ayrıca UV-Vis spektrum analizleri, her iki amin için anottaki reaksiyon hızının katottaki reaksiyon hızından çok daha yüksek olduğunu göstermiştir.

TABLE OF CONTENTS

LIST OF FIGURES

LIST OF TABLES

CHAPTER 1

INTRODUCTION

1.1. The Need for CO_2 Capture

Anthropogenic carbon dioxide (CO_2) emission is a major emission source contributing to global warming. It has been observed that the global average temperature has increased by 0.06^oC every ten years since 1880, and since 1970 this rate has almost tripled and reached 0.16^oC. The reason for this increase in temperature is directly related to the CO_2 concentration in the atmosphere due to greenhouse effect (Stern et al., 2013).

The natural greenhouse effect is a process that allows life to exist by heating the earth's surface. When the sun's energy reaches the earth's atmosphere, some of the energy is reflected into space while the rest is absorbed and re-emitted by greenhouse gases. Thus, these greenhouse gases in the atmosphere warm the earth by trapping the incoming energy. This process keeps the earth's temperature 33^oC warmer than it would normally be, allowing life to exist on earth. However, increased human activities with industrialization increased the concentration of greenhouse gases in the atmosphere and significantly affected the course of the natural process (web1).

Figure 1.1 show the global average CO_2 concentration over the years. While the CO_2 concentration was about 278 ppm in 1750, it reached ca. 377 ppm in 2004 with a rapid increase of 19% from 1960 to 2004, as seen in Figure 1.1.a. Figure 1.1.b shows the CO_2 concentration from 2005 to the present. The CO_2 concentration was 378.4 ppm in 2005, and CO_2 concentration was 417 ppm as of early 2022. As can be seen, with the Industrial Revolution that started in the mid-1700s, human activities increased the atmospheric CO_2 concentration by 50%. If no measures are taken for the current situation, CO_2 concentration is expected to exceed 750 ppm by 2100 (Dugas, 2009; Wang et al., 2011; web2).
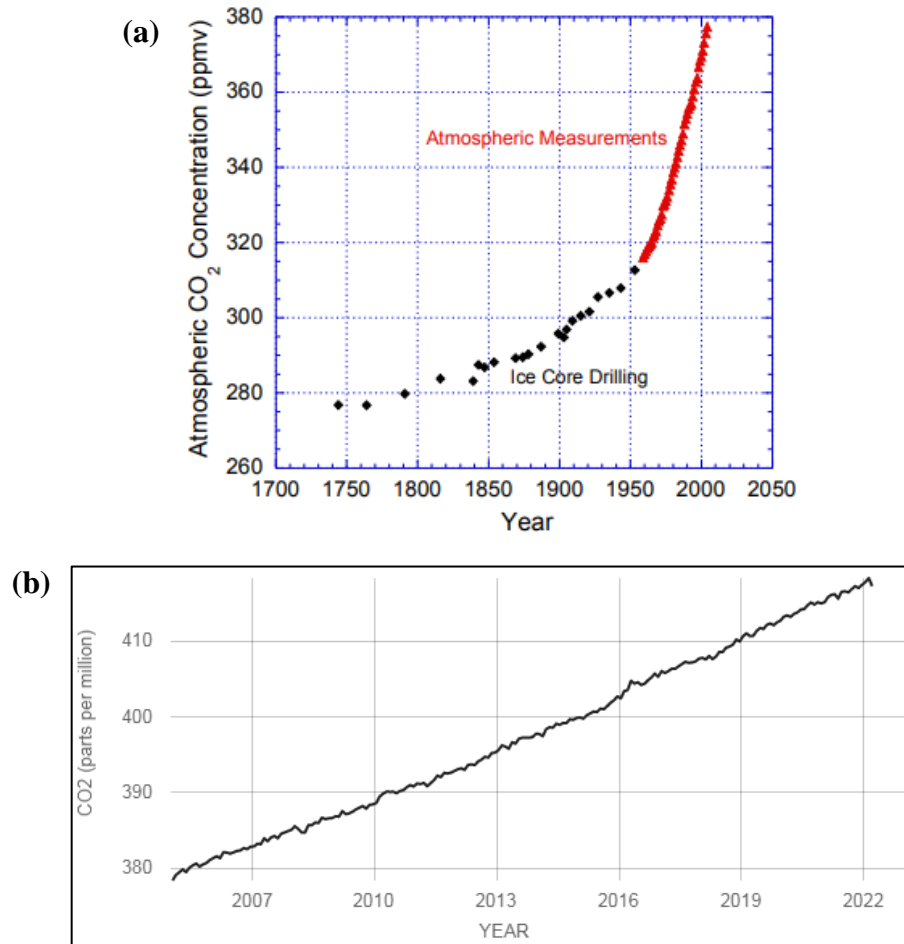
Figure 1. 1. Atmospheric CO_2 concentration by years, (a) CO_2 concentration in the years 1750-2004 (Dugas, 2009), (b) CO_2 concentration 2005-present (web2).

Figure 1.2 shows the global temperature anomaly from 1880 to 2021. The anomaly value, for which the initial value was recorded as -0.16°C (the reference point is the average of the global surface temperature measured from 1951 to 1980), increased since 1970 and it was recorded as 0.85°C in 2021. Interestingly, the significant temperature anomaly increase after 1960s in Figure 1.2 follows a similar trend to the CO_2 concentration shown in Figure 1.1.a. This shows a relationship between the CO_2 concentration and global temperature anomaly.
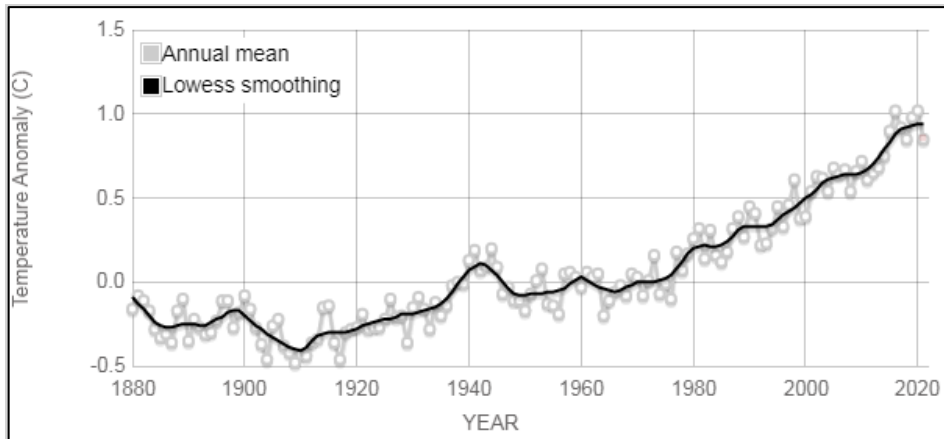
Figure 1. 2. Global temperature anomaly between 1880 and 2020. The average of the measured global surface temperature from 1951 to 1980 was taken as the reference point for these anomalies (web2).

Global energy demand has increased drastically since the Industrial Revolution. Fossil-based fuels (coal, natural gas and oil) play an important role by meeting 82% of this energy demand. Therefore, these fossil fuels constitute the majority of CO_2 emissions. According to a study conducted in 2011, it was determined that fossil fuels constitute 42% of the total CO_2 emissions (Rexed et al., 2015). Looking at Figure 1.3, it is seen that the share of CO_2 emitted due to fossil fuel use increased to 57% in 2019 (Arachchige, 2019). Although there are many sources of atmospheric carbon dioxide, fossil fuels continue to be the main source of CO_2 emissions.
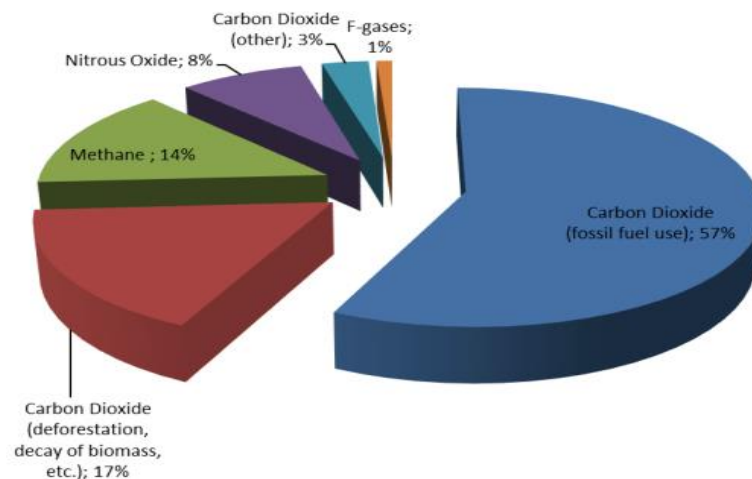
Figure 1. 3. Emission shares of greenhouse gases in 2019 (Arachchige, 2019).

Carbon dioxide is produced in large quantities in many industries such as coal and gas fired power plants, natural gas treatment, cement production, steel production,

chemical and petrochemical production (Arachchige, 2019; Chowdhury et al., 2013). Electricity generation in coal-fired power plants is the largest source of CO_2 emissions due to fossil fuel use. Approximately 40% of human-induced CO_2 emissions in the world originate from power plants working with fossil fuels (Mikkelsen et al.,2010; Pennline et al., 2010; Yang et al., 2008). Typically, about 1 tonne of CO_2 is released for 1000 kWh (=1 MWh) power generation in coal-fired power plants (Boot-Handford et al., 2014). In a study, it was reported that a coal-fired power plant with an installed capacity of 500 MW produced 3200 tons of flue gas per hour, of which 480 tons were CO_2 (gas mixture is 15% CO_2, 15% H_2O, 65% N_2, 4% O_2 and the remainder NO and SO_2 by volume at 1 bar pressure and 40°C) (Liu et al., 2009). Coal is a major fuel of the energy sector because its reserves are very large. Around the world, there is 500 GW of coal-based electricity generation capacity under the age of 10, which is more than a third of the global total coal-based capacity. It is estimated that 1000 GW of coal-based capacity will be installed in the next two decades. It is clearly seen that this increase in coal-fired power plants will significantly contribute to the CO_2 concentration in the atmosphere (Jorgensen et al., 2012; Sjöstrand & Yazdi, 2009; Stern & Hatton, 2014).

The fact that increasing CO_2 concentration in the atmosphere causes global warming has gained awareness in the last years. In order to limit global warming, the Paris Agreement was signed with the participation of 175 countries in 2015 and the steps to be taken to reduce the carbon footprint were determined. According to the IPCC (Intergovernmental Panel on Climate Change) report that forms the basis of the Paris Agreement, the global temperature increase caused by the anthropogenic greenhouse effect should be limited to a maximum of 2°C compared to the pre-industrial period in order to prevent climate change. In order to keep the temperature increase at this limit, CO_2 emissions should be reduced by 42-72% until 2050 (IPCC, 2018).

Various options have been proposed by scientists to mitigate CO_2 emissions. Although the transition to green energy sources (solar, wind, etc.) seems like a possible option, they are intermittent by nature and the lack of cheap, scalable technology and insufficient infrastructure prevents this transition. Therefore, in the near future, fossil fuels will continue to be the main source that meets the world's energy demand due to their energy density, process efficiency, process maturity, reliability, flexibility and accessibility. For this reason, there is a need for technologies that will enable the cleaner use of fossil fuels with effective CO_2 emission reduction strategies such as carbon capture

(and storage (CCS)) (Arachchige, 2019; Kothandaraman, 2010; Mac Dowell et al., 2013; Wang et al., 2011; Wang et al., 2019 (1)).

1.2. Overview of CO_2 Capture Systems

Carbon capture and storage (CCS) is the general name for technologies based on the removal of carbon dioxide emitted from fossil fuel power plants and large industrial CO_2 sources to reduce the amount of carbon in the atmosphere. CCS can also be defined as the process of separating CO_2 from any CO_2-rich gas stream and storing it permanently (Ciftja & Svendsen, 2014; Rexed et al., 2015).

Carbon capture and storage (CCS) technologies are generally grouped under three main headings, as shown in Figure 1.4. These technologies are namely pre-combustion, oxy-fuel combustion and post-combustion capture. In pre-combustion capture, CO_2 is captured before the fuel is burned. In this process, called gasification, the fuel is decomposed into hydrogen and CO_2 using oxygen and water vapor at high pressure and temperature. Pre-combustion capture technology requires expensive equipment which increases the investment cost, so pre-combustion capture technology is not common. In oxy-fuel combustion technology, the fuel is burned with pure oxygen (O_2) instead of air. The gases formed after the combustion reaction contain a high percentage of CO_2 and water. The formed CO_2 is separated from other gases. The most important disadvantage of this technology is its high cost due to the constant need for pure O_2. In the post-combustion capture technology, CO_2 gas is separated from the exhaust gas formed after the fuel is burned. The post-combustion capture technology is an advantageous method over the other two technologies: Post-combustion capture is compatible with the infrastructure of existing coal-based power plants, it does not require a significant change in the main combustion technology, it can be easily integrated into the plant, it has a flexible use and it does not interfere with the operation of the power plant if the CO_2 capture plant is shut down. In comparison, the closure of the capture facility using pre-combustion and oxy-fuel combustion technologies causes the existing facility to be shut down as well. In addition, when gas-fired power plants are considered, post-combustion technology is the first method that comes to mind because oxy-fuel and pre-combustion technology are not suitable for these plants (Herzog et al., 2009; Madeddu et al., 2018).

Therefore, post-combustion CO_2 capture technology can be stated as the most viable method to reduce CO_2 emissions in power industry.
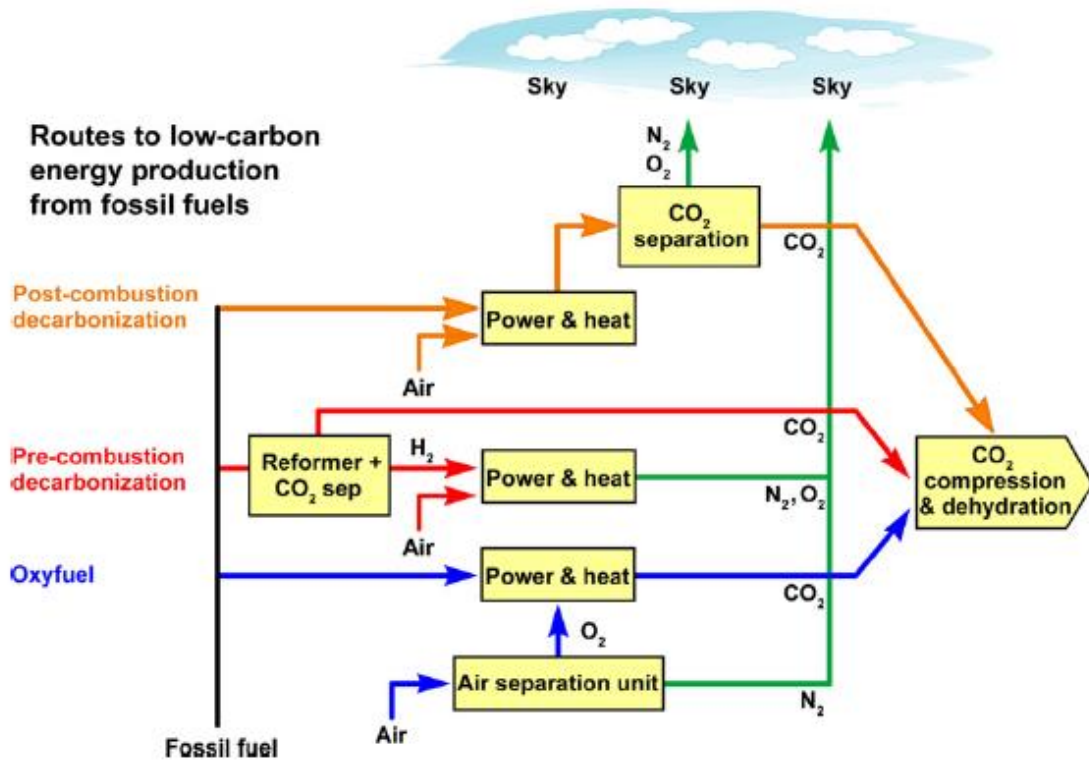
Figure 1. 4. CO_2 capture methods (Merkel et al., 2010).

Post-combustion capture technology is based on the separation of CO_2 gas from the exhaust gas released as a result of fuel combustion. Different methods have been developed to achieve the separation. These post-combustion CO_2 capture methods are called adsorption, cryogenic separation, membrane separation, physical absorption and chemical absorption.

1.3. Chemical Absorption/Stripping as Conventional CO_2 Capture Process

Among the post-combustion capture methods, the adsorption method has low CO_2 removal ability due to poor selectivity. High pressure liquid CO_2 is produced in the cryogenic separation method, but it is not economical due to the high cooling cost and can only be applied to gas mixtures with very high CO_2 concentration. Membrane separation technology requires high purity flue gas flows (Arachchige, 2019). On the other hand, the chemical absorption method is a low-cost technology that can be easily

6

integrated into the existing plant, has higher selectivity compared to other methods, and can produce highly pure CO_2 (high efficiency) (Wu et al., 2014). Among the mentioned methods, it is seen that the chemical absorption method is the best post-combustion CO_2 capture technology. The chemical absorption method has been the most preferred method by nearly all commercial post-combustion CO_2 capture plants developed to date (Herzog et al., 2009). This method is the preferred method applied in proprietary and commercial processes developed by companies such as Fluor, Alstom, Siemens, Mitsubishi and HTC Purenergy (Wu et al., 2014).

1.3.1. Process Description of Typical Absorption/Stripping Process

The conventional chemical absorption/stripping method consists of two main processes. These are the absorption and solvent regeneration (stripping) processes, a general representation of which is given in Figure 1.5. Each process takes place in two separate columns. Packed-bed columns are generally used as absorption and stripping columns. This is because packed-bed columns provide a high contact area between the liquid and gas phases and provide small pressure drop. In the absorption process, the flue gas is brought into countercurrent contact with a liquid absorber solution selective for CO_2 in a column. Upon this contact, CO_2 is transferred from the vapor/gas phase to the liquid phase. While flue gas enters the column from the bottom, the solution enters the column from the top. Absorber temperature is about 40^oC and pressure is about 1.1 bar. Unreacted gases exit from the top of the absorption column and the CO_2-rich solution exits from the bottom of the column. The CO_2-rich solution is heated to $110\text{-}120^oC$ using a cross heat exchanger and pumped to the top of the stripping column for thermal regeneration of the absorption liquid. The stripping column operates approximately at 112^oC and 1.9 bar. Here, the CO_2 is separated from the solvent and sent to the condenser to be compressed at a high purity (about 98%). From the bottom of the stripping column, the regenerated absorber solution is returned to the absorption column to capture CO_2 again (Arachchige, 2019; Herzog et al., 2009; Kothandaraman, 2010; Madeddu et al., 2018; Wang et al., 2011; Wu et al., 2014).
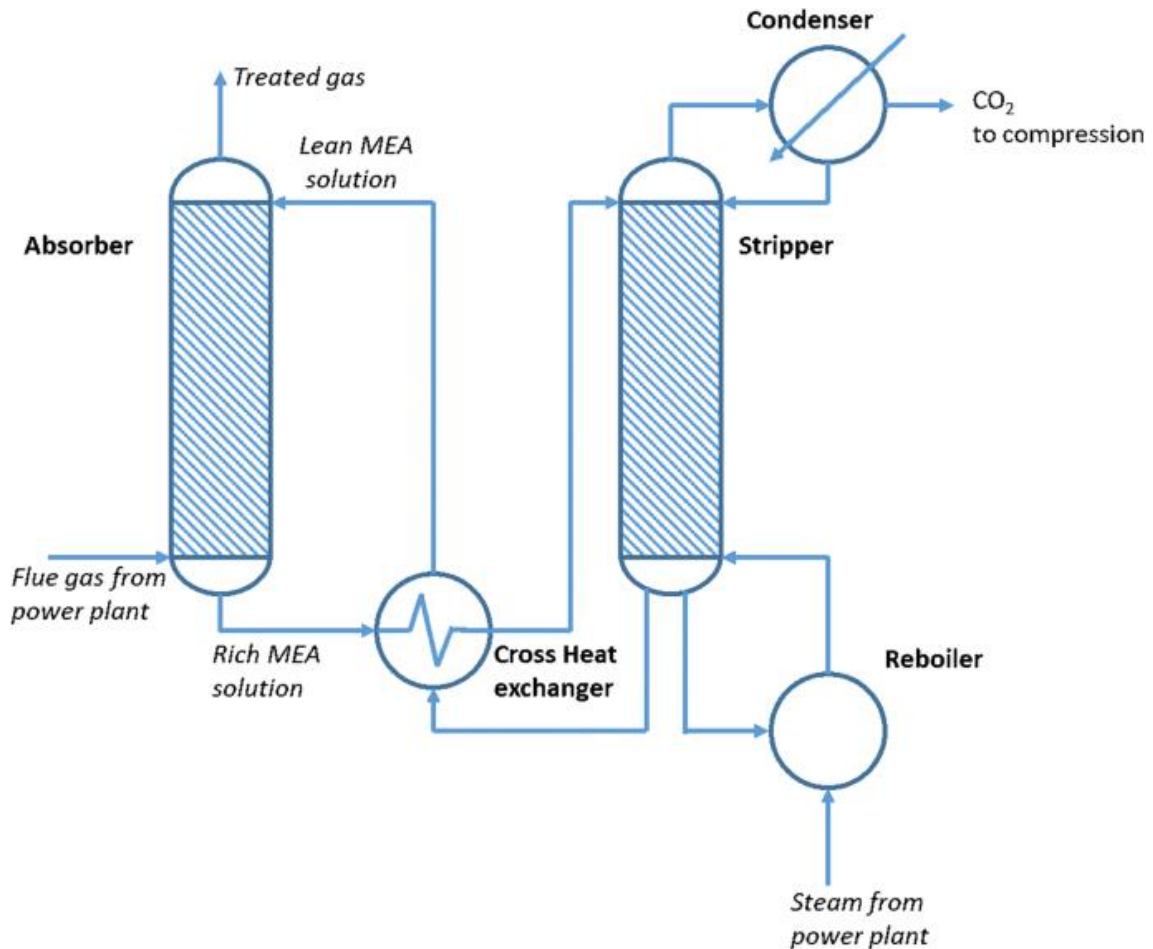
Figure 1. 5. Schematic representation of the conventional CO_2 capture process based on chemical absorption method (Lecomte et al., 2010).

1.3.2. Solvents for Chemical Absorption Process
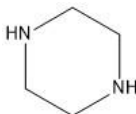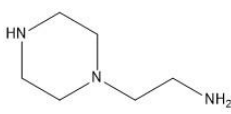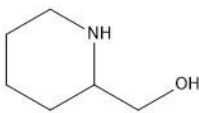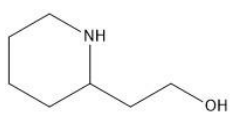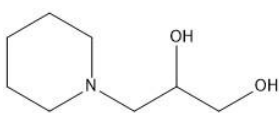
In the chemical absorption method used to CO_2 capture, solvents that will react with CO_2 are used. In the packed absorption column, CO_2 and solvent react and CO_2 is captured by the transfer from the gas phase to the liquid phase. While potassium carbonate solutions were used in the early systems used to capture CO_2 in industrial gas streams, the most widely used solvent today is monoethanolamine (MEA). This is due to the low selectivity of potassium carbonate, slow absorption rate and corrosion effect on equipment. In comparison, when looking at a chemical absorption system using MEA, 4 MJ of heat is required for each kilogram of CO_2 captured during the regeneration of MEA. This heat requirement reduces plant efficiency by 35-40% (Asif et al., 2018). About 80% of the total energy consumption in CO_2 capture comes from the solvent regeneration. Due to the low CO_2 concentration in the flue gas, high concentrations of MEA should be used

8

(up to 2 kg solvent/tonne of CO_2). In addition, MEA is corrosive to equipment material and thermally degrades. These factors significantly increase the capital and operating costs of the chemical absorption plant using MEA. Therefore, all these disadvantages mentioned require the development of a new solvent to be used to capture CO_2. The following criteria should be considered in the selection of the new solvent type to be developed (Arachchige, 2019; Asif et al., 2018):

- Solvent must be thermally stable so it will resist degradation.
- The vapor pressure of the solvent should be low to avoid losses.
- It should have high absorption capacity and rate. This reduces the size of the column and therefore the cost of the process.
- Solvent must have a low regenerating temperature. The low temperature will also reduce the amount of energy required during regeneration.
- A non-corrosive solvent should be chosen. Otherwise, the equipment cost will be high.
- The solvent should be a cheap and readily available.
- From an environmental point of view, the solvent should be less toxic and more environmentally friendly.

For these reasons, amines stand out as the most popular solvent group. In a study conducted by Puxty et al. in 2009, the CO_2 absorption ability of 76 different amines was investigated. In that study, piperazine and its derivatives were observed to be a promising solvent. It has been reported that piperazine and its derivatives, whose CO_2 capture properties are given in Table 1.1, have higher CO_2 absorption capacity and rate compared to other amines, are resistant to thermal and oxidative degradation, and provide less energy consumption. As seen in the table, homopiperazine has the highest CO_2 absorption rate and 3-piperidino-1,2-proandiol has the highest CO_2 absorption capacity (Puxty et al., 2009).

Table 1. 1. Chemical structures and CO_2 capture abilities of amines (Puxty et al., 2009).

Name	Chemical Structure	CO_2 Capture Capacity (n_{CO2}/n_{amine})	CO_2 Capture Rate ($n_{CO2}/(n_{amine}.min)$)	pK_a
monoethanolamine		0.56	0.013	9.5
piperazine		0.65	0.031	9.73
homopiperazine		0.70	0.045	11.0
1-(2-aminoethyl)piperazine		0.23	0.014	10.1
2-piperidinemethanol		1.0	0.012	10.6
2-piperidineethanol		1.0	0.011	10.9
3-piperidino-1,2-propanediol		1.1	0.008	8.91

1.3.3. Mechanism of Absorption and Desorption for Conventional Method

The zwitterion mechanism introduced by Caplow (Caplow, 1968) and re-examined by Danckwerts (Danckwerts,1979) is widely used to explain the absorption of CO_2 in aqueous amine solutions. This mechanism, for which the reactions of which are given in Table 1.2, consists of two steps. In the first step, the nucleophilic nitrogen atom in the amine provides an electron pair to form a chemical bond with the electrophilic

carbon atom in CO_2. As a result, an unstable compound called zwitterion is formed (zwitterion is a neutral compound with same number of positive and negative functional groups). Then, the zwitterion formed reacts with any basic compound (OH^- or amine molecules) in the solution to form a carbamate (amine-CO_2 complex). This reaction in the absorber column takes place at about 40^oC. According to the zwitterion mechanism, the CO_2 absorption rate is directly proportional to the amine concentration (Blauwhoff et al.,1983; Caplow, 1968; Danckwerts, 1979). As the amine concentration decreases as a result of the reaction with CO_2, the rate of CO_2 absorption decreases and eventually the CO_2 absorption rate is reset by reaching the thermodynamic equilibrium state.

Table 1. 2. Reactions that take place during the absorption and desorption steps in the conventional CO_2 capture process (Yousefzadeh et al., 2022).

$$2H_2O \underset{k_{-1}}{\overset{k1}{\rightleftharpoons}} H_3O^+ + OH^-$$

$$CO_2 + 2H_2O \underset{k_{-2}}{\overset{k_2}{\rightleftharpoons}} HCO_3^- + H_3O^+$$

$$HCO_3^- + H_2O \underset{k_{-3}}{\overset{k_3}{\rightleftharpoons}} CO_3^{2-} + H_3O^+$$

$$R_1R_2NH + H_3O^+ \underset{k_{-4}}{\overset{k_4}{\rightleftharpoons}} R_1R_2NH_2^+ + H_2O$$

$$R_1R_2NH + HCO_3^- \underset{k_{-5}}{\overset{k_5}{\rightleftharpoons}} R_1R_2NCOO^- + H_2O$$

$$R_1R_2NCOO^- + H_3O^+ \underset{k_{-6}}{\overset{k_6}{\rightleftharpoons}} R_1R_2NH^+COO^- + H_2O$$

The regeneration of the amine from the CO_2-saturated amine solution (desorption process) is the opposite of the absorption process. However, an important difference from the absorption process is that the carbamate from the absorber column must be heated at high temperatures (120^oC-140^oC). In the desorption process given as reverse reactions in Table 1.2, the carbamate formed during the absorption is heated to separate the amine and CO_2 (Lv et al., 2015). A general schematic of absorption and desorption processes is given in Figure 1.6.
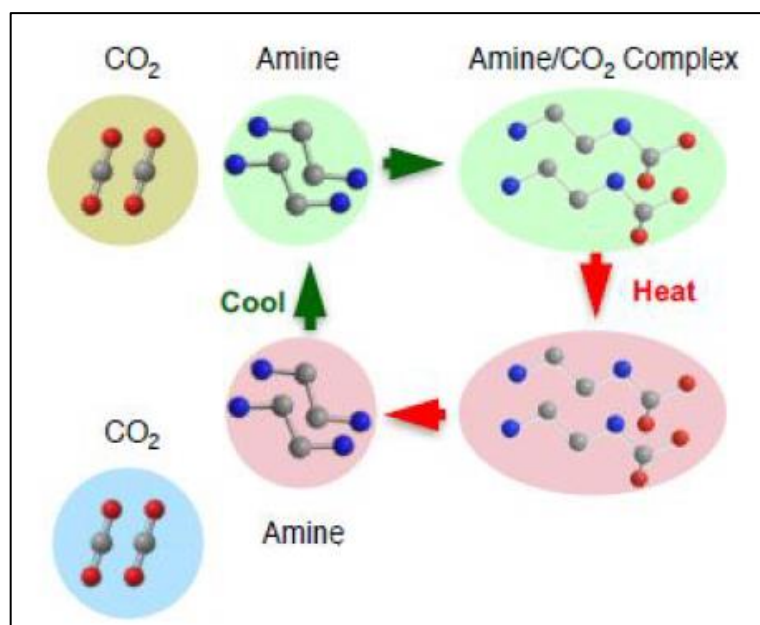
Figure 1. 6. General representation of the processes taking place in the absorber and stripping column in the conventional CO_2 capture method using ethylenediamine as the absorber molecule (Hatton, 2021).

1.3.4. Disadvantages and Improvement Point of Conventional Process

The most important disadvantage of the conventional thermal chemical absorption process in which MEA is used is the high energy requirement for solvent regeneration. As mentioned in Section-1.3.2, in the CO_2 capture process using MEA, the efficiency of the facility decreases by 30-40%, and 80% of the total energy consumption in the facility is used in MEA regeneration. In addition, the high corrosion rates observed in the MEA process and the emergence of toxic nitrosamine and nitramine compounds formed by MEA degradation are also important disadvantages of the MEA process (D'Alessandro et al., 2010; Leung et al., 2014; Rheinhardt et al., 2017; Yang, et al., 2008). Therefore, considering all these disadvantages, new studies are required to mitigate the aforementioned shortfalls. Studies can be carried out in development of a new amine or a new capture process. New solvents and new methods could provide the opportunity to realize significant energy and cost savings.

1.4. Electrochemical CO_2 Capture Process

First introduced by Stern et al. (Stern et al., 2011) in 2011, the amine-based electrochemical CO_2 capture technology has significant advantages over the conventional CO_2 capture process. The high amount of energy required during solvent regeneration is the main disadvantage of amine-based CO_2 capture systems. Electrochemical CO_2 capture technology, which is a new method in the literature on CO_2 capture, stands out with its potential to directly eliminate the high energy consumption in the amine regeneration process, as it is a process carried out at low and constant temperatures. This is because the Gibbs free energy is interconvertible with electrical energy and the electrochemical method is therefore not limited by the Carnot efficiency unlike conventional temperature variation methods (e.g., stripping column). In addition, electrochemical CO_2 capture technology reduces electrical losses and prevents side reactions by precise control of potential (Hatton, 2021; Rheinhardt et al., 2017; Stern & Hatton, 2014).

1.4.1. Process Description of Electrochemical CO_2 Capture Process

In electrochemical technology, the same type of absorption column and the same operating conditions for absorption are used as in conventional CO_2 capture technology. However, the rest of the process is completely different. The temperature of the CO_2-rich solution is not increased and not sent to the desorption column, instead CO_2-rich solution is passed through the anodic and cathodic sides of the electrochemical cell.

In the electrochemical CO_2 capture process, a general representation and reactions of which are given in Figure 1.7, the CO_2 capture step and the CO_2 release step are performed by different processes. In the CO_2 capture step, CO_2 is captured in an absorption column using the amine molecule as in the conventional process (the amine-CO_2 adduct is formed). Then, this amine-CO_2 adduct, unlike the conventional process, it is pumped to the anode of an electrochemical cell and the CO_2 release step is carried out electrochemically. In the CO_2 release step, metal ions (e.g., Cu(II)) dissolved by the potential applied to the anode form a complex with the amine, allowing the amine-CO_2 adduct to release CO_2. The resulting Cu(II)-amine complexes are pumped to the cathode in the electrochemical cell, and the amine is released and recovered by reduction of the

metal ion (reduced Cu(II) accumulates as Cu(s) on the cathode). The cycle is restarted by returning the free amine to the absorption column, and CO_2 capture is performed in a continuous process (After long cycles, the polarity in the electrochemical cell is changed to prevent the metal from accumulating in one electrode and completely wasting the other electrode) (Stern & Hatton, 2014).
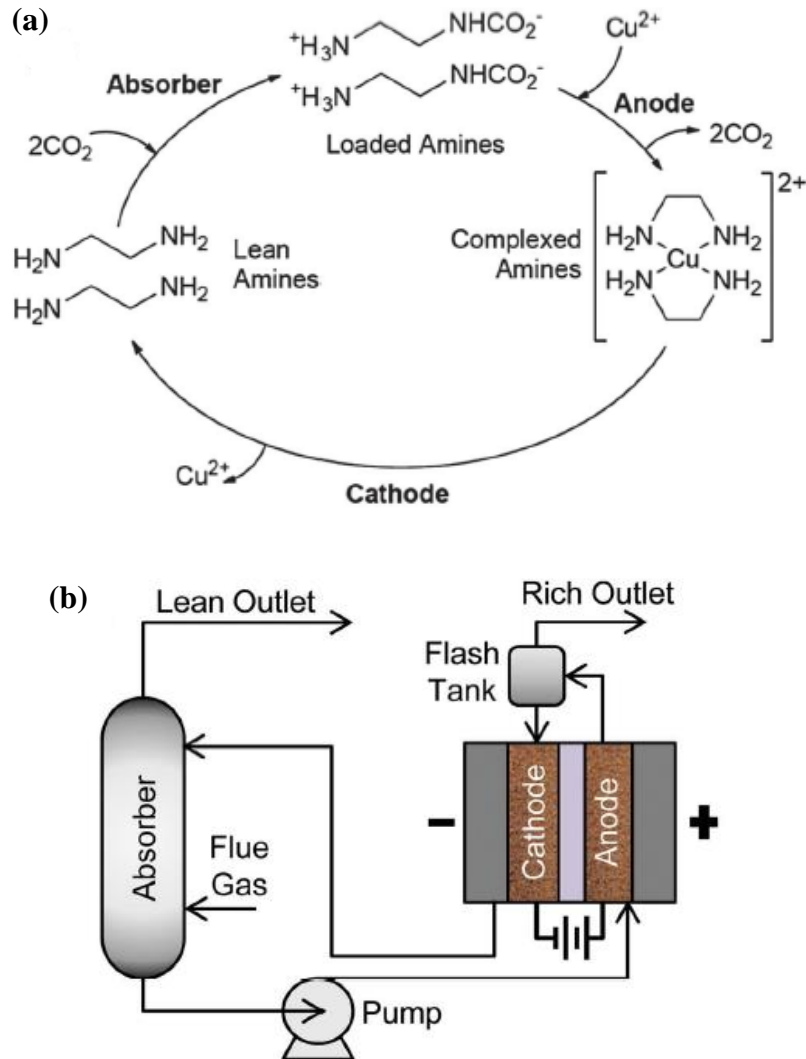
Figure 1. 7. (a) Chemical reactions for electrochemical process, (b) Schematic representation of the electrochemical process (Stern & Hatton, 2014).

1.4.2. Selection of Metal in Electrochemical Process

In electrochemical CO_2 capture technology, the CO_2 capture process takes place in the same way as the conventional process. The reactions at this stage can be explained by the zwitterion mechanism as described in Section-1.3.3. However, the reactions that

14

take place in the anode and cathode parts of the electrochemical cell to which it is sent are completely different from the conventional process. These reactions are carried out with metal ions in the electrochemical process.

At the anode, it is necessary to use redox active metals to release the captured carbon dioxide. In particular, oxidation of transition metals yields cations with sufficient Lewis acidity to compete with CO_2 at amine linking groups. Metal cations, which dissolve into the solution with the effect of the applied potential, tend to form higher complexes with the amine compared to CO_2. Therefore, metal ions break the bond formed between CO_2 and amine, forming an amine-metal complex and releasing CO_2 (Stern & Hatton, 2014). In the cathode part of the electrochemical cell, reduction takes place and the metal ions in the amine-metal complex precipitate on the electrode and the amine is regenerated.

There are some criteria for selecting the metal ion to be used in the process. Based on several criteria, such as cost, complexing power with amine, and resistance to undesirable oxidation by hydrogen formation, the best metal candidate for CO_2 capture is selected.

In order for amines to be used in the electrochemical CO_2 release process, they must maintain a stable coordination with metal ions. If the coordination is not provided or the coordination they provide is weak, it causes the formation of metal-hydroxide precipitate. In the literature, it has been observed that only copper (Cu), zinc (Zn) and nickel (Ni) are suitable metals to form metal-amine complexes. However, only Cu has been shown to adapt to electrochemical methods without undergoing hydrogen formation (i.e., water splitting). In addition to that, its relatively low cost, high affinity towards amines, and oxidative stability make copper (Cu) the most suitable candidate (Hatton, 2021; Stern & Hatton, 2014).

In Figure 1.8, the cell part of the electrochemical process is shown and the reactions taking place at the anode and cathode with the use of copper ions are given. In this process, 1 mole of Cu^{+2} ion at the anode releases 2 moles of CO_2 gas. At the cathode, a positively charged amine-Cu complex is reduced by taking 2 electrons (e^-) and the regeneration of the amine is provided.

$$Am(aq) + mCO_2(g) \rightleftharpoons Am(CO_2)_m(aq)$$

$$\frac{2}{m}Am(CO_2)_m(aq) + Cu(s) \rightleftharpoons CuAm_{2/m}^{2+}(aq) + 2CO_2(g) + 2e^-$$

$$CuAm_{2/m}^{2+}(aq) + 2e^- \rightleftharpoons Cu(s) + \frac{2}{m}Am(aq)$$
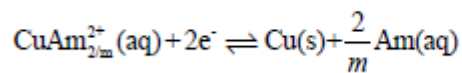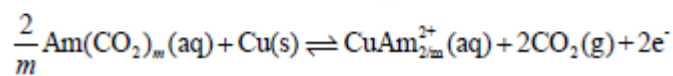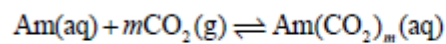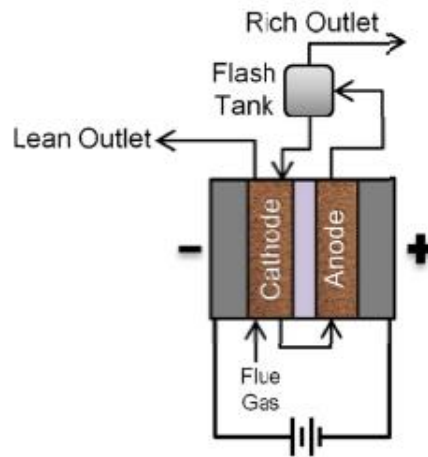
Figure 1. 8. The schematic of an electrochemical cell used in electrochemical CO_2 capture process and the reactions occurring in the anode and cathode compartments of the electrochemical cell in presence of copper ions (Stern & Hatton, 2014).

1.5. Aim of Thesis

The aim of this thesis is to investigate the electrochemical CO_2 capture process using homopiperazine (HPZ). The use of homopiperazine (HPZ) in electrochemical CO_2 capture process is not carried out before in the literature. A new cell design was made based on the literature and a laboratory scale electrochemical CO_2 capture process was developed. Comparisons were done between the use of HPZ and MEA in the electrochemical CO_2 capture process.

1.6. Structure of Thesis

This thesis consists of five chapters. In the first chapter, the effects of the increasing amount of CO_2 in the atmosphere on global warming, the main factors that increase the CO_2 concentration, the methods used to reduce the CO_2 emission are briefly discussed. For this purpose, the chemical absorption process, which is the conventional method, is overviewed and an introduction to the electrochemical CO_2 capture technology

is provided. In the second chapter, Literature Survey, previous studies on the electrochemical CO_2 capture system were discussed and important points affecting the electrochemical process were emphasized. In Chapter 3, the chemicals used in the study are introduced, the details of the absorption experiment, the design of the electrochemical cell, and the electrochemical cell experiments are given. In addition, derivations of the necessary equations were made to calculate the absorption rate, amine capacity and CO_2 release rate. In Chapter 4, titled "Results and Discussion", the results of all experiments are given and these results are examined. In the last chapter, Chapter 5, the results are briefly summarized and suggestions for future studies are given.

CHAPTER 2

LITERATURE SURVEY

2.1. Criteria Followed in Literature Survey

Although there are many studies on CO_2 capture technologies in the literature, CO_2 capture by electrochemical method is a new technology for this field. In order not to miss the focus of the thesis and to customize the literature search in accordance with this thesis, the following criteria were determined for article selection:

- Chemical absorption method should be used to capture CO_2 from flue gas.
- The amine compounds, especially monoethanolamine (MEA), ethylenediamine (EDA) or, if available, homopiperazine (HPZ) should be used as absorbent.
- Electrochemical method should be used in the desorption stage.
- Electrochemical cell design should be made, and the details of the design should be given.
- Copper (Cu) metal should be used as the electrode, and details should be given about whether the electrode is porous or plate.
- Details regarding the supporting electrolyte used in the experiments should be given.

A few studies come to the fore when literature research is conducted in line with the given criteria. In the following sections, studies that meet these criteria are examined according to the amine selection, metal selection, cell design, electrode and electrolyte details, which are important for the development of the electrochemical method. In the last section of this chapter, the lessons learned from the literature survey are summarized.

2.2. Literature Studies Satisfying the Criteria

2.2.1. Amine Selection

In a study by Stern (Stern, 2013), fourteen different types of amines, including monoamines, diamines and polyamines given in Table 2.1, were compared for the selection of amines to be used in the electrochemical CO_2 capture system in terms of the solution stability in presence of copper ions.

As seen in Table 2.1, it has been determined that monoamines are not suitable for the electrochemical process due to their tendency to precipitate with copper ions. Amino acids are not effective candidates due to their complex structure with CO_2. In addition, it has been observed that 1 molecule of CO_2 is released per two electrons in systems using amino acids. The low CO_2 yield per electron also increases the required current densities. On the other hand, ethanolamines, diamines and polyamines will release 2 molecules of CO_2 per two electrons. Besides, these amines do not produce precipitates with copper ions.

Table 2. 1. The studied amines and corresponding comments on their solution stability performance in electrochemical CO_2 capture studies conducted in (Stern, 2013).

Abbrev.	Full Chemical Name	Comments
MEA	Monoethanolamine	Precipitate observed during CO_2 capacity measurement
DEA	Diethanolamine	Precipitate observed during CO_2 capacity measurement
MDEA	N-Methyldiethanolamine	Precipitate observed during CO_2 capacity measurement
Gly	Glycine	Precipitate observed during CO_2 capacity measurement
Sar	Sarcosine	CO_2 capacity experiments not performed
Tar	Taurine	CO_2 capacity experiments not performed
EDA	Ethylenediamine	No precipitate observed in target concentration range
dmEDA	N,N-Dimethylethylenediamine	No precipitate observed in target concentration range
deEDA	N,N-Diethylethylenediamine	Precipitate observed during CO_2 capacity measurement
tmEDA	Tetramethylethylenediamine	Amine was too volatile for CO_2 capacity measurement
AEEA	Aminoethylethanolamine	No precipitate observed in target concentration range
DACH	Trans-Diaminocyclohexane	Precipitates immediately when exposed to cupric ions
DETA	Diethylenetriamine	Copper powder formed during CO_2 capacity experiments
TETA	Triethylenetetramine	No precipitate observed in target concentration range

Copper ions have high stability constants in presence of polyamines. Their ability to strongly chelate metal cations makes polyamines a promising chemical for

electrochemical CO_2 capture. Polyamines with copper ions appear to be the most effective combination for electrochemical CO_2 capture studies. The four polyamines tested in this study were EDA, AEEA, TETA and DETA. It was determined that EDA had the highest CO_2 capacity among these four polyamines.

In another study by Hatton (Hatton, 2021), a different set of amines were also compared. MEA, DEA, DETA, 2-Amino-2-methyl-1-propanol (AMP), EDA, pentamethyldiethylenetriamine (PMDTA), AEEA, TETA and piperazine (PZ) were studied as possible CO_2 absorbents. In the study, pH titrations, open-circuit potential measurements and cyclic voltammetry measurements were carried out to assess the stability constants of metal ion-amine interaction. The binding of the amine and metal must be strong enough to overcome the amine-CO_2 complex so that CO_2 can be released from amine-CO_2 complex by formation of amine-metal ion complex instead, but it should not be that strong to cause high power consumption to regenerate free amine by breaking up amine-metal ion complex and reducing metal ion to neutral metal. While choosing the convenient amine for the electrochemical CO_2 capture process, attention was paid to the stability of the metal-amine complex and not to form precipitation. In line with the results obtained, it was seen that only the Cu-EDA complex have high stability in a broad pH range and its stability could be adjusted by electrochemical means without causing hydrogen formation (water splitting).

2.2.2. Metal Selection

The combination of metals and amines is an important criterion for an electrochemical CO_2 capture technology. In the study by Stern (Stern, 2013), vanadium, tin, chromium, zinc, manganese, iron, cobalt, nickel and copper metals were compared to determine the best combination between metals and EDA.

Vanadium, tin, nickel and cobalt are not suitable candidates because they are expensive. An important criterion is the stability constant of the amine-metal complex. The amine-metal complex should have a stronger bond than the amine-CO_2 complex. In this case, it was observed that only Cr(III), Fe(III), Co(II), Co(III), Ni(II) and Cu(II) ions had strong enough interactions with EDA. However, these metals, except copper, tin and lead, have the potential to be oxidized even in the absence of oxygen.

Copper (Cu(II)) is a redox active competitor to the amine-CO_2 complex, relatively low cost, resistant to oxidation that may occur due to hydrogen formation, and has high affinity for complexing with amines. Therefore, considering these properties, Stern stated that Cu(II) is the most suitable candidate for the electrochemical CO_2 capture process in presence of EDA (Stern, 2013).

In the study by Hatton (Hatton, 2021), the precipitation state of metal-amine pairs was investigated. It was observed that some amines (AEEA, MEA, PZ, TETA, AMP) used in the study mentioned in the amine selection section precipitated with Co^{2+}, Fe^{3+}, Fe^{2+}, Cr^{2+} ions. However, no precipitation was observed with Cu^{2+} using EDA, DETA and AEEA, with Zn^{2+} using DETA and with Ni^{2+} using EDA and DETA. According to the results obtained, it was seen that only Cu, Zn and Ni were suitable for electrochemical treatment, but it was concluded that only the Cu-EDA complex was not prone to hydrogen formation and was resistant to oxidation.

2.2.3. Conceptual Configurations for Electrochemically Modulated Complexation

Stern et al. conducted another study on electrochemical mediated separation systems to separate CO_2 from gas mixtures (Stern et al., 2011). For this purpose, separation processes called electrochemically modulated complexation (EMC) were developed and four possible process configurations were analyzed.

The EMC process is an electrochemically mediated process consisting of absorption-desorption cycles. In this process, whose applicability is seen in gas absorption processes, the electrochemically active sorbents form redox state sensitive complexes with the target species. Separation takes place in four steps given in configuration A in Figure 2.1. These four steps are the activation of the sorbent (Stage 1), the capture of the target molecules (Stage 2), the deactivation of the sorbent (Stage 3), and the release of capture molecule (Stage 4). The EMC system was examined in this study by testing the configurations B, C and D shown in Figure 2.1.
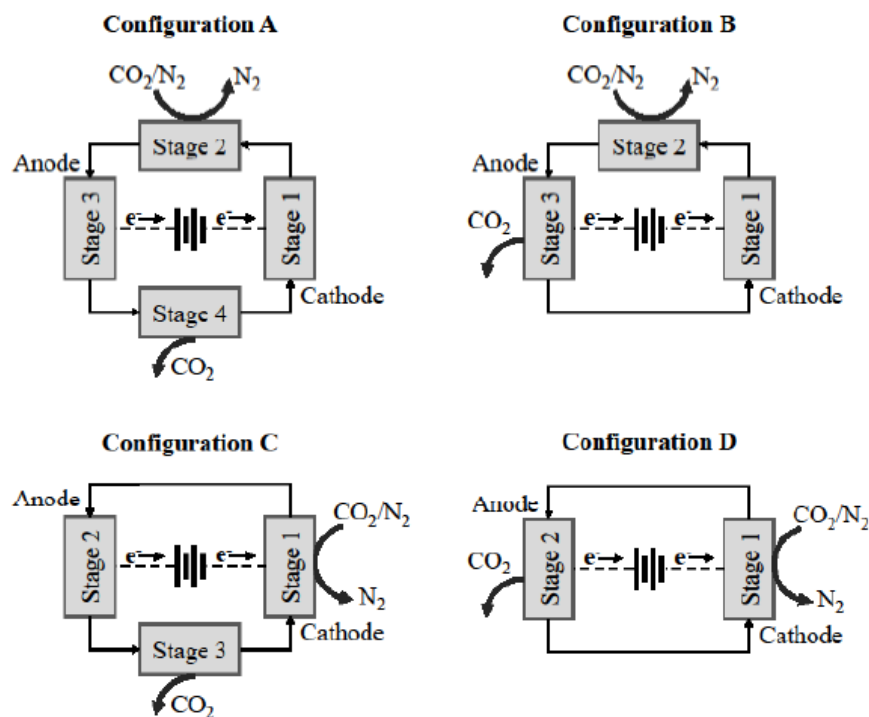
Figure 2. 1. Possible configurations for an electrochemically modulated complexation (EMC) system (Stern et al., 2011).

Figure 2.2 shows the energy efficiency of each of the four configurations. The axis of approach to ideality shown in the figure is defined as the energy efficiency of the configuration relative to the completely reversible single-stage thermodynamic limit. The reduction fraction shows the electron transferred (reduction amount) according to the maximum possible limit (reduction fraction of zero means neutral state). As can be seen, in systems without integration at the cathode (configurations A and B), high efficiency losses occur when the reduction ratio reaches a value greater than 0.5. In systems without integration at the anode (configurations A and C), the efficiency decreases as the reduction fraction increases. The best performance is given by fully integrated systems (D configuration) with >95% ideality.
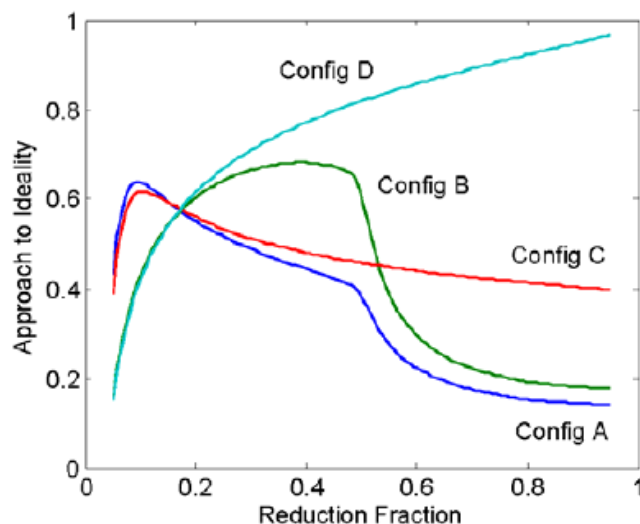
Figure 2. 2. Energy efficiencies of four possible configurations shown in Figure 2.1 (Stern et al., 2011).

2.2.4. Electrochemical Cell Design

Various studies were carried out by Stern on electrochemical cell design (Stern, 2013). These designs, each being an improved version of the previous one, are named as second generation, third generation (EMAR 3) and fourth generation (EMAR 4).

In the second generation design, polypropylene was used as the main construction material in the system, which is given in assembled and disassembled state as shown in Figure 2.3. Polypropylene was proposed as to remain chemically stable in aqueous amine solutions. Although the design was well-structured and the material of construction was resistant to chemicals and waterproof, the geometry of the design was not suitable for electrochemical reactions. The reason was the very deep flow channel preventing the effective utilization of the electrode.
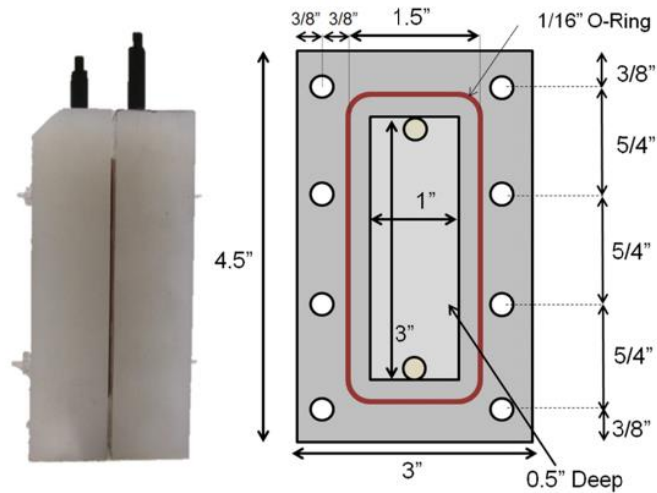
Figure 2. 3. Second generation EMAR cell (Stern, 2013).

The third generation system (EMAR 3) is shown in Figure 2.4 is well designed. However, the polycarbonate used as the main building material in this design swelled and was found to be unstable. The fact that a hole was drilled in the chassis from the back of the system for the electrical connection created difficulties in sealing. Nafion, which was used as a membrane in EMAR 3, was found to discolor due to impregnation of copper-amine complexes, but gave stable and effective results. Although the third generation system is short-lived due to the main material used, it has been seen that the system was effective in design.
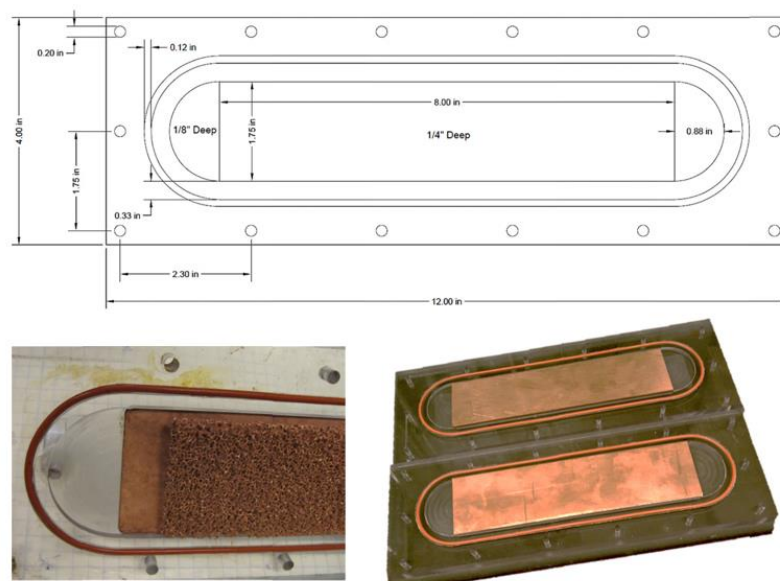
Figure 2. 4. Schematic diagram and disassembled state of third generation system (EMAR 3) (Stern, 2013).

The fourth generation system, called EMAR 4, is the main focus of this study. In this design, method of assembly and disassembly, flow geometry and stability were improved with respect to previous designs. The chassis material was selected as aluminum, not plastic unlike in the previous designs. The design details of EMAR 4 are given in Figure 2.5.
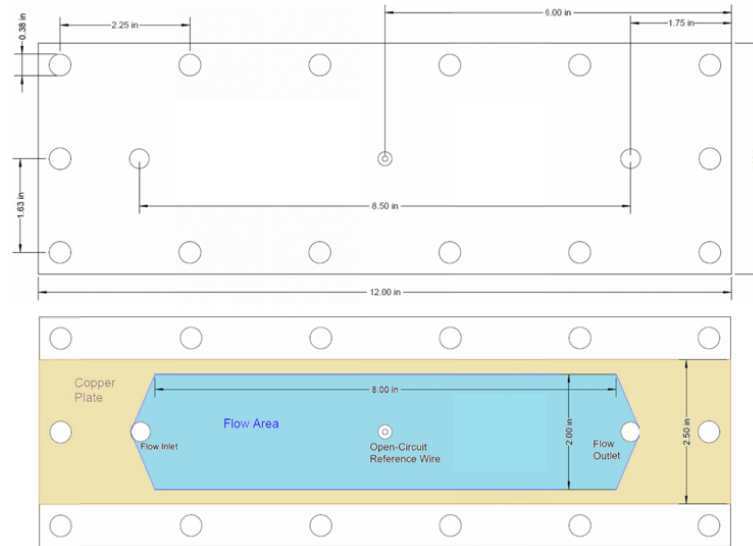
Figure 2. 5. Schematic representation of EMAR 4 (Stern, 2013).

Another function of aluminum chassis was to be used as a current collector. In this design, the power supply is connected to the more accessible aluminum chassis instead of the copper electrode. As seen in Figure 2.6, foam is placed between the copper plate and the aluminum chassis. This foam was used to prevent liquid from leaking into the space between the two metals. For the electrical connection, two metals are soldered in places cut in the silicon foam. Aluminum and copper have significantly different oxidation potentials and, the bonding of these two metals observed to cause galvanic oxidation at the end of the experiments.
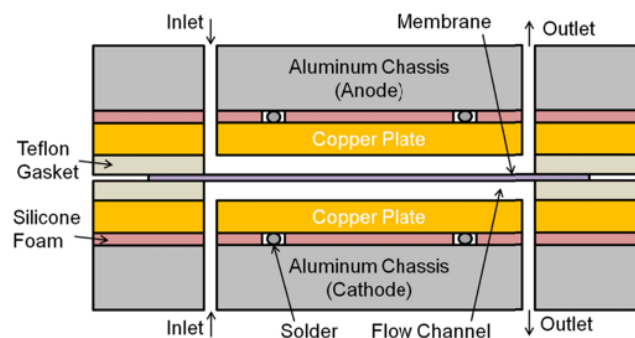
Figure 2. 6. Cross-sectional view of EMAR 4 (Stern, 2013).

25

Another challenge in the EMAR 4 design was to avoid the contact of the membrane and the copper electrode. The coating of surfactant coated polypropylene membranes with copper-amine complexes and contact of the coated membrane to the copper electrode would cause a short circuit in the system after a while. For this reason, a fabric was placed between the copper electrode and the membrane, as shown in Figure 2.7. Thus, the system was ensured to operate without short circuit. However, the flow distribution was significantly affected due to presence of fabric, and accumulation and dissolution occurred at the outer edges of the flow area. The inability to use the flow field effectively was a major problem of the EMAR 4 system.
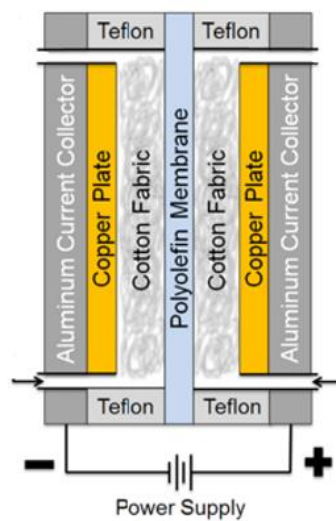
Figure 2. 7. Cross-sectional view of EMAR 4 with cotton fabric (Stern, 2013).

Another study on electrochemical cell design was conducted by Eltayeb (Eltayeb, 2015). The cells discussed in this study are an improved version of Stern's designs (Stern, 2013). The aim here was to develop the electrochemical cell designs given by Stern in his thesis and to obtain the most suitable design. For this, Eltayeb has developed three cell designs.

Eltayeb stated that the cell design called EMAR 4 in Stern's study was to prove the feasibility of the EMAR process. Eltayeb developed new designs by considering the shortcomings of the design EMAR 4, listed as follows:

- The fabric used to prevent the collapse of the membrane increases the contact resistance, causes uneven copper accumulation and accordingly the formation of dendrites. Dendrite formation was undesirable because it caused short circuit.

- The use of aluminum plates as both external chassis and current collector brought about undesirable situations. The solder to provide the electric current flow between the aluminum and the copper electrode was being broken. The space between the chassis and the electrodes caused the fluid to leak constantly and the structure of the chassis to deteriorate, and some side reactions occurred. These reduced energy efficiency.

- The force applied to close the cell caused deformation in Teflon gaskets used in the flow area. Therefore, it required care to balance the force to be applied. Therefore, assembly and disassembly of EMAR 4 were difficult and time-consuming.

EMAR 5, shown in Figure 2.8, was designed to allow quick creation and placement of flow fields, reusability of electrodes, and quick assembly and disassembly. In addition, problems such as dendrite formation and chassis degradation were also addressed in this design. For this purpose, the current collector function was separated from the external chassis and conductivity was provided with copper wires soldered to the holes drilled into the electrode. Thus, the aluminum chassis was isolated from the solution and current. Teflon gaskets were replaced with silicon sheets. Easily cut into complex shapes, silicone acted as a more leak-proof gasket that can withstand high sealing pressures. In order to prevent membrane collapse, Teflon gasket with small sections opened along the flow direction was used.

Figure 2. 8. EMAR 5 cell (Eltayeb, 2015).

The EMAR 6 cell was designed as a multi-electrode cell, where the applied voltage or current can be precisely controlled using more than one electrode portions. Thus, more efficient and stable design could be obtained by adjusting the working conditions and flow area. The sketch images of EMAR 6 design are shown in Figure 2.9. In this design, pieces of electrodes that are electrically insulated from each other were used. Aluminum was used as the chassis and a polypropylene layer was placed between

the aluminum chassis and copper electrodes for insulation. Electrode parts with wires soldered behind them for electrical connection were placed in a pocket formed by a polypropylene layer. Here, polypropylene was used as both insulation and building material. Flow channels and sealing were provided with silicone.
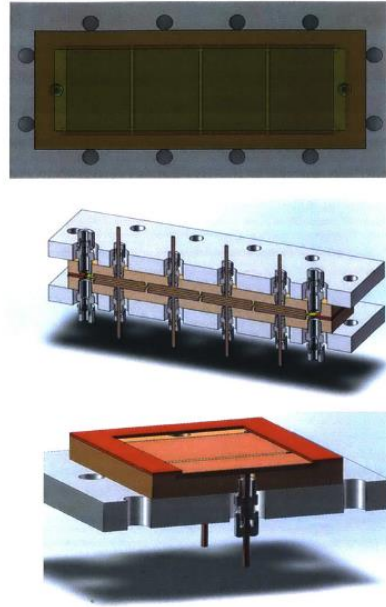
Figure 2. 9. Sketch images of EMAR 6 (Eltayeb, 2015).

The EMAR 6 prototype was designed to be used in a bench-scale system with more than one power sources. Thanks to this design, variations within the cell could be investigated and their interactions with different parameters could be examined. The images of EMAR 6 cell are given in Figure 2.10.
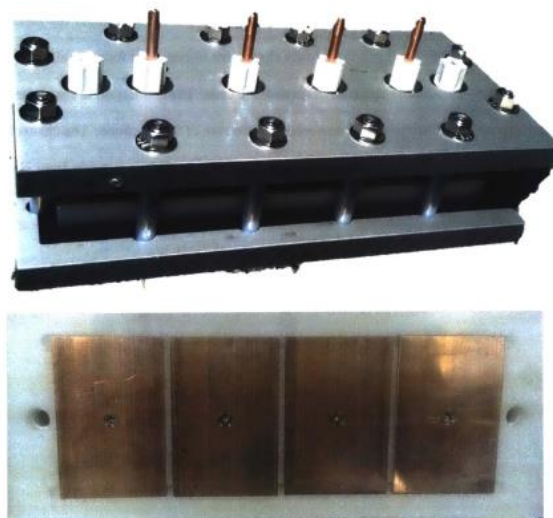
Figure 2. 10. Photos of EMAR 6 cell (Eltayeb, 2015).

Eltayeb stated that these prototypes could be operated at higher temperatures, but are not suitable for high pressures (Eltayeb, 2015). For this purpose, he developed the EMAR 7 prototype shown in Figure 2.11. In this design, safety was given priority taking into account the corrosive properties of amines and high pressure operating conditions. For this, an o-ring was used to contain the high pressure solution and to provide sealing. The connection to the electrode was made of copper wire, and the outer chassis was made of chemical resistant PEEK (polyether ether ketone).
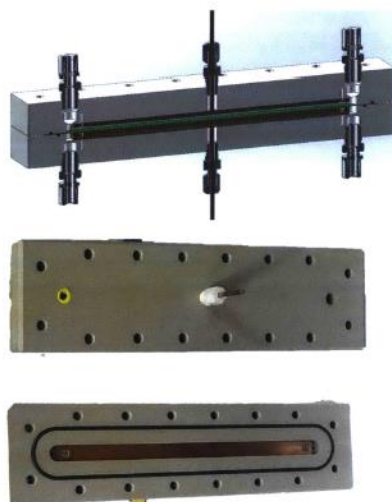
Figure 2. 11. EMAR 7 cell (Eltayeb, 2015).

Eltayeb's study showed that design parameters and operating conditions have a significant impact on CO_2 capture performance. He stated that EMAR 5 was a suitable design for exploring design variables, EMAR 6 was suitable for analytical experiments and model validation, and EMAR 7 was suitable for safe and high pressure operation.

Another study in which the design of the electrochemical cell was developed was conducted by Shaw (Shaw, 2019). In this study, EMAR 8.x designs were studied based on cell designs up to EMAR 7. The purpose of these designs was to enable the EMAR system consisting of a single unit cell to transition to stack geometry.

EMAR 8.x offered two options to run in parallel or serial configurations. In the parallel configuration shown in Figure 2.12, the polarity of voltage was reversed between each consecutive unipolar copper plates. In the series configuration, each copper plate acted as a bipolar plate. The parallel system EMAR 8.1 required high current and low potential operation. The serial system, EMAR 8.2, on the other hand, was suitable for low current and high potential operating conditions. Both systems had a geometry similar to

a flat plate heat exchanger. This allows the scale of desorption to be increased at the anode.

(a) Parallel Configuration   (b) Series Configuration
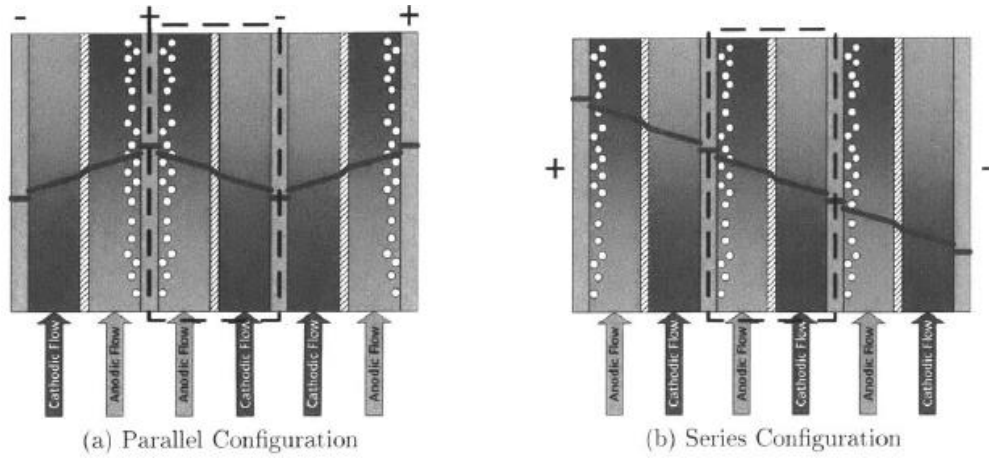
Figure 2. 12. Parallel and series stack configurations of EMAR 8.x (Shaw, 2019).

Finally, in a project carried out by Hatton, the mentioned studies were evaluated (Hatton, 2021). He stated that the operability of EMAR 8.x has been proven, but the size of the stack, its volume and the absorption of CO_2 by the regenerated amine created difficulties, and the simplicity and integratability of EMAR systems designed as single cells would be more suitable for experiments. Thanks to the cell design shown in Figure 2.13, gas output and voltage/current behavior could be monitored more carefully, and electron usage and energy calculations could be done more accurately.
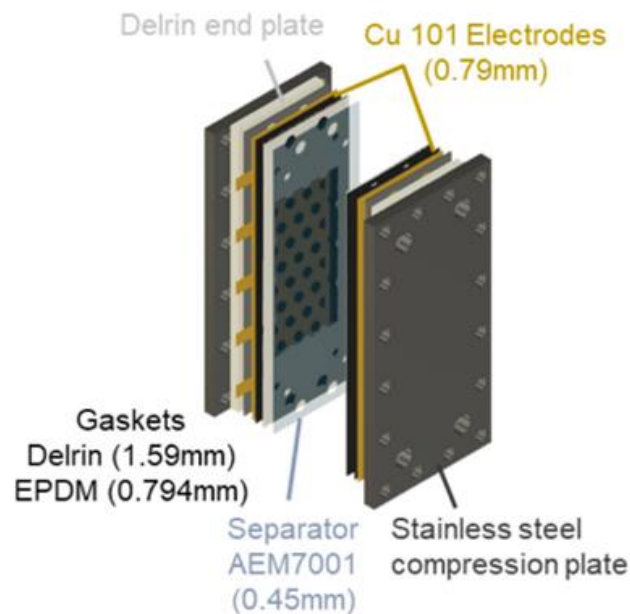
Figure 2. 13. Design image of single flow cell (Hatton, 2021).

2.2.5. Electrode Type

Electrode type selection is an important criterion in electrochemical systems. Stern compared flat plate electrode systems and porous electrode systems (Stern, 2013). He found out that the porous copper electrode was superior in terms of requiring low overpotential. It was observed that the flat plate electrode operates at an overpotential close to 100 mV, while the porous electrode operates at about 50 mV. Porous electrodes increased the effective electrode surface area to reduce the overpotential. However, it was noticed that the performance of the porous electrode systems started quite high and decreased over time. The reason was stated to be the trapping of the bubbles inside the pores.

In the study by Hatton (Hatton, 2021), porous carbon electrodes and flat copper plates were compared. According to Hatton, porous electrodes should be used for lowering energy requirement for the electrochemical process. It was shown that porous carbon electrodes have higher deposition efficiency than copper plates, uniform copper deposition and low reaction resistance.

2.2.6. Supporting Electrolyte Selection

Electrolyte selection is an important factor affecting the kinetics and thermodynamics of the system. For this purpose, Stern compared nitrate and chloride salts (Stern, 2013). With the tests using $NaNO_3$ and $NaCl$, it was observed that chloride salts had some minor effects on the EDA system, but had no significant effect on the thermodynamics of the system. Stern argued that the type of salt should have a significant effect on the kinetics of the system due to the complex structures formed by chloride salts and copper ions. He found out that the kinetics of a chloride-free system were extremely slow and required high potentials. In systems where nitrate salts are used, it was observed that the systems were more stable and higher Faradaic efficiency was obtained. On the other hand, the systems with chloride salts require lower potential. However, the corrosion of aluminum chassis in presence of chloride salts was problematic.

Another study comparing supporting electrolytes was carried out in one of Hatton's projects (Hatton, 2021). Hatton did comparisons with chloride, sulfate and nitrate salts in the study. It was observed that the kinetics of the system using chloride was very

fast and the chloride electrode required a lower overpotential compared to the system using sulfate. Consistent with Stern's findings (Stern, 2013), Hatton also noted that the reduction kinetics of copper ions was slow in presence nitrate compared to that of chloride. The reason was stated to be that chloride stabilized the cuprous intermediate and facilitated the further reduction reaction.

2.2.7. Energetics of EMAR Process

In a study by Wang et al. (Wang et al., 2019(2)), the EMAR process was modeled, and the amount of energy required by EMAR process was examined and compared with the conventional capture process. In this theoretical study, the desorption process of EMAR was defined as a "plug and play" operation since the carbon capture unit was completely independent from the main system. The amount of energy required to capture CO_2 and compress it at 150 bar pressure was calculated as 37-52 kJ/mol CO_2, making the EMAR process competitive with conventional CO_2 capture processes (about 40-64 kJ/mol CO_2 in the conventional amine-based process including compression to 150 bar (Boot-Handford et al., 2014)).

In another study by Wang et al. (Wang et al., 2019 (1)), the theoretical results of the EMAR system were tried to be experimentally verified. For this purpose, a system in which CO_2 flow and electron usage was monitored was operated continuously for 50 hours and the obtained results were analyzed. According to this study, EMAR process showed an electron utilization above 80%. CO_2 was captured with a capacity of 0.12-0.62 mol CO_2/mol amine, and the electrical energy consumption was measured to be 40-80 kJ/mol CO_2.

2.3. Lessons Learned from the Literature Survey

The important lessons learned from the literature survey section are listed below:

- What should be considered in the selection of amines are the chelating abilities and CO_2 capacities to be modulated with metal cations.

- The bonding between the amine-metal should be strong enough to overcome the amine-CO_2 complex and weak enough not to require high energy for amine regeneration.

- Metal selection should be made by considering its combination with amines. The metal's affinity for complexing with amines and the stability constants of the metal-amine complexes to be formed should be high.

- The formed metal-amine complex should not precipitate.

- Polyamines and piperazine derivatives and copper ions are suitable amine-metal ion combinations for EMAR process.

- Electrochemical cell design is a very important task in EMAR process design. While designing the cell, all details including sealing, placement of gaskets, main construction material, electrical connection, depth of flow channel should be considered. The cell design given in Figure 2.13 appears to be the best design so far.

- Regarding the types of electrodes to be used in the cell, porous electrodes provide higher energy efficiency than flat plate electrodes, while the compression of gas bubbles trapped in the pores is problematic.

- In the selection of the supporting electrolyte, the effect of the selected salt on the kinetics and thermodynamics of the system needs to be taken into account. Among the compared sulfate, chloride and nitrate salts, chloride salts provide the fastest kinetics, and lowest overpotential.

- The electrochemical CO_2 capture process has competitive energy requirements with the conventional CO_2 capture methods.

- As an advantage, the electrochemical CO_2 capture process can be easily integrated into existing coal-fired power plants.

CHAPTER 3

MATERIALS AND METHODS

3.1. Materials

Monoethanolamine (MEA) (C_2H_7NO) obtained from Tüpraş R&D center and homopiperazine (HPZ) ($C_5H_{12}N_2$) (98%) obtained from Sigma Aldrich were used in the CO_2 capture system. NaCl obtained from Merck was used as supporting electrolyte, and $CuCl_2$ and $Cu(NO_3)_2.3H_2O$ obtained from Merck were used as sources of copper ion (Cu(II)) in electrochemical cell experiments. CO_2 and N_2 gases were supplied from Güneş Gaz. De-ionized water with a resistivity of 15 MΩ.cm was obtained using a Millipore Elix 5 Essential Lab Water H_2O Purification System to prepare aqueous solutions. To simulate flue gas, a CO_2-N_2 gas mixture containing ca. 15% CO_2 by volume was obtained from Güneş Gaz.

3.2. Preparation of CO_2 Absorption System

First, a system for absorption of CO_2 from the CO_2-N_2 gas mixture is prepared. The flowchart of the prepared CO_2 absorption system is shown in Figure 3.1 and the photo of the prepared CO_2 absorption system is shown in Figure 3.2. A Hempel column with a diameter of 3 mm and a height of 50 cm was used as the absorption column. Glass beads with a diameter of 5-6 mm were randomly placed inside the column as packed material. The packed height is set to be 25 cm. Gas inlet and liquid outlet to the column were provided with a 2-necked 75° angled adapter connected to the bottom part of the column, while gas outlet and liquid inlet were provided with a 2-neck parallel adapter connected to the top part of the column. The CO_2-N_2 gas mixture was fed into the absorption column with the help of a mass flow controller (MFC; ALICAT, Model MC-10 SLPM-D). A check valve was used after the MFC to prevent any liquid from entering the MFC. Quick-fit elements and Teflon/POM flexible tubing were used for the piping processes in the

system. The chemical resistance of these materials against amine solutions was confirmed by chemical resistance tests in which they were kept in 1M aqueous amine solution for 5-7 days. The amine solution was sent from the top of the absorption column with the help of a peristaltic pump (Schencen-LabV1/V1). The amine solution sent to the column was returned to a 3-necked glass flask under the effect of gravity. In a real plant, the fresh amine solution is sent to the system in a single pass, absorbed the CO_2, regenerated, and fed back into the system as fresh amine solution. However, for the accuracy of the calculations to be made in our experiments, the amine solution fed to the absorption system was continuously recirculated between the 3-necked flask and the absorption column using the peristaltic pump. This ensured a complete saturation of amine solution with CO_2 and allowed a more precise calculation about the captured CO_2 amount. Gas and liquid flows in the absorption column were investigated at various flow rate ranges in order to prevent flooding and minimize channeling. For an acceptable gas-liquid contact, it was found that the gas can be fed at 1 bar at 25°C and with a flow rate of 250 mL/min, and the amine solution can be fed at 25°C with a flow rate of 170 mL/min. The gas at the absorption column outlet was sent to a CO_2 sensor after passing through the condenser. The condenser was kept at 5 °C using a recirculating cooler (CLS Scientific, CLRC-08C) to condense any trace amine vapor in the gas stream that might damage the CO_2 sensor. A CO_2 sensor (CO2meter-SprintIR®-W 100% CO_2 Sensor) was used to monitor the CO_2 concentration in the gas outlet after absorption in ppm units. In the sensor data that will also be given in the Results and Discussion chapter, when the amine starts to enter the column, the CO_2 concentration starts to decrease and becomes zero after a while. Absorption is considered to begin at this lowest CO_2 concentration seen in the sensor. As the amine solution begins to be saturated with CO_2, the concentration of CO_2 starts to increase. As the amine solution becomes completely saturated, the CO_2 concentration read on the sensor returns to the value that was before the amine solution was fed, and the absorption experiment is terminated at that point.
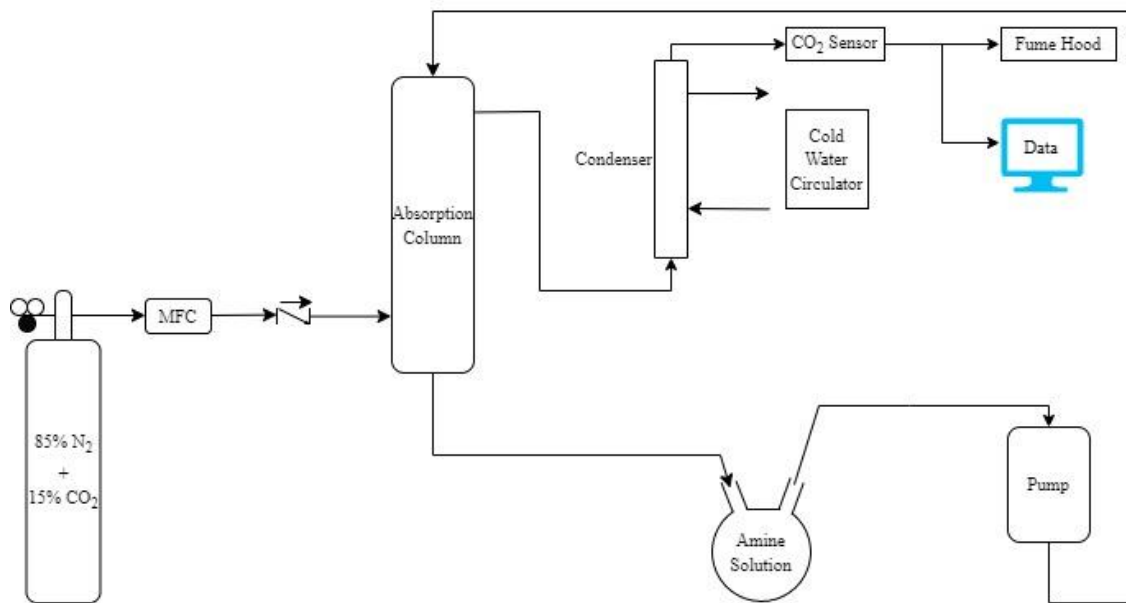
Figure 3. 1. Flowchart of the designed absorption system.

Figure 3. 2. Photo of the prepared CO_2 absorption system.

3.3. Derivation of Absorption Rate Equation

The absorption rate equation is derived by establishing the mass balances of the absorption experiment, the setup of which is given in Section 3.2. Two assumptions are made to derive this rate equation. The gas mixture is assumed to be an ideal gas and the system is assumed to be a CSTR. The equations given in Table 3.1 show the steps of deriving the rate equation starting from the ideal gas equations. In ideal gas equations and CO_2 ppm calculations, P, T and R are pressure (bar), temperature (K) and gas constant (83.145 $mL.bar.mol^{-1}.K^{-1}$), respectively. $\dot{V}$ and $\dot{n}$ represent the volume flow rate of gas mixture ($mL.min^{-1}$) and the gas mixture mole flow rate ($mol.min^{-1}$), respectively. In mass balance calculations, $N_{CO_2(g)}$ represents the mole amount of CO_2 in the gas phase (mol); F_{in}, $F_{CO_2,in}$, $F_{CO_2,out}$, $F_{N_2,in}$ represent the total gas mixture inlet molar flow rate, CO_2 inlet and outlet molar flow rate, and N_2 inlet molar flow rate ($mol.s^{-1}$), respectively. v_{in}, v_{out} represent the inlet and outlet volumetric flow rate ($mL.s^{-1}$), respectively. C_{in}, $C_{CO_2(g),out}$ represent the total inlet gas concentration and the output gas phase CO_2 concentration ($mol.mL^{-1}$), respectively. $y_{CO_2(g),in}$, $y_{CO_2(g),out}$ represent the inlet and outlet CO_2 mole fraction (ppm), respectively. V_g represents the volume of the uncaptured gas phase in the amine solution after absorption (Yousefzadeh et al., 2022). T_{in}, T_{out}, P_{in}, P_{out} represent the temperature and pressure of the inlet and outlet gas mixture (K, bar), respectively. t represents time (second), and finally $r_{absorption}$ represents the CO_2 capture rate ($mol.s^{-1}$).

Table 3. 1. Steps of derivation of the absorption rate equation

Equation	#
$P.\dot{V} = \dot{n}.R.T$	3.1
$\dot{V} = \dot{V}_{CO_2} + \dot{V}_{N_2}$	3.2
$\dot{n} = \dot{n}_{CO_2} + \dot{n}_{N_2} = \left(\dfrac{P}{R.T}\right).\left(\dot{V}_{CO_2} + \dot{V}_{N_2}\right)$	3.3

(cont. on the next page)

(Cont. of Table 3.1)

$$(CO_2)_{ppm} = \frac{\dot{n}_{CO_2}}{\dot{n}_{CO_2} + \dot{n}_{N_2}} = \frac{\dot{V}_{CO_2}}{\dot{V}_{CO_2} + \dot{V}_{N_2}} = \frac{\dot{V}_{CO_2}}{\dot{V}_T}$$	3.4
$$F_{CO_2(g),in} - F_{CO_2(g),out} - r_{absorption} = \frac{dN_{CO_2(g)}}{dt}$$	3.5
$$F_{CO_2(g),in} = F_{in} \cdot y_{CO_2,in} \text{ and } F_{CO_2(g),out} = F_{out} \cdot y_{CO_2,out}$$	3.6
$$N_{CO_2} = C_{CO_2} \cdot V_g$$	3.7
$$F_{in} \cdot y_{CO_2(g),in} - F_{out} \cdot y_{CO_2(g),out} - r_{absorption}$$ $$= V_g \cdot \frac{dC_{CO_2(g)}[\text{in gas phase control volume}]}{dt}$$	3.8
$$C_{CO_2(g),out} = \frac{F_{CO_2(g),out}}{\upsilon_{out}}$$	3.9
$$C_{in} = \frac{F_{in}}{\upsilon_{in}} = \frac{P_{in}}{R \cdot T_{in}} \text{ and } C_{out} = \frac{F_{out}}{\upsilon_{out}} = \frac{P_{out}}{R \cdot T_{out}}$$	3.10
$$\upsilon_{out} = \upsilon_{in} \cdot \left(\frac{F_{out}}{F_{in}}\right) \cdot \left(\frac{T_{out}}{T_{in}}\right) \cdot \left(\frac{P_{in}}{P_{out}}\right)$$	3.11
$$C_{CO_2(g),out} = \frac{F_{CO_2(g),out}}{\upsilon_{out}} = \frac{F_{CO_2(g),out}}{\upsilon_{in} \cdot \left(\frac{F_{out}}{F_{in}}\right) \cdot \left(\frac{T_{out}}{T_{in}}\right) \cdot \left(\frac{P_{in}}{P_{out}}\right)}$$ $$= \left(\frac{F_{in}}{\upsilon_{in}}\right) \cdot \left(\frac{F_{CO_2(g),out}}{F_{out}}\right) \cdot \left(\frac{T_{in}}{T_{out}}\right) \cdot \left(\frac{P_{out}}{P_{in}}\right)$$	3.12
$$y_{CO_2(g),out} = \frac{F_{CO_2(g),out}}{F_{out}}$$	3.13
$$T_{in} = T_{out} \text{ and } P_{in} = P_{out}$$	3.14
$$C_{CO_2(g),out} = C_{in} \cdot y_{CO_2(g),out}$$	3.15

(Cont. of Table 3.1)

$C_{CO_2(g)}$[in gas phase control volume] $= C_{CO_2(g),out}$ (CSTR assumption)	3.16
$F_{in} \cdot y_{CO_2(g),in} - F_{out} \cdot y_{CO_2(g),out} - r_{absorption} = C_{in} \cdot V_g \cdot \dfrac{dy_{CO_2(g),out}}{dt}$	3.17
$y_{CO_2(g),out} = \dfrac{F_{CO_2(g),out}}{F_{CO_2(g),out} + F_{N_2(g),out}} \Rightarrow F_{CO_2(g),out}$ $= F_{N_2(g),out} \cdot \left(\dfrac{y_{CO_2(g),out}}{1 - y_{CO_2(g),out}} \right)$	3.18
$F_{out} = F_{CO_2(g),out} + F_{N_2(g),out} = F_{N_2(g),out} \cdot \left(\dfrac{1}{1 - y_{CO_2(g),out}} \right)$	3.19
$F_{N_2(g),in} = F_{N_2(g),out}$	3.20
$r_{absorption} = F_{in} \cdot y_{CO_2(g),in} - F_{N_2,in} \cdot \left(\dfrac{y_{CO_2(g),out}}{1 - y_{CO_2(g),out}} \right) - C_{in} \cdot V_g \cdot \dfrac{dy_{CO_2(g),out}}{dt}$	3.21
Total CO_2 capture capacity (mol) $= \displaystyle\int_0^{t_s} r_{absorption} \cdot dt$	3.22

Thanks to this rate equation that obtained as a result of all the steps and given in the table as Equation-3.21, the CO_2 capture rate by the amine solution sent to the system can be calculated, and the total amount of CO_2 captured can be found by integrating this equation with respect to time (Equation-3.22). With these two equations, the CO_2 capture rate and capacity were easily calculated.

3.4. Electrochemical Cell Design

The design of the electrochemical cell, the mechanical details of which are given in Figure 3.3, is a complex field where many detailed considerations must be taken into account, such as the end-plate flow field depth, depth, type and location of fluid entry and exit into the flow pool, type of flow channels, thickness and placement of electrodes, how

to make an external electrical connection to the electrodes, how to attach the electrodes to the end plates, how to fix the membrane to the cell, what type of seals to use in the electrochemical cell, the design of the gaskets, the locations and types of fittings, placement and dimensions of bolts, etc. Considering these factors, a plausible mechanical design was made by us using the SOLIDWORKS program. The designed cell was manufactured with the help of a CNC milling machine using Teflon and tested for repeatability in sealing and cell assembling.
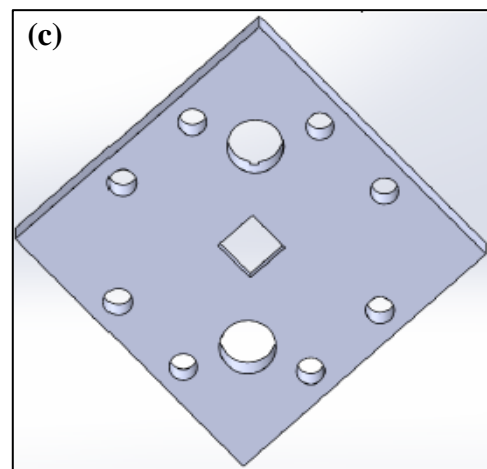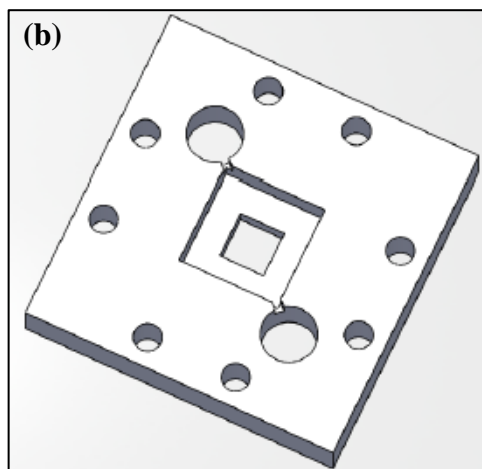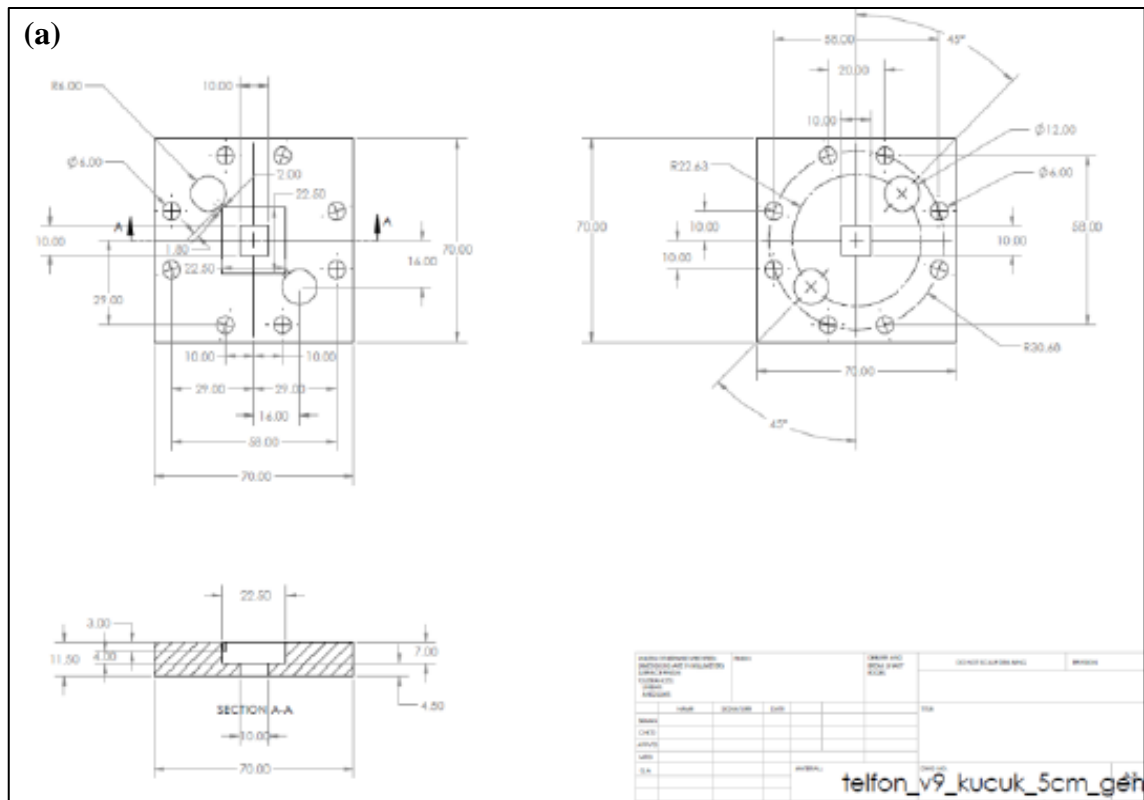
Figure 3. 3. Designed electrochemical cell (end plate part), (a) Technical drawing of the design, (b) perspective from the inside of the 3D model of the design for

which technical drawing is given (the center grove is the location where the copper plate will be placed), (c) perspective from the outside of the 3D model of the design whose technical drawing is given (this is the side where the fittings will be installed and the electrical connection to the copper plate will be done).

The manufactured electrochemical cell and components of electrochemical cell are shown in Figure 3.4.a. As seen in the figure, electrochemical cell, Teflon end plates containing flow field (pool); silicone gaskets; flow channels (baffles) made of silicone gasket; bolts and washers; ¼" NPT fittings; POM pipes attached to fittings with double ferrules (front and back); stoppers suitable for fittings (for use when needed); square copper plates with an area of 5 cm^2 with a copper wire soldered on one side; and an appropriate anion exchange membrane (AEM, bright yellow component in the middle of the figure). Figure 3.4.b. shows the assembled form of the cell components.
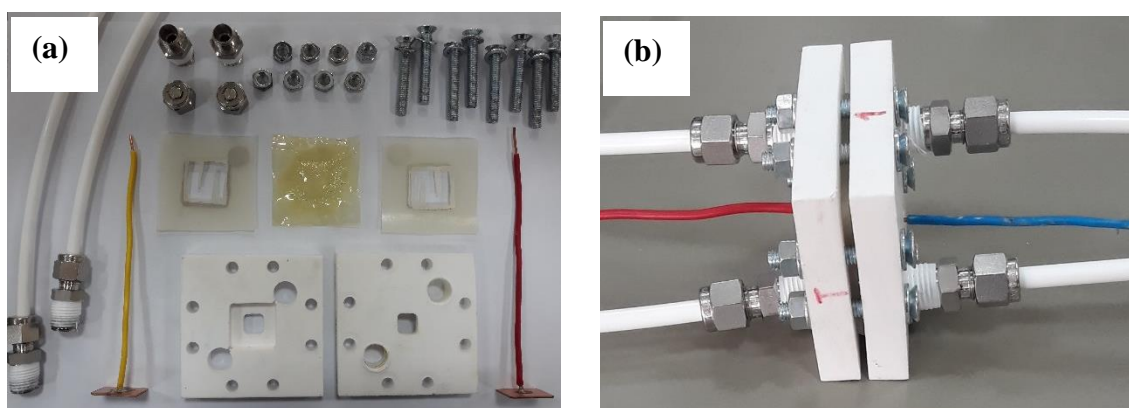
Figure 3. 4. Electrochemical cell, (a) open state of components, (b) the assembled state of the electrochemical cell.

The purity of the copper plates is 99.9% according to the information received from the seller. For the cleaning of copper plates, the copper plate was first polished with sandpaper and then kept in 0.1M HNO$_3$ for at least 10 minutes to remove any chemical contaminants. After this process, copper plate was washed with de-ionized water and dried. The copper plates were seated in the grooves inside the Teflon end plates using a silicone-based liquid sealant.

3.5. Activation of Anion Exchange Membrane (AEM)

The membrane to be used in the electrochemical cell must be activated before it can be used. Fumasep FAA-3-50 membrane from Fumatech was used as anion exchange membrane (AEM). This membrane is supplied in Br^- form and covered on one side with a protective PET layer. In order for the electrochemical cell to complete the electrochemical circuit, the membrane must be in the form of the dominant anion used on both sides of the cell. The dominant anion is the anion of the supporting electrolyte used on the anode and cathode side. For example, if NaCl is used as the supporting electrolyte, the AEM must be converted to the Cl^- form; if $NaNO_3$ is used as the supporting electrolyte, the AEM must be converted to the NO_3^- form. In order to learn how to convert the membrane into Cl^- and NO_3^- forms, the membrane manufacturer company Fumatech was contacted directly (phone and email), and a membrane activation protocol was prepared with the information obtained from these interviews. According to this protocol, when the membrane is desired to be formed to its Cl^- form, first the PET layer is removed and the membrane is kept in 0.5M NaCl solution in a closed container covered with aluminum foil for 24 hours. Then, the membrane is placed in 1.5M NaCl solution to convert it to Cl^- form for 48-72 hours. When it is desired to convert it to NO_3^- form, the membrane is placed in 1.5M $NaNO_3$ solution for 48-72 hours. The membrane is then washed with de-ionized water and placed inside the electrochemical cell without waiting for it to dry.

3.6. Preparation of Electrochemical Cell Test Setup

In preliminary studies of the electrochemical cell, a setup was designed to verify the completion of the electrochemical circuit in the cell as shown in Figure 3.5. An aqueous solution containing a Cu(II) source and supporting electrolyte was added to the anode compartment of the cell and the compartment was closed with plugs. A solution containing CO_2-absorbed amine, Cu source and supporting electrolyte was pumped between the cathode compartment and a beaker.
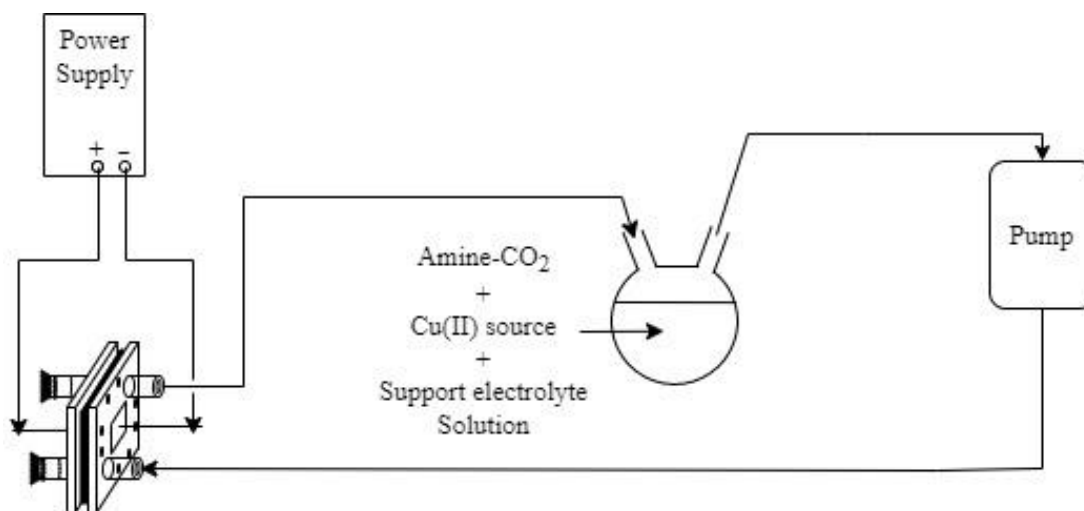
Figure 3. 5. Schematic representation of designed experimental setup to test the completion of the electrochemical circuit.

3.7. UV-Vis Spectrometer Analysis

UV-Vis spectroscopy measurements of the inlet and outlet solutions of the electrochemical cell were made to understand the behavior of the cell and to examine the course of the reactions taking place in the cell. A Perkin Elmer Lambda 25 UV-Vis Spectrometer was used for the measurements. Measurements were made using a quartz cuvette in the 190-1000 nm range. De-ionized water was used as a reference. If needed, dilutions of solutions were made using de-ionized water.

3.8. Obtaining Calibration Curves of Solutions for UV-Vis Spectroscopy Measurements

In order to interpret the absorbance plots obtained by UV-Vis spectroscopy measurements, calibration curves were prepared with respect to the copper concentration (dissolved $CuCl_2$) of the anode and cathode solutions prepared using MEA and HPZ. Thus, the concentration of copper ions dissolved at the anode, the concentration of copper ions deposited at the cathode and the Faradaic efficiency of these processes could be calculated. For this purpose, solutions were prepared in which amine-CO_2 and NaCl concentrations for the anode, and amine and NaCl concentrations for the cathode remained constant, and the concentrations of $CuCl_2$ for both anode and cathode increased gradually, and UV-Vis measurements of the prepared solutions were carried out. In

addition, while these solutions were being prepared, qualitative information about solubility of $CuCl_2$ in amine and amine-CO_2 solutions was obtained as given in Appendix A.

Based on the UV-Vis measurements performed, the absorbance values at the peak points were collected and the calibration curves according to the Cu concentration were obtained. Using the calibration curves, the equations giving the relationship between the absorbance values and $CuCl_2$ concentration values were derived. Thanks to these equations and Faraday's law, the Faraday efficiency of the electrochemical cell was calculated for each experiment. Below is an example of how to calculate the calibration curve for 1M MEA.

- The solution that enters the anode compartment of the cell contains amine-CO_2 complex and NaCl. Since this solution dissolves Cu ions upon entry to the anode and contains amine-Cu complex at the anode exit, a series of solutions for UV-Vis analysis is prepared: 1M MEA-CO_2+1M NaCl, 1M MEA-CO_2+1M NaCl+0.025M $CuCl_2$, 1M MEA-CO_2+1M NaCl+0.05M $CuCl_2$, 1M MEA-CO_2+1M NaCl+0.075M $CuCl_2$, 1M MEA-CO_2+1M NaCl+0.1M $CuCl_2$ and 1M MEA-CO_2+1M NaCl+0.125M $CuCl_2$. UV analyzes could not be performed for solutions containing 0.1M and 0.125M Cu $CuCl_2$ were blurry indicating a possible oversaturation. UV-Vis curves of the other solutions are given in Figure 3.6.
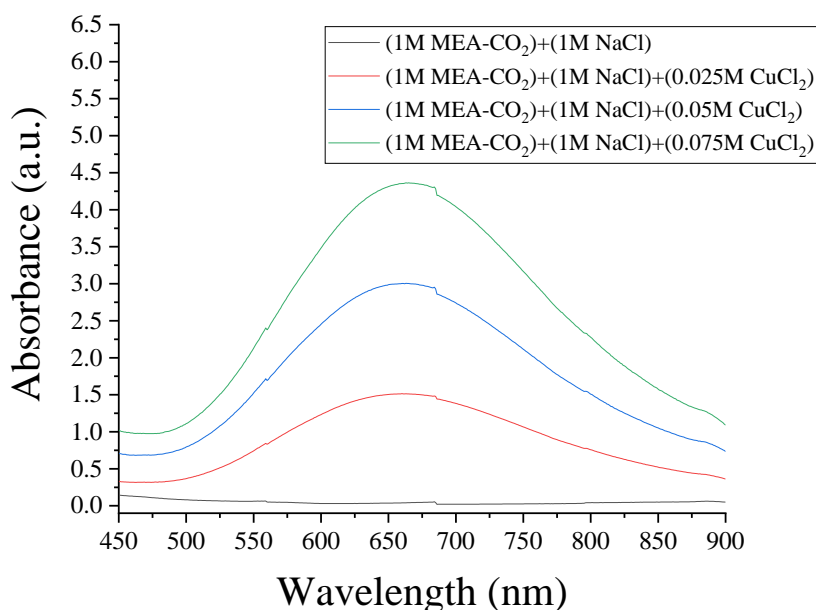
Figure 3. 6. UV-Vis spectroscopy measurements of the solutions prepared for the CuCl2 calibration curve of the anode solution containing 1M MEA.

- The wavelength at which these solutions gave their peaks was found to be ca. 663 nm and the absorbance values at this wavelength were read as 0.0408, 1.5136, 3.0051 and 4.3628, respectively. Then, the calibration curve was drawn according to the $CuCl_2$ concentrations and the maximum absorbance values. Using this curve whose equation is given in Figure 3.7, the concentration of Cu ions in the samples collected from the anode compartment of the cell was calculated.
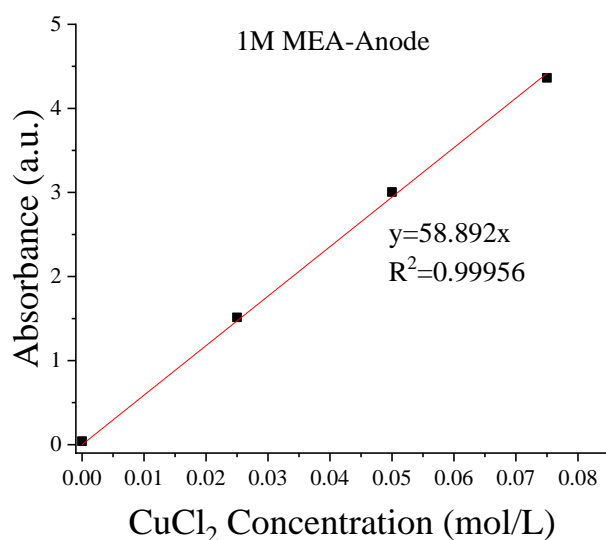
Figure 3. 7. Calibration curve of anode solution for 1M MEA.

- The same procedure was repeated for the solution to be used in the cathode compartment of the cell. Unlike the anode compartment, an amine-Cu complex will enter the cathode compartment instead of an amine-CO_2 complex. Therefore, to obtain a calibration curve, the following solutions were prepared: 1M MEA+1M NaCl, 1M MEA+1M NaCl+0.025M $CuCl_2$, 1M MEA+1M NaCl+0.05M $CuCl_2$, 1M MEA+1M NaCl+0.075M $CuCl_2$, 1M MEA+1M NaCl+0.1M $CuCl_2$, 1M MEA+1M NaCl+0.125M $CuCl_2$ and 1M MEA+1M NaCl+0.15M $CuCl_2$. As in the anode solution, UV-Vis measurements were made and absorbance values were read at the peak wavelength (600 nm). The calibration curve and its equation is given in Figure 3.8.
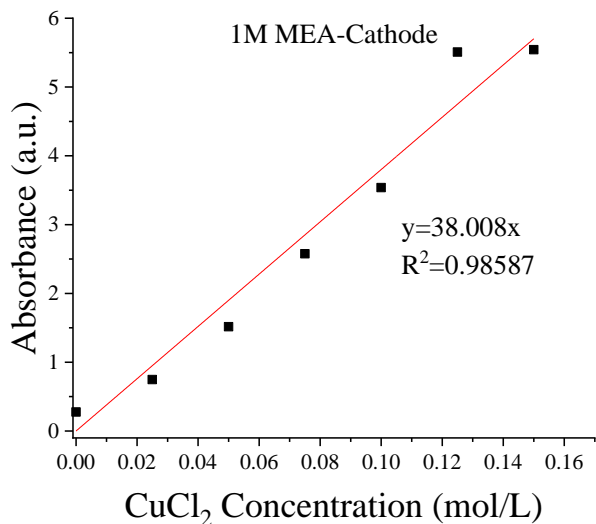
Figure 3. 8. Calibration curve of the cathode solution for 1M MEA.

Similar to the example described above, calibration curves for anode and cathode solutions were obtained for the solutions using 0.1M MEA, 0.1M HPZ and 1M HPZ. The detailed calculations are given in Appendix B. All of the obtained calibration curves are shown in Figure 3.9.
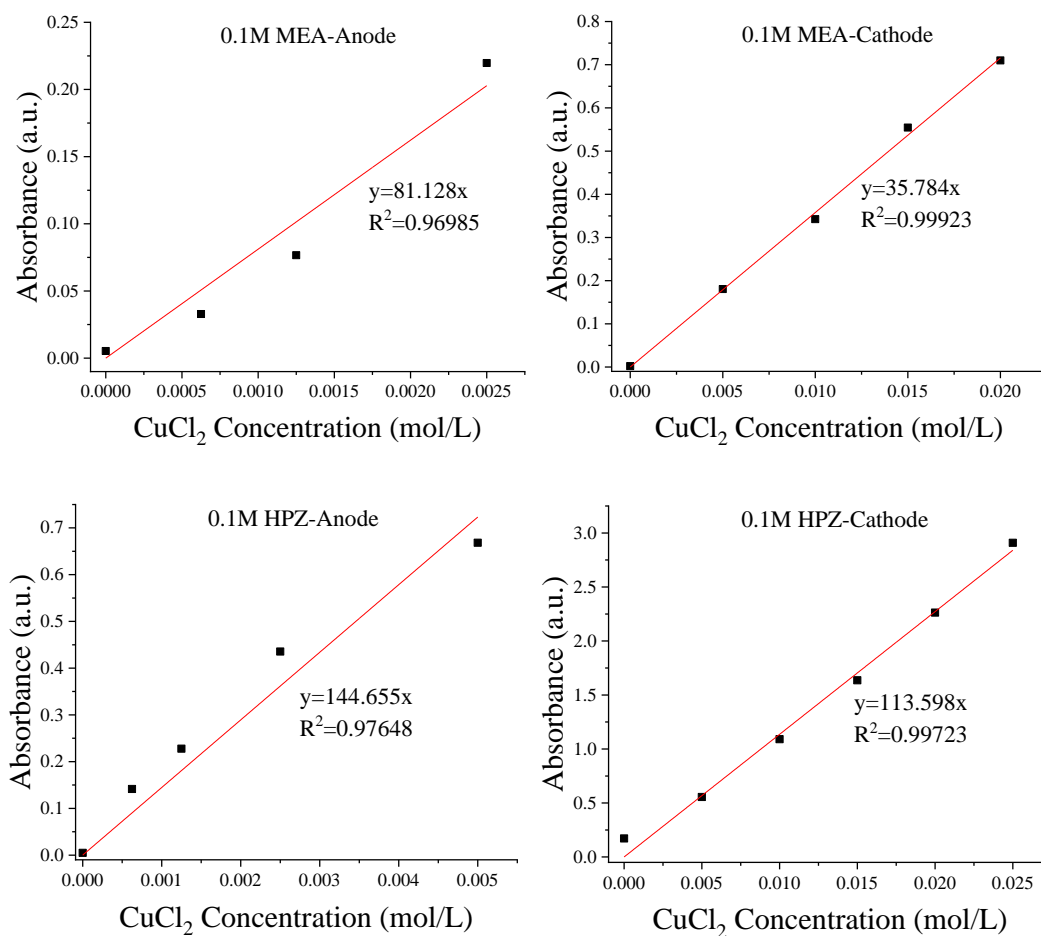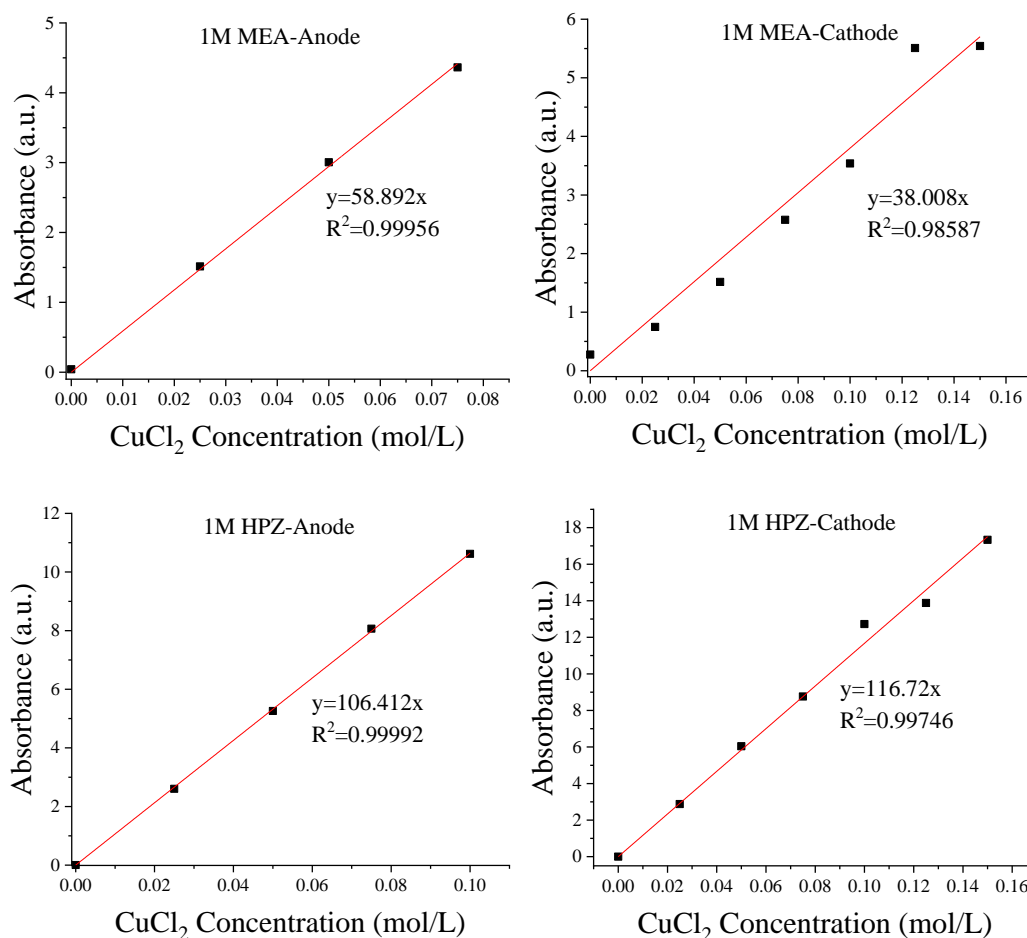
Figure 3. 9. CuCl$_2$ calibration curves of 0.1M MEA, 0.1M HPZ, 1M MEA and 1M HPZ
solutions, from top to bottom, respectively. The left plots are for the anode,
the right plots are for the cathode.

3.9. Continuous Cycle and Single-Pass Electrochemical Cell Experiments

The UV-Vis spectroscopy to be applied to the anode and cathode solutions to examine the reactions taking place in the anode and cathode compartments of the cell has been described above. With the UV-Vis spectroscopy technique, the increasing Cu concentration with the dissolution of Cu plate in the anode compartment of the cell is expected to increase the absorbance value of the solution in the visible region. At the cathode, it is expected that the Cu ions contained in the cathode solution will deposit onto the copper plate, thereby reducing the absorbance value of the solution. Two kinds of experiments were conducted to observe the changes in absorbance values. These two tests differ according to the way the samples were collected.

In the first kind of the experiments schematically shown in Figure 3.10, two separate solutions were prepared for the anode and the cathode compartments. The solution prepared for the anode compartment was sent to the anode compartment of the cell and collected again in the beaker containing the solution. The anode solution was circulated between the anode compartment and the beaker with the help of a peristaltic pump. Likewise, the solution prepared for the cathode compartment was circulated between the cathode compartment of the cell and the beaker containing the cathode solution using another peristaltic pump. Due to the continuous recirculation, this first experiment was called the continuous cycle electrochemical cell experiment. With continuous cycle cell experiments, it is aimed to understand the cumulative behavior of the cell for a certain duration. The cell was supplied with a current of 0.2A, pump rates were set at 17 mL/min and the experiment was run for 30 minutes. The experiment was carried out under the same conditions for 1M MEA and 1M HPZ. The anode solution contained 1M amine-CO_2 and 1M NaCl; the cathode solution contained 1M amine, 1M NaCl and 0.025M $CuCl_2$. Before the start of the experiment (at the entrance), at the 15th minute and at the end of the experiment (at the 30th minute), three samples were taken from both beakers and UV-Vis spectrometry measurements were performed.
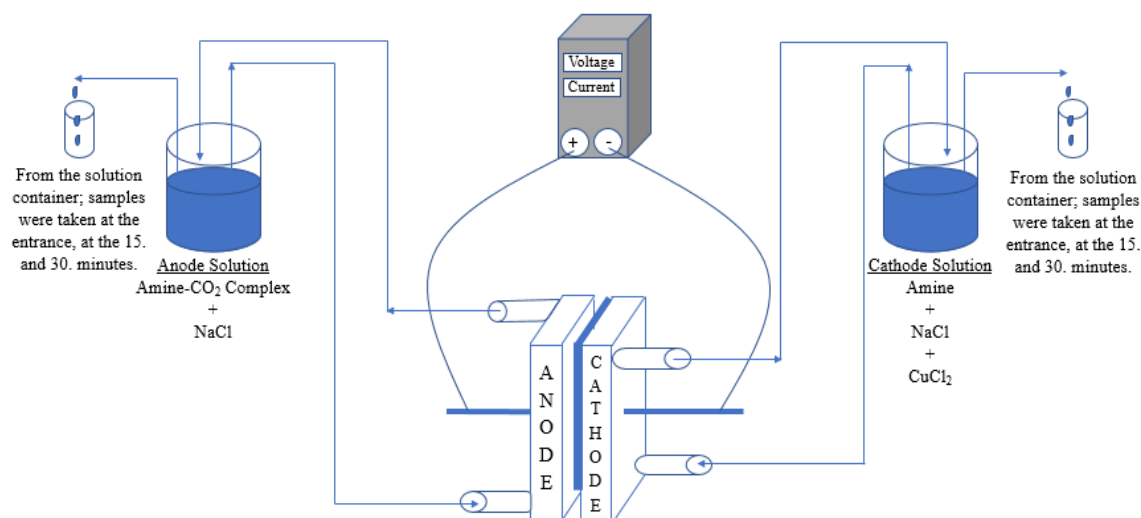
Figure 3. 10. Schematic representation of the continuous cycle electrochemical cell experiments.

Afterwards, in order to better understand a real electrochemical CO_2 capture process, it was decided to conduct experiments in which the solutions were not cycled continuously, instead the solutions passed through the anode and cathode compartments

of the cell in one go, unlike the continuous cycle experiments. The solutions passing through the anode and cathode compartments of the cell were collected at certain intervals and UV-Vis spectroscopy measurements were performed. Due to one pass of solutions from the cell compartments, these experiments were called the single-pass cell experiments. As can be seen in Figure 3.11, the solutions coming out of the anode and cathode compartments were at once collected directly into sample tubes at certain time intervals.
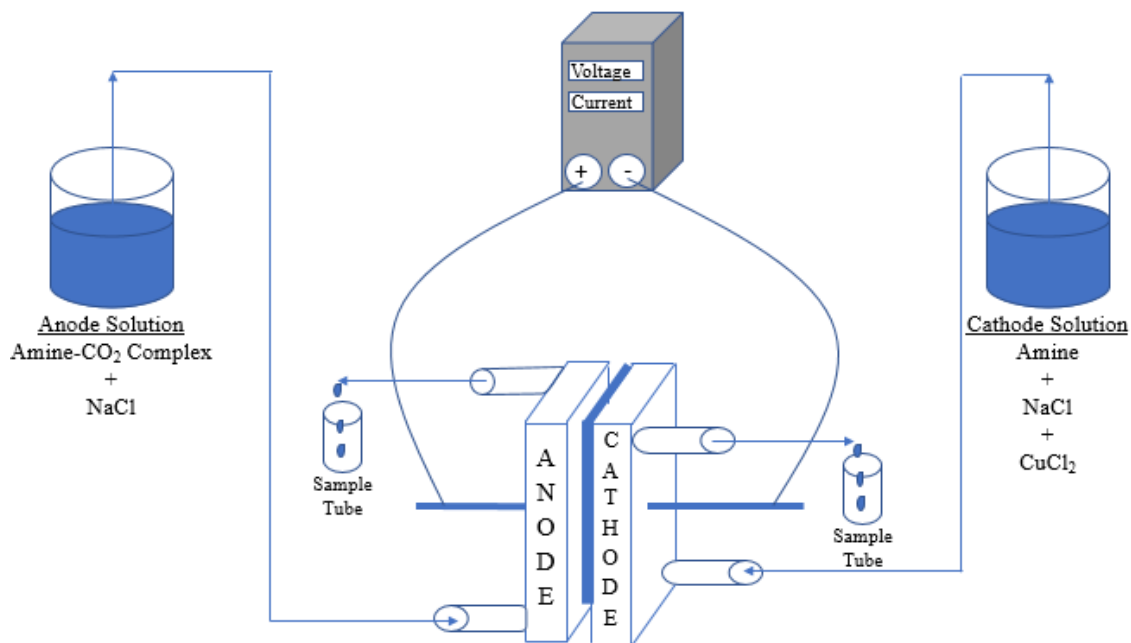
Figure 3. 11. Schematic representation of the single-pass electrochemical cell experiments.

3.10. Compilation of Reactions Used for Faradaic Efficiency Calculation

The general equations of the expected reactions in the electrochemical cell are given in Equation-3.23, Equation-3.24 and Equation-3.25 for the absorption column, the anode compartment of the cell and the cathode compartment of the cell, respectively (Stern et al., 2013). Here, 'Am' given in the reaction equations represents any amine, and 'm' represents the coefficient obtained by dividing the number of amine functional groups contained in the amine used by 2.

$$Am(aq) + mCO_2(g) \leftrightarrow Am(CO_2)_m(aq) \qquad \text{(Equation-3.23)}$$

$$(2/m)Am(CO_2)_m(aq) + Cu(s) \leftrightarrow CuAm_{2/m}^{2+}(aq) + 2CO_2(g) + 2e^- \qquad \text{(Equation-3.24)}$$

$$\text{CuAm}_{2/m}{}^{2+}(aq) + 2e^- \leftrightarrow Cu(s) + (2/m)Am(aq) \qquad \text{(Equation-3.25)}$$
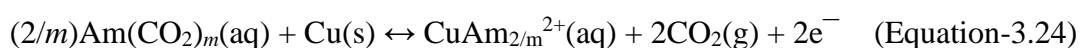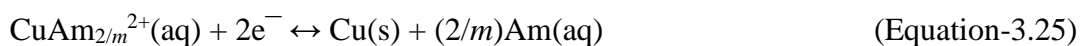
MEA and HPZ were used as amines in the electrochemical cell experiments. The equations of the reactions given above in general form are given below according to these two amines.

The chemical formula of MEA is given in Figure 3.12 and this amine contains 1 amine functional group as seen. Accordingly, the coefficient m is ½ for MEA. The absorption, anode reaction and cathode reaction equations for MEA are given in Equation-3.26, Equation-3.27 and Equation-3.28, respectively.
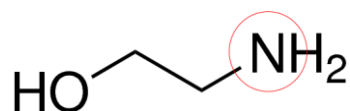
Figure 3. 12. Chemical structure of MEA.

$$\text{MEA}(aq) + (1/2)CO_2(g) \leftrightarrow MEA(CO_2)_{1/2}(aq) \qquad \text{(Equation-3.26)}$$

$$\text{4MEA}(CO_2)_{1/2}(aq) + Cu(s) \leftrightarrow CuMEA_4{}^{2+}(aq) + 2CO_2(g) + 2e^- \qquad \text{(Equation-3.27)}$$

$$\text{CuMEA}_4{}^{2+}(aq) + 2e^- \leftrightarrow Cu(s) + 4MEA(aq) \qquad \text{(Equation-3.28)}$$
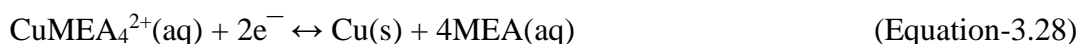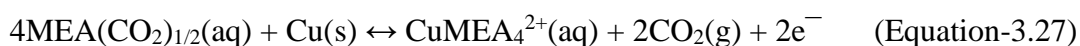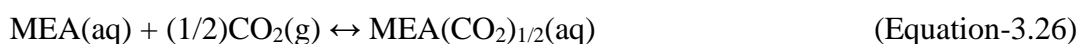
The chemical formula of HPZ is given in Figure 3.13 and HPZ contains 2 amine functional groups. Accordingly, the coefficient m is 1 for HPZ. The absorption, anode reaction and cathode reaction equations for HPZ are given in Equation-3.29, Equation-3.30 and Equation-3.31, respectively.
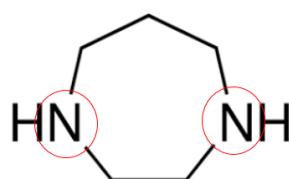
Figure 3. 13. Chemical structure of HPZ.

$$\text{HPZ}(aq) + CO_2(g) \leftrightarrow HPZ(CO_2)(aq) \qquad \text{(Equation-3.29)}$$

$$\text{2HPZ}(CO_2)(aq) + Cu(s) \leftrightarrow Cu(HPZ)_2{}^{2+}(aq) + 2CO_2(g) + 2e^- \qquad \text{(Equation-3.30)}$$

$$\text{Cu}(HPZ)_2{}^{2+}(aq) + 2e^- \leftrightarrow Cu(s) + 2HPZ(aq) \qquad \text{(Equation-3.31)}$$
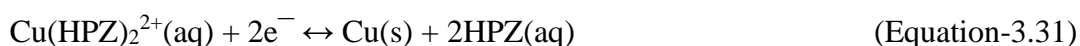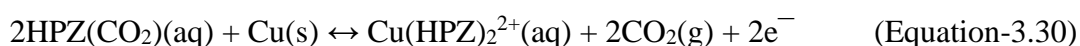
3.11. Measuring the Released Flow Rate of CO_2 at the Anode

The schematic representation of the designed experimental setup to measure the release rate of CO_2 at the anode of the electrochemical cell and the photo of the prepared setup are given in Figure 3.14. Faradaic efficiency calculations were made by considering this experimental setup and the reactions given above.
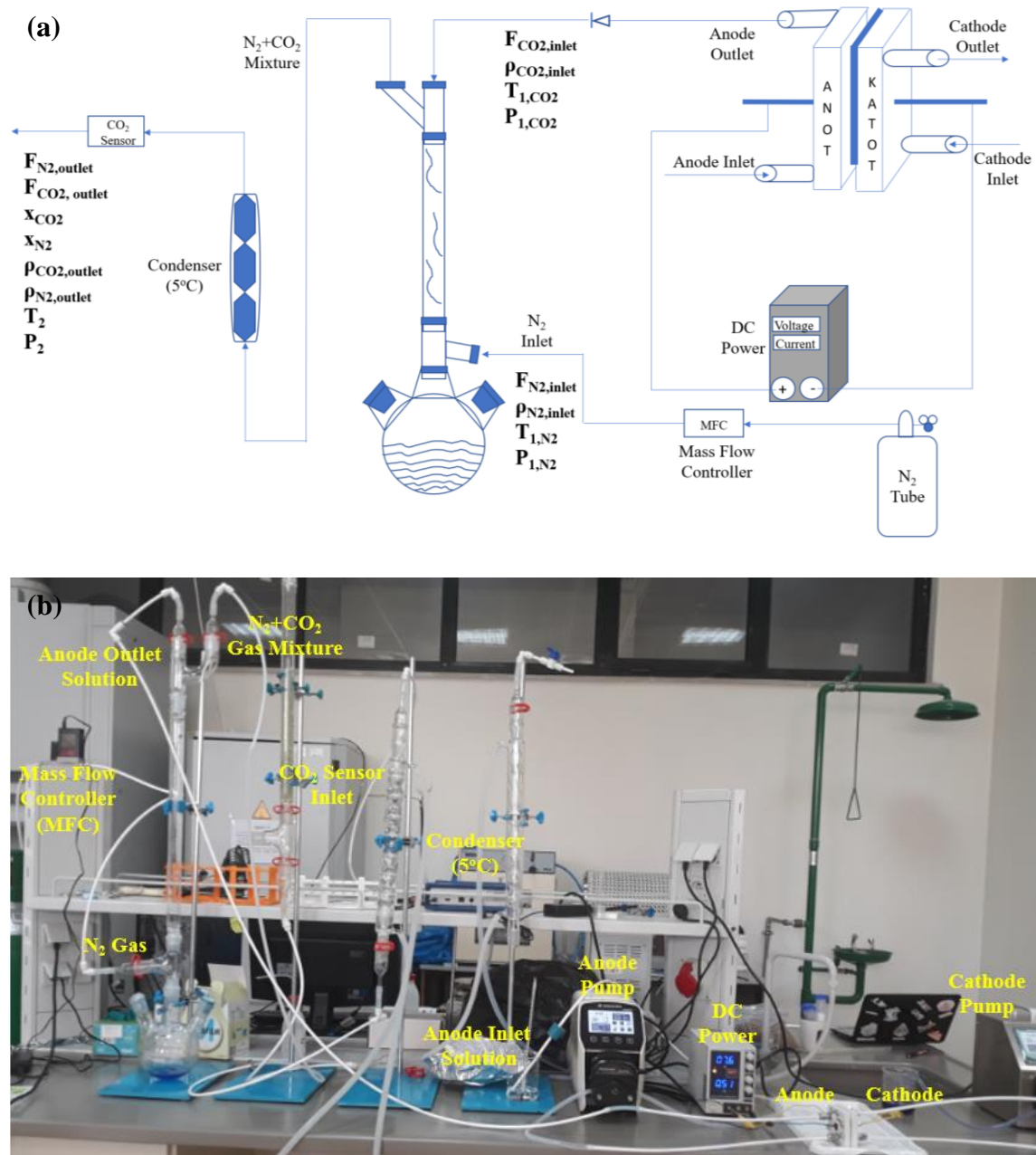
Figure 3. 14. Experimental setup to measure the release flow rate of CO_2 gas, (a) schematic representation, (b) photo of the prepared setup.

In this experiment, N_2 gas was used as the sweep gas. Pure N_2 gas was fed to the system with the help of MFC with a volumetric flow rate of 200 mL/min. The mixture exiting the anode compartment which was presumed to contain amine-CO_2 complex, amine-Cu complex and gaseous CO_2 was sent from the top of the column. The CO_2 gas in this mixture was swept towards the CO_2 sensor with the help of N_2 gas, and the CO_2 concentration was measured in ppm unit in the sensor. In order to prevent the amine vapor from damaging the sensor, the gas mixture was passed through a condenser column before the sensor. A coolant was circulated at $5^{\circ}C$ in the jacket of the condenser. The liquid part of the mixture coming from the anode compartment was collected in a tightly sealed 3-necked glass container (balloon) to prevent gas escape. All connections were carefully made for a complete gas tightness in the setup. In the cathode compartment of the cell, the cathode solution is prepared in accordance with the anode and contains the same amount of amine, the same amount of NaCl and a certain amount of copper salt. The prepared cathode solution was passed through the cathode with a peristaltic pump during the experiment to complete the electrochemical circuit.

In order to calculate the CO_2 flow rate, the mass balance equations derived in the designed experimental setup were used. Figure 3.14.a shows the parameters that need to be measured and calculated. Densities of N_2 and CO_2 gases were taken from NIST Chemistry WebBook database at the measured temperature and pressure values (web3). N_2 inlet pressure was measured with the help of MFC. N_2 inlet and anode outlet pressures were considered equal, and the sensor outlet pressure was accepted as atmospheric pressure. N_2 inlet temperature was also measured with MFC, and sensor outlet temperature was measured with a thermocouple connected to the sensor. The anode outlet temperature was assumed to be equal to the anode inlet temperature, and the temperature of the anode inlet solution was measured with a thermometer immersed in the solution. The derivation of the equations used to calculate the CO_2 flow rate is given in Table 3.2. The release rate of CO_2 gas can be calculated using Equation-3.50. $F_{CO2, \text{ inlet}}$, $F_{CO2, \text{ outlet}}$, $F_{N2, \text{ inlet}}$ and $F_{N2, \text{ outlet}}$ given in the equations are the inlet and outlet volumetric flow rates (mL/min) of CO_2 and N_2 gases, respectively; $\rho_{CO2,inlet}$, $\rho_{CO2,outlet}$, $\rho_{N2,inlet}$ and $\rho_{N2,outlet}$ are the density of CO_2 and N_2 gases at the inlet and outlet (g/mL), respectively; x_{CO2} and x_{N2} are the mole fractions of CO_2 and N_2 gases at the outlet, respectively; $P_{1,CO2}$, $P_{1,N2}$ and P_2 are respectively the pressure of CO_2 and N_2 gas at the inlet, and the pressure of the gas mixture at the outlet (bar); $T_{1,CO2}$, $T_{1,N2}$ and T_2 represent the temperature of the CO_2 and

N_2 gas at the inlet, and the total temperature (K) of the gas mixture at the outlet, respectively.

<p align="center">Table 3. 2. Derivation of the equations to calculate the CO_2 flow rate</p>

$F_{CO2,inlet} \cdot \rho_{CO2,inlet} + F_{N2,inlet} \cdot \rho_{N2,inlet} = F_{CO2,outlet} \cdot \rho_{CO2,outlet} + F_{N2,outlet} \cdot \rho_{N2,outlet}$	3.32
$F_{CO2,inlet} \cdot \rho_{CO2,inlet} + F_{N2,inlet} \cdot \rho_{N2,inlet} = F_{Total,outlet} \cdot x_{CO2} \cdot \rho_{CO2,outlet} + F_{Total,outlet} \cdot x_{N2} \cdot \rho_{N2,outlet}$	3.33
$x_{N2} = 1 - x_{CO2}$	3.34
$F_{CO2,inlet} \cdot \rho_{CO2,inlet} + F_{N2,inlet} \cdot \rho_{N2,inlet} = F_{Total,outlet} \cdot x_{CO2} \cdot \rho_{CO2,outlet} + F_{Total,outlet} \cdot (1 - x_{CO2}) \cdot \rho_{N2,outlet}$	3.35
$F_{Total,outlet} = F_{CO2,outlet} + F_{N2,outlet}$	3.36
$F_{CO2,inlet} \neq F_{CO2,outlet} \qquad \text{and} \qquad n_{CO2,inlet} = n_{CO2,outlet}$	3.37
$P_{1,CO2} \cdot F_{CO2,inlet} = n_{CO2,inlet} \cdot R \cdot T_{1,CO2}$	3.38
$P_2 \cdot F_{CO2,outlet} = n_{CO2,outlet} \cdot R \cdot T_2$	3.39
$F_{CO2,inlet} \cdot P_{1,CO2} \cdot T_2 = F_{CO2,outlet} \cdot P_2 \cdot T_{1,CO2}$	3.40
$F_{CO2,outlet} = (F_{CO2,inlet} \cdot P_{1,CO2} \cdot T_2)/(P_2 \cdot T_{1,CO2})$	3.41
$a = (P_{1,CO2} \cdot T_2)/(P_2 \cdot T_{1,CO2})$	3.42
$\mathbf{F_{CO2,outlet} = a \cdot F_{CO2,inlet}}$	3.43
$F_{N2,inlet} \neq F_{N2,outlet} \qquad \text{and} \qquad n_{N2,inlet} = n_{N2,outlet}$	3.44
$P_{1,N2} \cdot F_{N2,inlet} = n_{N2,inlet} \cdot R \cdot T_{1,N2}$	3.45
$P_2 \cdot F_{N2,outlet} = n_{N2,outlet} \cdot R \cdot T_2$	3.46
$F_{N2,inlet} \cdot P_{1,N2} \cdot T_2 = F_{N2,outlet} \cdot P_2 \cdot T_{1,N2}$	3.47
$F_{N2,outlet} = (F_{N2,inlet} \cdot P_{1,N2} \cdot T_2)/(P_2 \cdot T_{1,N2})$	3.48
$F_{CO2,inlet} \cdot \rho_{CO2,inlet} + F_{N2,inlet} \cdot \rho_{N2,inlet} = a \cdot F_{CO2,inlet} \cdot x_{CO2} \cdot \rho_{CO2,outlet} + F_{N2,outlet} \cdot x_{CO2} \cdot \rho_{CO2,outlet} + a \cdot F_{CO2,inlet} \cdot (1 - x_{CO2}) \cdot \rho_{N2,inlet} + F_{N2,outlet} \cdot (1 - x_{CO2}) \cdot \rho_{N2,outlet}$	3.49
$\mathbf{F_{CO2,inlet} \cdot [\rho_{CO2,inlet} - a \cdot x_{CO2} \cdot \rho_{CO2,outlet} - a \cdot (1 - x_{CO2}) \cdot \rho_{N2,outlet}] = F_{N2,outlet} \cdot x_{CO2} \cdot \rho_{CO2,outlet} + F_{N2,outlet} \cdot (1 - x_{CO2}) \cdot \rho_{N2,outlet} - F_{N2,inlet} \cdot \rho_{N2,inlet}}$	3.50

In order to a better understanding of the experiments and calculations, the CO_2 release experiment performed at 0.5A current using 1M MEA and the calculations of this experiment are explained in detail below:

- In order to prepare the solution to be sent to the anode compartment of the electrochemical cell, first 1M MEA solution was allowed to reach the saturation by absorbing CO_2. At the end of the absorption process, a 300 mL anode solution containing 1M MEA-CO_2 complex (obtained from absorption) and 1M NaCl was prepared. For the cathode compartment, a 300 mL solution containing 1M MEA, 1M NaCl and 0.025M $CuCl_2$ was prepared. Solutions were sent to both compartments of the cell separately with the help of peristaltic pumps operating at a flowrate of 8.5 mL/min. After making sure that the solutions entered the compartments, the power supply current value was adjusted to 0.5A. The CO_2 sensor was calibrated to read a CO_2 value '0 ppm' at the beginning of the experiment. As soon as the current was turned on, the time on the sensor (current start time) was recorded. The plot of the CO_2 values read during the experiment period, including the opening and closing times of the flow, is shown in Figure 3.15. As expected, the amount of CO_2 first increased and then almost stabilized at the point where the current and voltage values reached stability. When the solutions were consumed, the power supply was turned off and the reading time was recorded. In this experiment, current was applied to the cell for 2030 seconds.
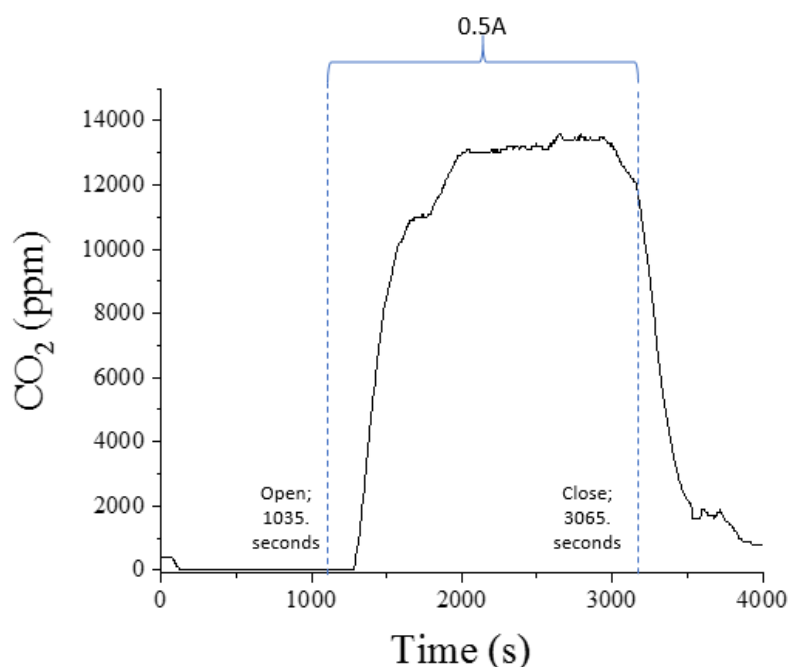
Figure 3. 15. Plot of CO_2 concentration versus time obtained from the CO_2 sensor in the 1M MEA-0.5A experiment.

- The parameters measured during the experiment were:

  $F_{N2,inlet}$=200mL/min, $T_{1,N2}$=294.36K, $P_{1,N2}$=1.06bar, $\rho_{N2,inlet}$=0.0012136g/mL

  $T_{1,CO2}$=291.15K, $P_{1,CO2}$=1.06bar, $\rho_{CO2,inlet}$=0.0019382g/mL

  T_2=292.15K, P_2=1.06bar, $\rho_{N2,outlet}$=0.0012228g/mL, $\rho_{CO2,outlet}$=0.001931g/mL

  $F_{N2,outlet}$ was calculated using Equation-3.48 in Table 3.2 as follows;

  $F_{N2,outlet}$=$(F_{N2,inlet}.P_{1,N2}.T_2)/(P_2.T_{1,N2})$

  $F_{N2,outlet}$=[(200mL/min).(1/60s).(1.06bar).(292.15K)]/[(1.013bar).(294.36K)]

  $F_{N2,outlet}$=3.461mL/s

  The relationship between $F_{CO2,inlet}$ and $F_{CO2,outlet}$ was found by using Equations-3.41, 3.42 and 3.43 from the equations in Table 3.2 as follows;

  $F_{CO2,outlet}$=$(F_{CO2,inlet}.P_{1,CO2}.T_2)/(P_2.T_{1,CO2})$

  $F_{CO2,outlet}$=(1.050).$F_{CO2,inlet}$

- The CO_2 ppm values given in Figure 3.15 represent the x_{CO2} values ($x10^6$), which were the CO_2 mole fraction values in the gas mixture at the outlet measured throughout the experiment duration (2030s). For each x_{CO2} value read during 2030 seconds, the parameters known above, the calculated $F_{N2,outlet}$ value and the found $F_{CO2,inlet}$ and $F_{CO2,outlet}$ relation are written in their place in the Equation-3.50 given in Table 3.2. Thus, the $F_{CO2,\ inlet}$ rates were calculated. Multiplying the $F_{CO2,\ inlet}$ values by 1.050, the CO_2 release flow rate versus time plot shown in Figure 3.16 was obtained.
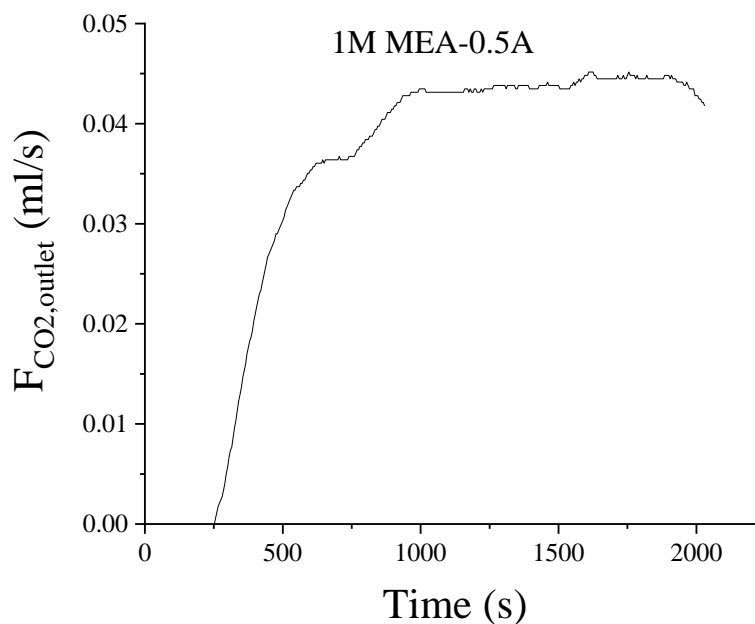
Figure 3. 16. Plot of $F_{CO2,outlet}$ (mL/s) versus time for 1M MEA-0.5A experiment.

- In order to calculate the Faradaic efficiency according to the CO_2 release of the reaction taking place at the anode, the number of moles of CO_2 released at the outlet must be calculated. To calculate the number of moles of CO_2 released at the anode, the data in the $F_{CO2,outlet}$ (mL/s)-time plot (Figure 3.16) were multiplied by $\rho_{CO2,outlet}$ and divided by the molecular weight of CO_2. Then, the resulting mole flow rate (mol/s)-time plot was integrated over time with the help of OriginPro 2019b program and the amount of CO_2 release was calculated in moles. According to the integrated plot in Figure 3.17, the outlet value of n_{CO2} was calculated as 0.0030 mol. This calculated value is the amount of CO_2 released at the anode experimentally.
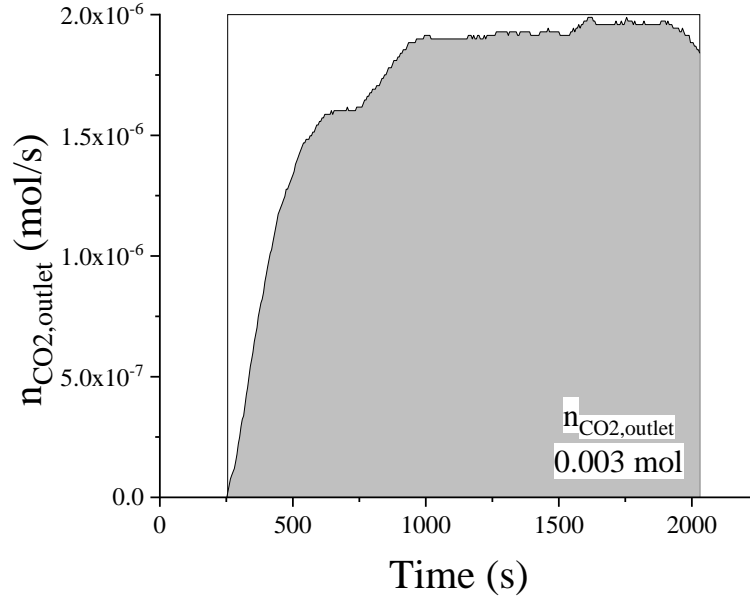
Figure 3. 17. Calculation of the mole amount of CO_2 at the outlet.

The amount of CO_2 that the electrochemical cell should have desorbed was calculated using the Faraday's law. This calculated value is the theoretical amount of CO_2 released. For the calculation of Faradaic efficiency, the amount of electrons required to desorb one mole of CO_2 was taken into account, starting from the reaction equation given as Equation-3.27 above. According to the reaction equation, 1 mol of e- is required for 1 mol of CO_2 release. In this case, the Faradaic efficiency of CO_2 emissions for 1M MEA at 0.5A was found to be 28.57% as follows:

$$n_{CO2} = \frac{I.t}{n.F} \qquad \text{(Faraday's Law) (Equation-3.51.a)}$$

The n_{CO2} given in the Equation-3.51.a is the amount of CO_2 released in moles, I is the current in Amperes, t is the time in seconds, n is the amount of electrons required to release one CO_2 molecule (dimensionless), F is the Faraday's constant (96485 A.s.mol^{-1}).

$$n_{CO2} = \frac{I.t}{n.F} = \frac{(0.5A).(2030s)}{1.(96485A.\frac{s}{mol})}$$

$$= 0.0105 \text{ mol (amount of } CO_2 \text{ that should theoretically be released)}$$

$$\text{Faradaic efficiency\%} = \frac{\text{Experimentally released amount of } CO_2}{\text{amount of } CO_2 \text{ that should theoretically be released}} \times 100$$

$$\text{Faradaic efficiency\%} = \frac{0.003 \text{ mol}}{0.0105 \text{ mol}} \text{x}100 = \%28.57$$

- During the experiment, the power supply was kept constant at 0.5A and the voltage value was recorded continuously. The average voltage value for 1M MEA solution was calculated as 7.95V, and the standard deviation was 0.612V. The amount of energy required for the release of 1 mole of CO_2 was obtained by dividing the energy calculated with multiplication of the average voltage obtained during the experiment, the current held constant throughout the experiment and the experiment time, by the total number of moles of CO_2 released during the experiment. Accordingly, 2354.83 kJ/mol CO_2 was found to be required to release 1 mol of CO_2 in the 1M MEA-0.5A experiment.

CHAPTER 4

RESULTS AND DISCUSSION

4.1. Absorption System of MEA and HPZ Solutions

Amine concentration is an important parameter that affects the CO_2 capture capacity and rate. To observe the effect of this parameter, MEA and HPZ amines were used, and 0.1M and 1M aqueous solutions of these amines were prepared. In this section, CO_2 breakthrough curves were obtained by using 0.1M MEA, 0.1M HPZ, 1M MEA and 1M HPZ solutions as initial concentration with the experimental setup shown in Figure 3.2. Mass balance validation was performed using the equations given in Table 3.1 and it was confirmed that the absorption system was working properly. For the absorption of CO_2, the details were given in Section 3.2. The CO_2-N_2 gas mixture was sent from the bottom of column at a pressure of 1 bar with a flow rate of 250 mL/min. Similar conditions were used for all amine solutions. Absorption was investigated versus time with the help of a CO_2 sensor located at the end of the gas outlet line at the top of the column (after the cooling column). Then, using the equations in Table 3.1, plots of F_{CO2} and absorption values versus time were generated. The total number of moles of CO_2 sent to the absorption system was found by multiplying the F_{CO2} value after the absorption reached equilibrium with the total experiment time. In order for mass balance to hold, the sum of number of moles of CO_2 obtained from the integrals of the CO_2 flow rate versus time plot and CO_2 absorption rate versus time plot given for each amine must be equal to the total number of moles of CO_2 sent to the absorption system.

4.1.1. Breakthrough Curves of MEA and HPZ Solutions

CO_2 capture breakthrough curves were plotted with the data taken from the CO_2 sensor. In the absorption experiments performed with 0.1M amine concentrations given in Figure 4.1.a, zero CO_2 concentration was not recorded at the outlet at the beginning of

the absorption experiment. A possible reason might be low amine concentration which could not absorb all CO_2 sent to the absorption column. While evaluating the breakthrough curves of the experiments done using 0.1M, the point where the absorption started was accepted as the point with lowest value recorded in the sensor. In the 1M amine solution trials, the CO_2 was completely captured and the zero value was recorded at the beginning of the absorption experiment. After zero value recorded for a certain period of time, the CO_2 concentration at the outlet increased rapidly from the breakthrough point. The experiment was continued until the amine saturation point was reached where amine solution could not capture any more CO_2 and the breakthrough curve is flattened.

In the experiments for which MEA was used, the breakthrough point was obtained faster than HPZ. In the 0.1M amine experiments given in Figure 4.1.a, the breakthrough points were obtained at approximately in 100 seconds for MEA and in 250 seconds for HPZ. The saturation points were obtained at 3000 seconds and 2665 seconds for MEA and HPZ, respectively. In Figure 4.1.b, the breakthrough results for 1M amine experiments are given. Breakthrough points were obtained approximately at 3000 seconds for MEA and 8500 seconds for HPZ. The saturation points at 1M amine concentration were obtained at 17700 seconds and 14000 seconds for MEA and HPZ, respectively. It was observed that the MEA reached the breakthrough point the fastest but the saturation point the latest for both concentrations. At low initial amine concentrations, the breakthrough point and saturation points were obtained earlier for both amine solutions.
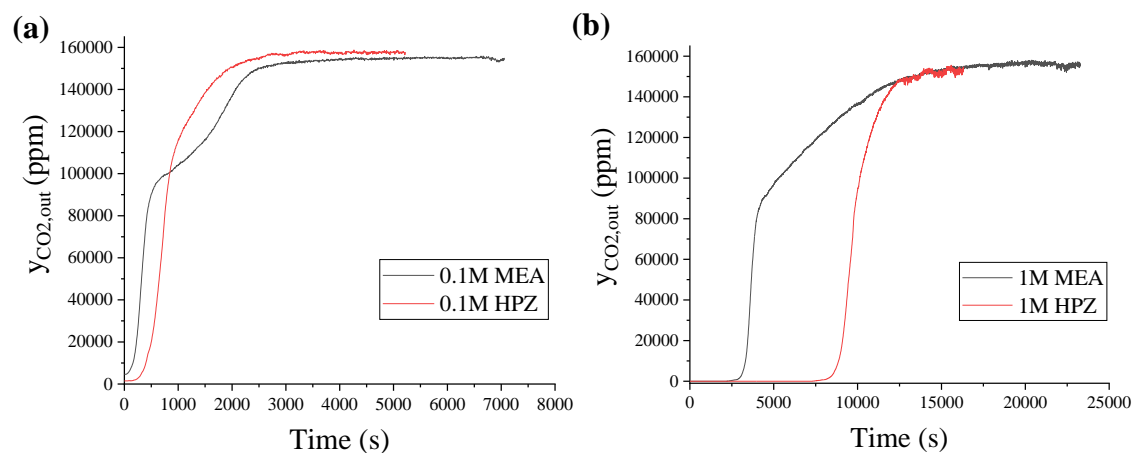
Figure 4. 1. Breakthrough curves for aqueous amine solutions: (a) initial amine concentration of 0.1M, (b) initial amine concentration of 1M.

4.1.2. CO_2 Capture Rates of MEA and HPZ Solutions

The CO_2 capture rate calculations of amines were made according to the rate equation in Equation-3.21 by using the breakthrough curves given in Figure 4.1. The CO_2 capture rates were plotted against time for both 0.1M and 1M amine concentrations as shown in Figure 4.2. It was found that CO_2 capture rate started at the highest rate at the start of the absorption experiments, stayed constant rate for a while, and decreased after a certain point as the saturation point was approached. For 1M amine concentration, a longer constant CO_2 capture period was observed since these solutions have a higher amine concentration than 0.1M amine concentration that enabled them to capture a larger amount of CO_2. It was observed that the constant period is longer for HPZ in both concentrations.
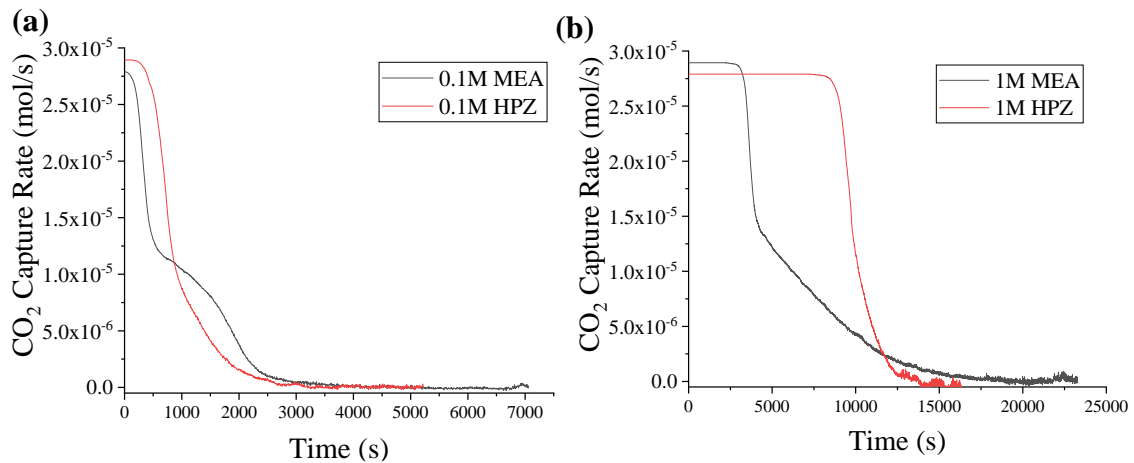
Figure 4. 2. CO_2 capture rate versus time plots, (a) 0.1M amine concentration, (b) 1M amine concentration.

4.1.3. CO_2 Capture Capacities of MEA and HPZ Solutions

The total amount of CO_2 absorbed and unabsorbed by the amines is given in Figure 4.3 0.1M and 1M aqueous MEA and HPZ solutions. The total amount of CO_2 absorbed was calculated based on the integrating the CO_2 capture rate curves against time. The amount of unabsorbed CO_2 was found by calculating the exit rate of the unabsorbed CO_2 gas according to Equation-3.18 and integrating the curve formed against time. The total amount of CO_2 entering the system was obtained by multiplying the value of F_{CO2}, calculated from the ideal gas equation, with the total absorption time. As seen in Figure 4.3, it was found that mass balances of CO_2 were verified to hold well for each case.
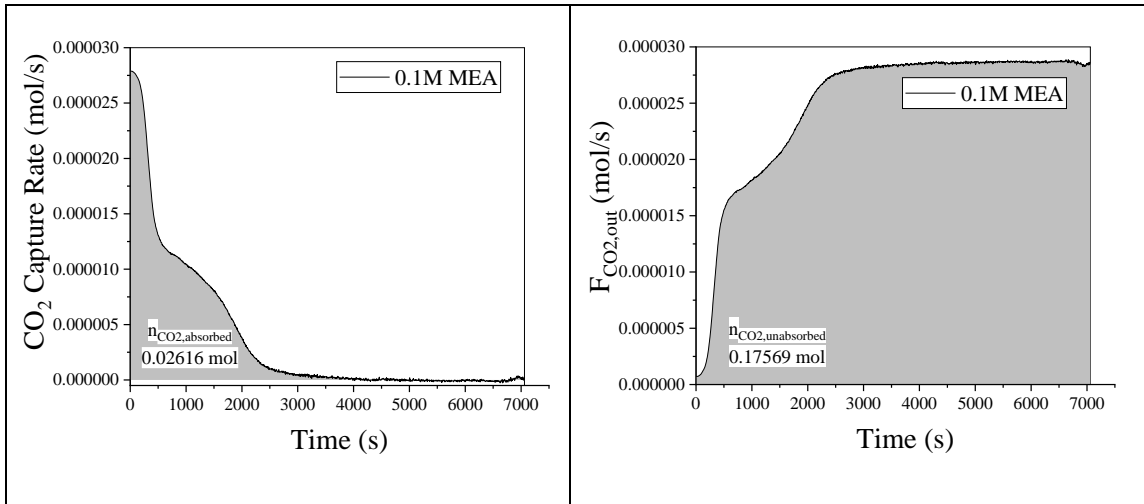
Amount of CO_2 entering = 0.20193 mol

Total amount of absorbed and unabsorbed CO_2 = (0.02616 + 0.17569) mol

0.20193 mol ≈ 0.20185 mol
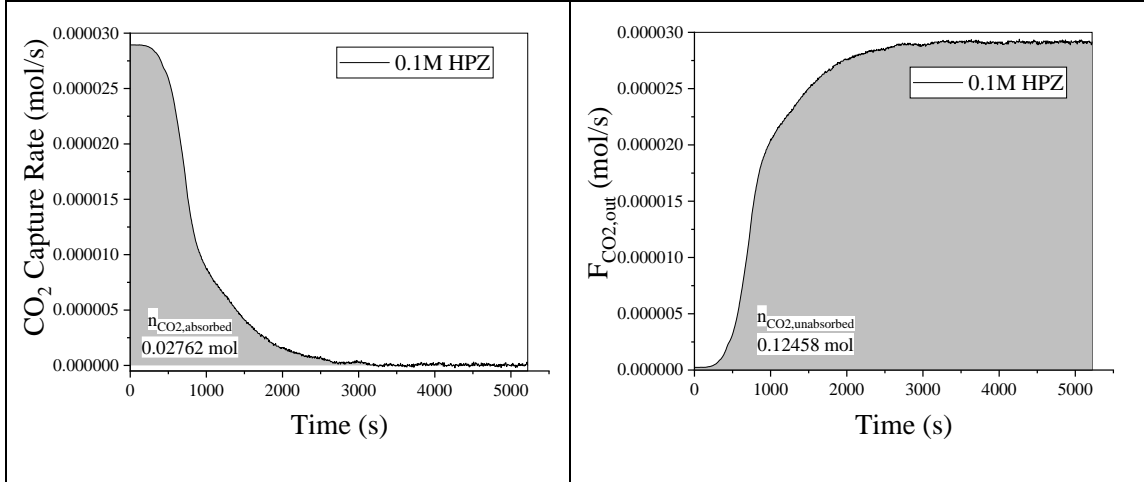
Amount of CO_2 entering = 0.15230 mol

Total amount of absorbed and unabsorbed CO_2 = (0.02762 + 0.12458) mol

0.15230 mol ≈ 0.15220 mol
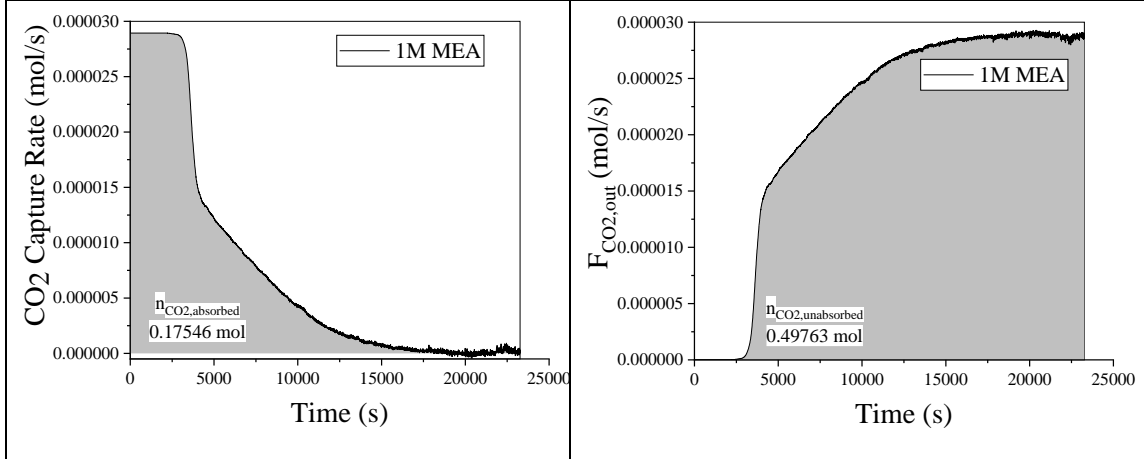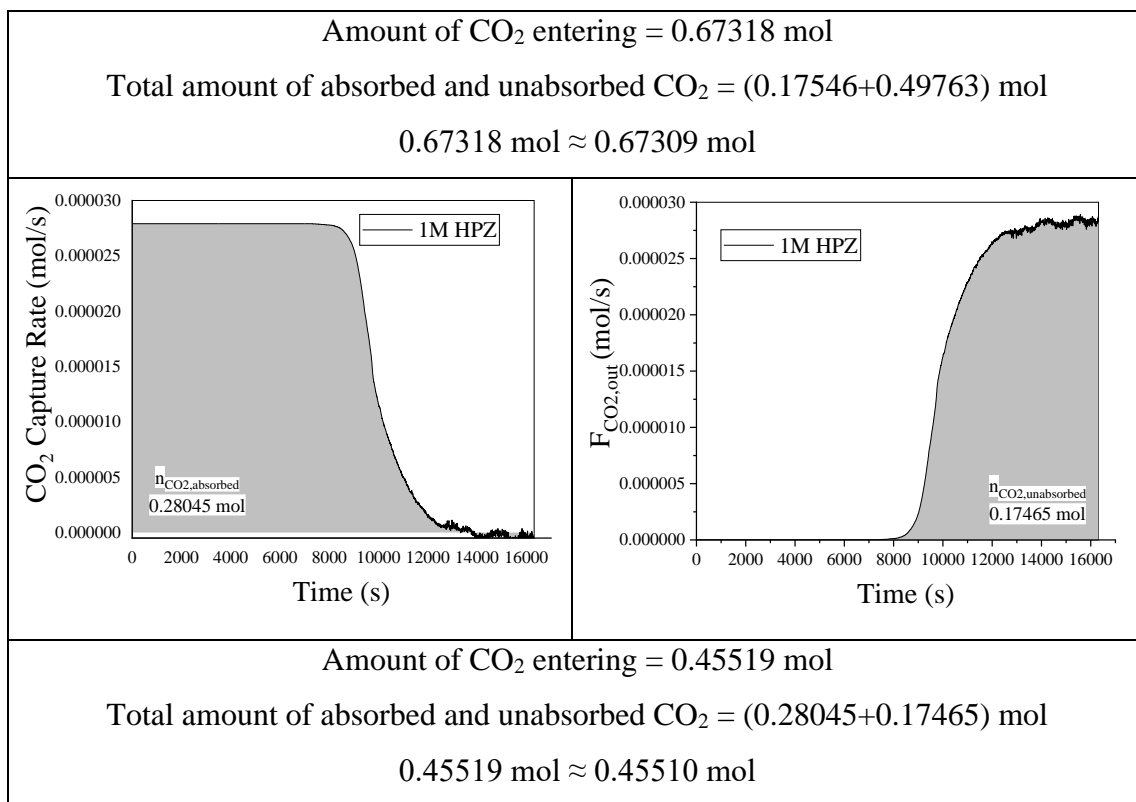
Figure 4. 3. Mass balances of the amount of CO_2 entering and leaving the system in absorption experiments.

The cumulative CO_2 capture capacity was calculated by dividing the absorbed CO_2 molar amounts by the initial amine molar amount (All amine solutions were prepared as 250 mL in the absorption experiments.). The calculated CO_2 capture capacities are shown in Table 4.1. As seen, HPZ is found to have a higher CO_2 capture capacity than MEA for 0.1M and 1M aqueous solutions.

Table 4. 1. CO_2 capture capacity according to concentrations for HPZ and MEA.

	CO_2 Capture Capacity (mol_{CO2}/mol_{amin})	
	0.1M MEA	1.0464
Amine Initial Concentration (mol/L)	0.1M HPZ	1.1048
	1M MEA	0.7018
	1M HPZ	1.1218

4.2. Preliminary Studies for Electrochemical Cell

The electrochemical cell is the core component of an electrochemical CO_2 capture process. In the electrochemical CO_2 capture process, the steps aimed to be realized in the cell are given below:

- CO_2-absorbed amine in the absorption column (CO_2-amine complex) comes to the anode compartment of the cell.
- The CO_2-amine complex coming to the anode reacts with the Cu(II) ions, which are produced by the oxidation of the copper plate (anode electrode), to form Cu(II)-amine complexes. In this way, CO_2 is released (i.e., desorbed).
- Then, the Cu(II)-amine complex formed at the anode compartment is sent to the cathode compartment of the electrochemical cell to regenerate the free amine by reducing Cu(II) ions to elemental copper to be deposited on the copper plate (cathode electrode).
- The free amine is returned to the absorption column for CO_2 re-absorption.

The functioning of an electrochemical circuit depends on the ionic conductivity of the membrane in the electrochemical cell, assuming proper electrolytes and electrodes are used and proper electrical connections are made. Considering the AEM, if the membrane is activated correctly, it will allow the anion with which it is activated to pass between the anode and cathode compartments and complete the circuit. For this purpose, it was tested whether the circuit was completed with a setup to be installed for the electrochemical desorption system. For this test, two AEMs, one in NO_3^- form and one in Cl^- form, were prepared and electrochemical cells were assembled. When AEM in the form of Cl^- was used, an aqueous solution containing 0.1M $Cu(NO_3)_2.3H_2O$ as copper ion source and 1M NaCl as support electrolyte was used at the anode compartment of the electrochemical cell; when AEM in NO_3^- form was used, an aqueous solution containing 0.1M $Cu(NO_3)_2.3H_2O$ as copper ion source and 1M $NaNO_3$ as supporting electrolyte was used at anode compartment of the electrochemical cell. After these solutions were added to the anode compartment of the electrochemical cell, the fittings were plugged. On the cathode compartment, a CO_2-absorbed 1M MEA solution containing 0.04M $Cu(NO_3)_2.3H_2O$ as copper ion source and 1M NaCl as support electrolyte in the case of AEM in the form of Cl^-, and 1M $NaNO_3$ supporting electrolyte in the case of AEM in the form of NO_3^- was used. The solution prepared for the cathode compartment was

pumped into the cathode compartment of the electrochemical cell by means of a peristaltic pump through a 3-neck glass flask and returned to this flask as circulation. The electricity was supplied to the electrochemical cell using a DC power source (UNI-T/UTP3315TFL) (anode: positive terminal, cathode: negative terminal). The photo of the prepared experimental setup, whose schematic diagram is given in Section 3.6, is given in Figure 4.4. In these experiments, the expectation was to measure a current value when a potential is applied to the electrochemical cell and to observe that this current value changes with the change of the potential.
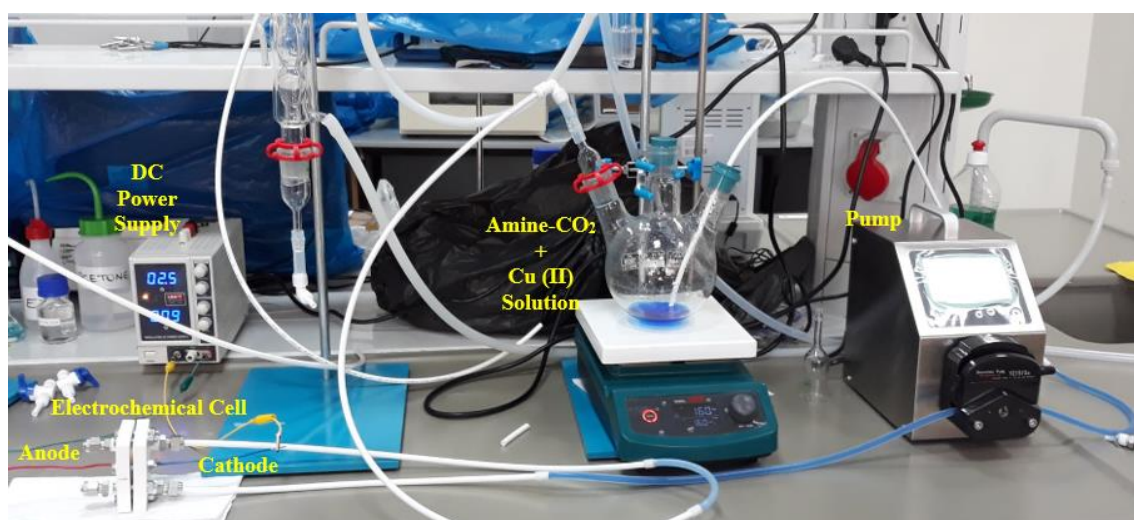
Figure 4. 4. Photo of the experimental setup prepared to test the completion of the electrochemical circuit.

The tests to see if the electrochemical circuit is complete (the Cl^- form and the NO_3^- form) were performed for both AEM forms. As seen in Figure 4.4, a current density of approximately 20 mA/cm^2 was obtained at voltages between 2.5-3V for both AEM forms. At the same time, current increase with potential increase and current decrease with potential decrease were also observed, as expected. This result revealed that AEMs provided the necessary ion transfer and the electrochemical circuit was completed.

The reactions expected to occur in the anode and cathode compartments of the electrochemical cell are the opposite of each other. At the anode, Cu ions are expected to dissolve from the electrode by oxidation and go into the solution, and at the cathode, Cu ions are expected to go from the solution to the electrode and to be deposited on the electrode by reduction. That is, copper dissolution will take place at the anode, and copper deposition will take place at the cathode. According to the reaction taking place at the

anode, the amine-CO_2 complex entering the anode will turn into an amine-Cu complex and release carbon dioxide, since the amine has a higher tendency to complex with Cu than with CO_2. At the cathode, Cu ions in amine-Cu complex will be reduced and the amine will be regenerated. This expected behavior of the copper plates in the cell has been confirmed by long-term experiments. As seen in Figure 4.5, as a result of these reactions, there will be dissolution in the electrode on the anode compartment of the cell and accumulation on the electrode on the cathode compartment.
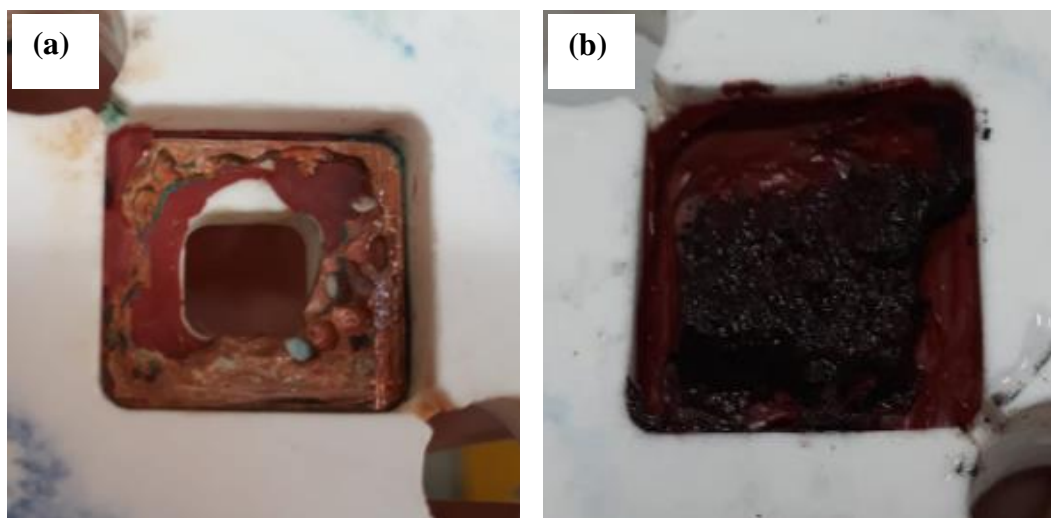
Figure 4. 5. Post-experiment photos of the copper plates used in the electrochemical cell experiments, (a) anode showing copper dissolution, (b) cathode showing copper deposition.

4.3. Basic UV-Vis Spectroscopy Analysis

UV-Vis spectroscopic measurements of anode and cathode solutions were used in order to characterize the electrochemical cell. To verify the UV-Vis spectroscopy measurements, a similar analysis made by Eltayeb was taken as an example (Eltayeb, 2015), and the measurements were compared. For this purpose, UV-Vis spectroscopy analyses of MEA, HPZ, $CuNO_3$, MEA-$CuNO_3$ and HPZ-$CuNO_3$ solutions were performed in the study. Figure 4.6.a is taken from Eltayeb's thesis, while Figure 4.6.b and Figure 4.6.c show the UV-Vis spectroscopy data obtained in our study. As can be seen, EDA, MEA and HPZ did not give peaks. The absorbance profile for Cu were very similar among the data. Looking at the amine-Cu curves, it is noticed that the amount of energy required for the excitation of the complex was close for all amines. The reason why the

absorbance values of the amine-Cu curves are different is due to the fact that the dilution ratio of the sample prepared for UV-Vis spectroscopy measurement was not specified in Eltayeb's thesis and EDA (ethylenediamine) was used as the amine in his experiments.
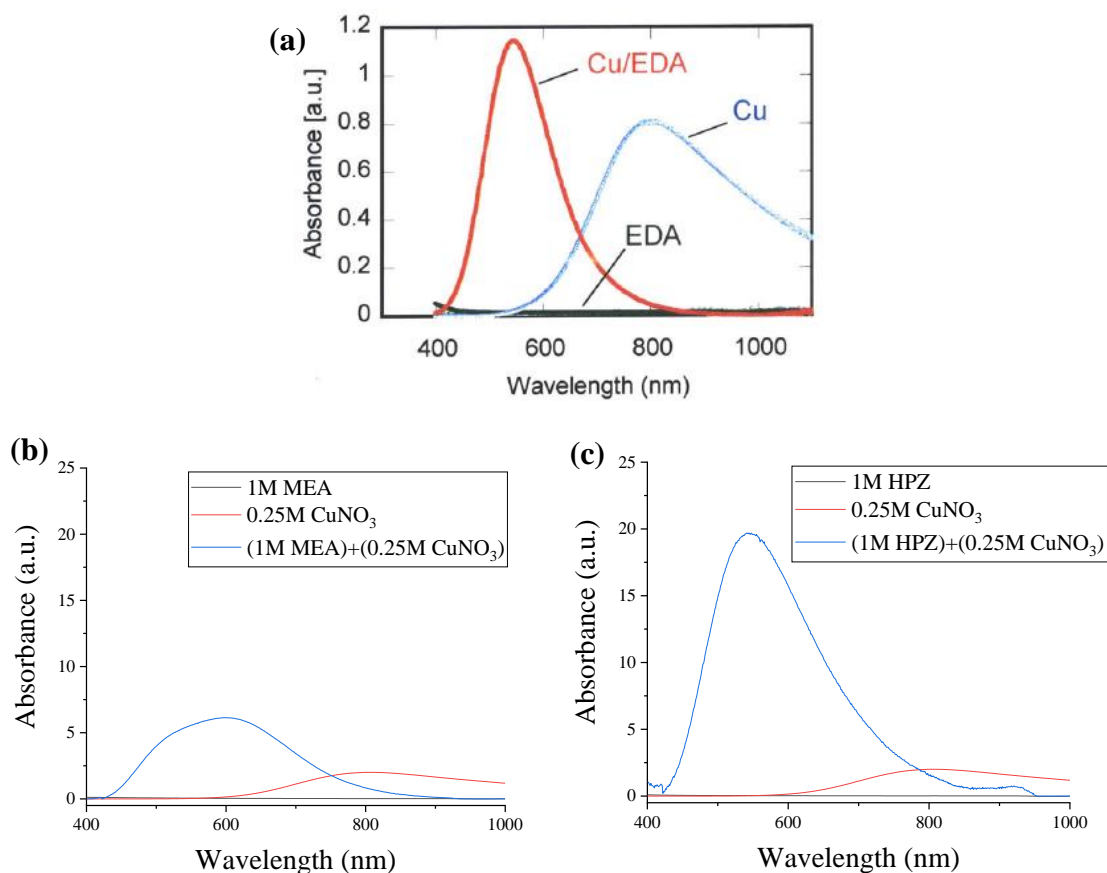
Figure 4. 6. UV-Vis spectra of amine, Cu salt, amine-Cu salt mixtures, (a) Eltayeb's thesis (in this thesis, 0.25M CuNO$_3$ was used as Cu salt) (Eltayeb, 2015), (b) MEA, Cu salt and MEA-Cu salt, (c) HPZ, Cu salt and HPZ-Cu salt.

In order to better analyze the UV-Vis spectroscopy measurements of the samples collected before and after absorption experiments, UV-Vis spectroscopy measurements of amine and amine-CO$_2$ solutions were made. The UV-Vis spectroscopy results are given in Figure 4.7, where the plots on the left show the results between 190-400 nm, the plots on the right show the results between 400-1000 nm. As seen, there were no peaks observed in the visible and part of near IR region for all samples (the plots on the right). The plots on the left (190-400 nm) were discussed below.

UV-Vis spectroscopy is based on the radiation absorbed by electronic transitions in molecules. The electronic transitions vary according to the chemical structure and concentration of the molecules. There are certain chromophores (such as C-C, C-H, C=C,

C=O, etc.) and auxochrome groups (-OH, -NH$_2$, -COOH, etc.) in organic compounds. Chromophore groups generally give absorbance below 300 nm, and auxochrome groups generally below 220 nm (web4). Looking at the amine and amine-CO$_2$ bond structures given in Figure 4.8, it is seen that the MEA and HPZ contains chromophore and auxochrome groups. In accordance, the absorbance values of the chemicals were not more than 250 nm, as shown in Figure 4.7.

When auxochrome groups bind to chromophore groups, auxochrome groups do not give absorbance themselves, but change the wavelength and absorbance value of chromophore groups. The shift of the absorption of the chromophore group to the long wavelength due to the effect of the auxochrome group is called the bathochromic effect (red-shift), and the shift to the short wavelength is called the hypsochromic effect (blue-shift). The decrease in the absorption intensity with the auxochrome effect is called the hypochromic effect, and the increase in the absorption intensity is called the hyperchromic effect (web4). As amines capture CO$_2$, new oxochrome groups (-NH and -COO$^-$) are formed (Figure 4.8). In addition, in the new chemical structure formed, the unbonded electron in the carboxyl group (-COO$^-$) resonates and causes a change in the spectrum (web5). Looking at all plots in Figure 4.7, it can be said that the formation of the new auxochrome group and the resonance effect cause hypsochromic (i.e., blue-shift) and hypochromic (i.e., decrease in absorbance value) effects on the absorption plot of the CO$_2$-captured amine.

68
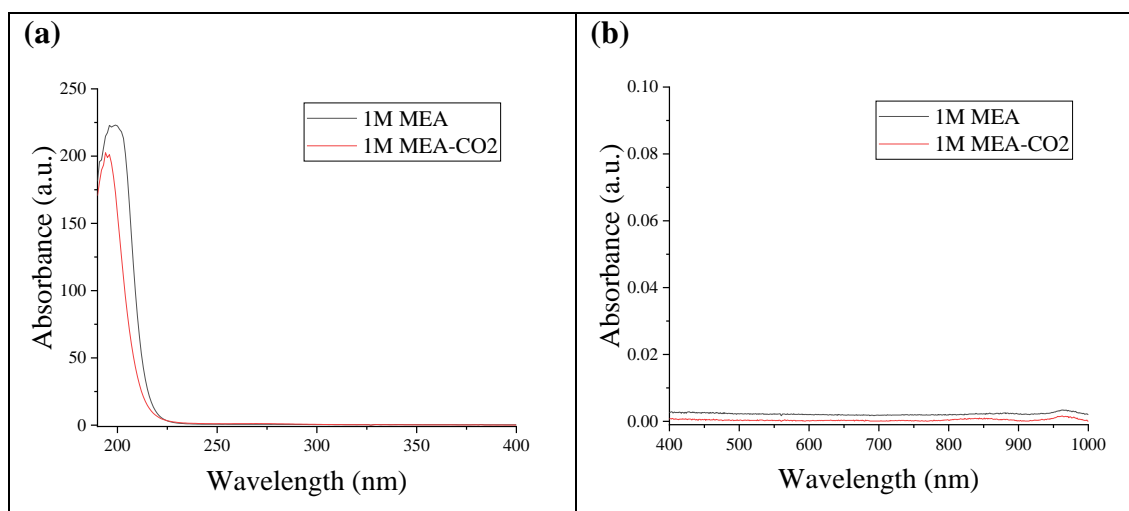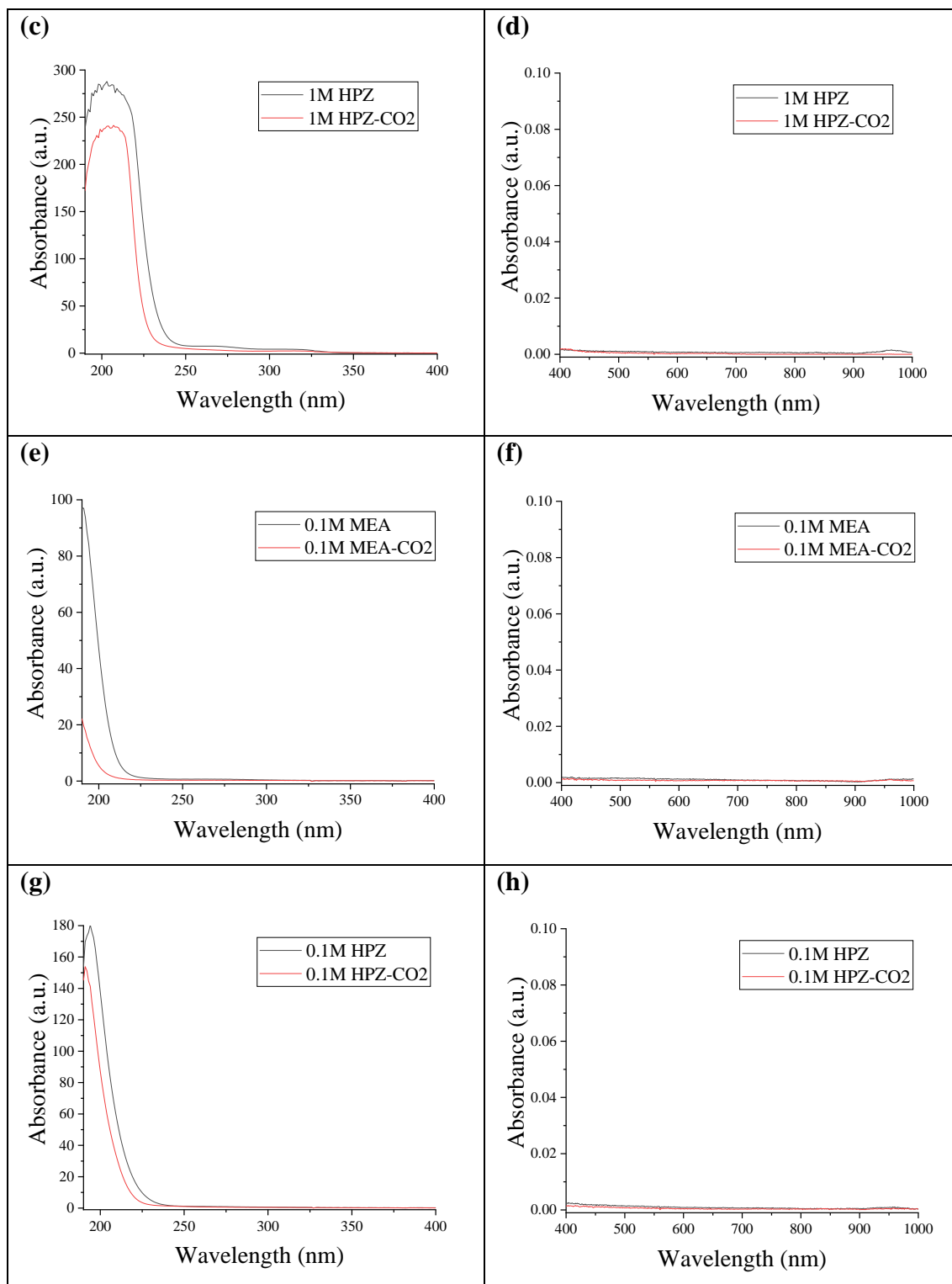
Figure 4. 7. UV-Vis spectrometers of amine and amine-CO_2 solutions, (a) 1M MEA vs. 1M MEA-CO_2, (b) measurements of 1M MEA and 1M MEA-CO_2 in the visible region, (c) 1M HPZ vs. 1M HPZ-CO_2, (d) measurements of 1M HPZ and 1M HPZ-CO_2 in the visible region, (e) 0.1M MEA vs. 0.1M MEA-CO_2, (f) measurements of 0.1M MEA and 0.1M MEA-CO_2 in the visible region,

(g) 0.1M HPZ vs. 0.1M HPZ-CO$_2$, (h) measurements of 0.1M HPZ and 0.1M HPZ-CO$_2$ in the visible region.
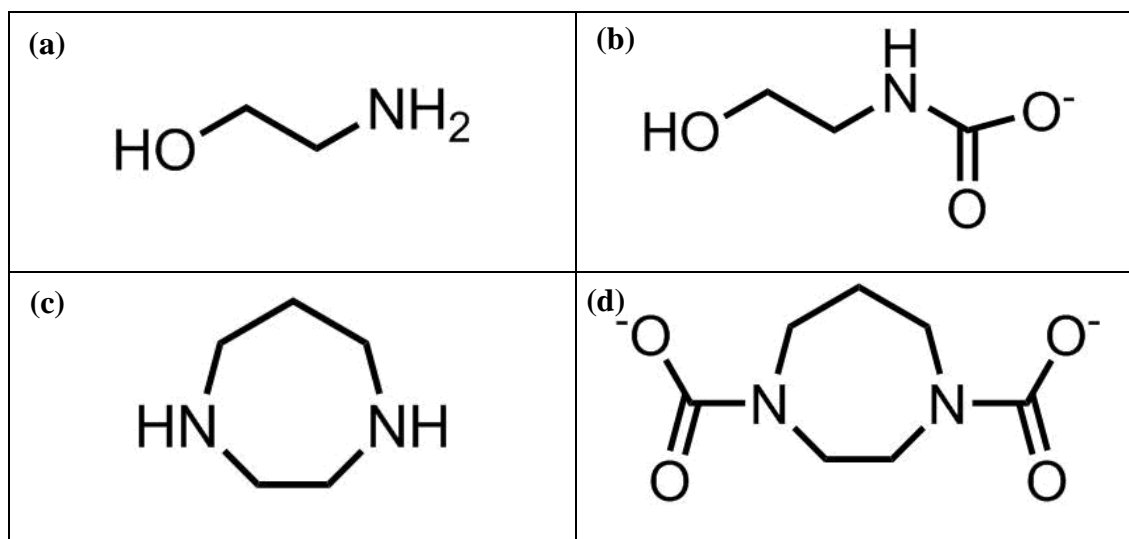
Figure 4. 8. Bond structures, (a) MEA, (b) MEA-CO$_2$, (c) HPZ, (d) HPZ-CO$_2$

Another set of basic UV-Vis spectroscopy measurement were done to understand the effect of the presence of Cu ions. This set of measurements were done for aqueous solutions of Cu salt, and amine-Cu and amine-CO$_2$-Cu solutions. The results are shown in Figure 4.9. Figure 4.9.a shows the measurements for varying concentrations of CuCl$_2$. Looking at Figure 4.9.a, it is found that the peaks were due to CuCl$_2$. Cu is a transition metal and the spectral properties of the transition metals result from electronic transitions between the various energy levels of the 3d and 4d orbitals. At the same time, transition metals show absorption in the visible region and their molar absorptivity is quite high (web6). It is also seen that the absorbance increases depending on the increase in concentration, which is in accordance with Beer-Lambert law.

Figure 4.9.b shows UV-Vis measurements of 1M MEA+0.025M CuCl$_2$, 1M MEA+0.25M CuCl$_2$, 1M MEA-CO$_2$+0.025M CuCl$_2$, 1M MEA-CO$_2$+0.25M CuCl$_2$ mixtures and Figure 4.9.c shows UV-Vis measurements of 1M HPZ+0.025M CuCl$_2$ and 1M HPZ-CO$_2$+0.025M CuCl$_2$ mixtures. These mixtures were prepared based on the interaction between amine-CuCl$_2$ and amine-CO$_2$-CuCl$_2$ (MEA-Cu, MEA-CO$_2$-Cu, HPZ-Cu and HPZ-CO$_2$-Cu) used in the experiments. Looking at Figure 4.9.b and Figure 4.9.c, it is seen that amine-Cu and amine-CO$_2$-Cu interactions showed absorption in the visible region. Unlike Figure 4.8.a, the peak wavelengths in the amine-CO$_2$-containing solution are shifted to longer wavelengths in the visible region with the presence of Cu ions in

solution. Also, the addition of $CuCl_2$ to amine solutions show an absorption profile blue-shifted with respect to $CuCl_2$ solution absorption profile shown in Figure 4.9.a. The solution with higher $CuCl_2$ concentration had higher absorbance values, as expected. When we examine the effect of CO_2 presence for MEA and HPZ solutions in Figure 4.9.b and Figure 4.9.c, the following conclusion can be reached: For MEA shown in Figure 4.9.b, in the case of 0.25M $CuCl_2$, the absorbance value appreciably decreased when a complex was formed with CO_2, while complex formation with CO_2 had a lesser effect on the absorbance value when 0.025M $CuCl_2$ was used. A much less effect on the absorbance value was observed for HPZ in presence of 0.025M $CuCl_2$, i.e., the absorbance values of HPZ and HPZ-CO_2 solutions are very close to each other.
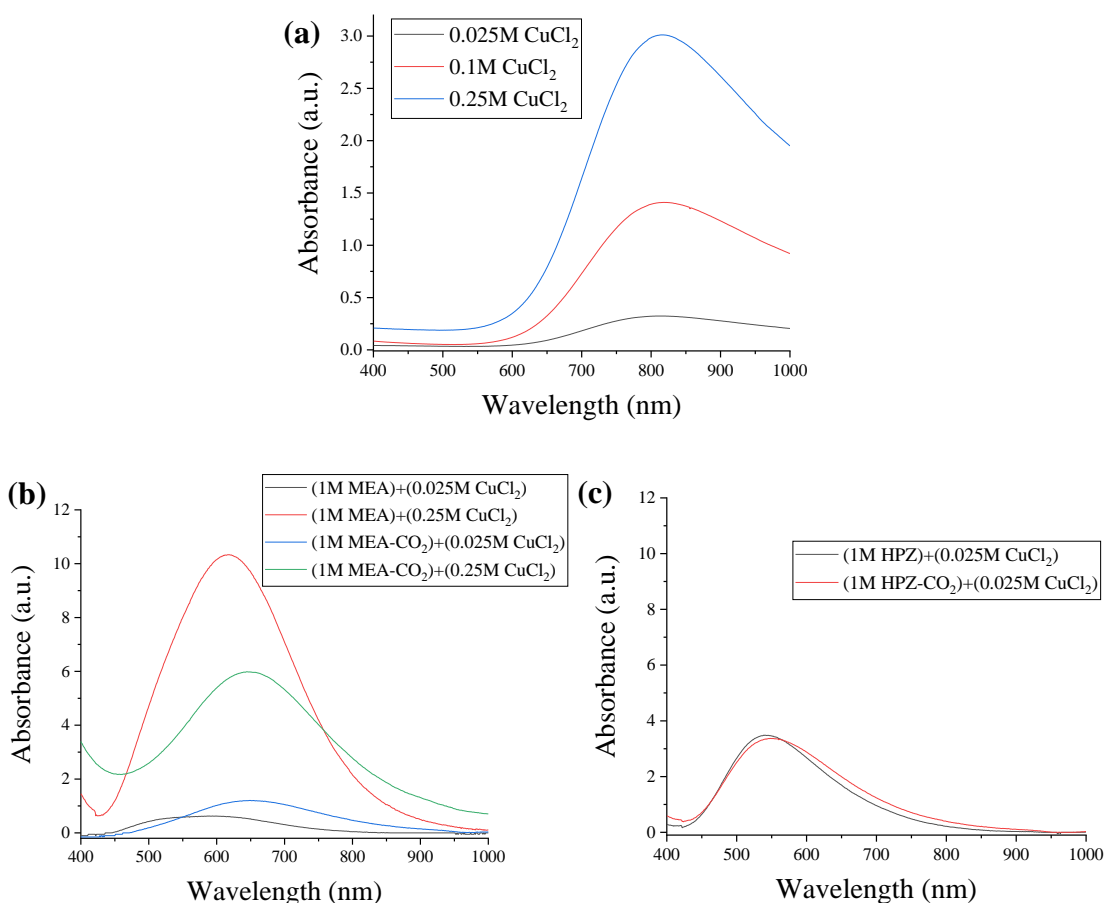
Figure 4. 9. UV-Vis measurements to study, (a) effect of Cu concentration, (b) interactions between Cu and MEA, Cu and MEA-CO_2, (c) interactions between Cu and HPZ, Cu and HPZ-CO_2.

4.4. CO₂ Desorption Studies in Electrochemical Cell

The next important step after absorption in the electrochemical CO_2 capture system is the desorption of CO_2 in the electrochemical cell. Desorption takes place at the anode of the electrochemical cell. In the experiments carried out to understand the desorption step, the prepared solutions were passed through the anode and cathode compartments of the cell, the voltage-current values were measured, and the UV-Vis spectroscopy measurements of the solutions coming out of the anode were evaluated. In order to make the findings easier to understand, in this section, first the UV-Vis spectroscopy results will be examined, and then the voltage-current values will be discussed.

Various parameters were determined to be examines the desorption step in the electrochemical cell, which was designed, manufactured and shown to be able to complete the electrochemical circuit. These parameters are namely anode solution flow rate, copper salt ($CuCl_2$) concentration and salt (NaCl) concentration as support electrolyte, and whether the cathode solution contains CO_2. (According to the designed experimental setup, the amine-CO_2 complex coming from the absorption column will come to the anode compartment of the cell and interact with the copper electrode here and will be sent to the flash column. Here, the amine-Cu complex, which is freed from the CO_2 gas, will be sent to the cathode compartment, where the Cu(II) ions will be reduced and the amine will be regenerated. However, the system may not have an ideal operation and the solution coming out of the anode may not contain only amine-Cu liquid and CO_2 gas. For this reason, the possibility that this solution, which comes out of anode and then returns to the cathode, might contain amin-CO_2 complex is considered as another parameter.) To that end, a total of 8 experiments were carried out in which at least one parameter was changed and MEA was used as the amine, as shown in Table 4.2. For example, according to this table, in the D1 experiment, MEA sent to the cathode compartment was not saturated with CO_2, the support electrolyte salt NaCl concentration was 1M, the copper salt concentration was 0.025M, and the flow rate of the solution sent to the anode compartment of the cell was 8.5 mL/min. The flow rate at the cathode was used as 18.5 mL/min in all experiments.

Table 4. 2. Experiments designed to understand the CO_2 desorption step in the electrochemical cell.

Experiment	Anode Flow Rate		Cathode Solution		NaCl Concentration		CuCl$_2$ Concentration	
	8.5 mL/dk	17 mL/dk	Cathode1 (0% CO$_2$)	Cathode2 (100% CO$_2$)	1M	0.25M	0.025 M	0.25 M
D1	x		x		x		x	
D2		x	x		x		x	
D3	x			x	x		x	
D4		x		x	x		x	
D5		x	x			x	x	
D6		x	x		x			x
D7		x		x	x			x
D8		x	x			x		x

Figure 4.10 shows the UV-Vis spectroscopy measurements of solutions entering the anode with different flow rates. While MEA was used in the cathode solutions of the D1-D2 experiments, MEA-CO$_2$ was used in the cathode solutions of the D3-D4 experiments. In the UV-Vis measurements shown in Figure 4.10.a and Figure 4.10.b, respectively, the rate of the fluid entering the anode in D1 and D3 was 8.5 mL/min, while the anode fluid rate in D2 and D4 experiments was 17 mL/min. The lower the flow rate, the greater the contact time of the solution with the electrode. As the contact time of the solution with the electrode increases, the copper ion concentration increases due to the longer duration of electrochemical dissolution of the copper plate. Increasing copper ion concentration breaks the adduct between MEA-CO$_2$ and causes the release of CO$_2$. Here, the increase in copper ion concentration and the breaking of adduct between MEA-CO$_2$ can be mentioned as two reasons for the increase in absorption at low flow rate (the absorption decreases when MEA forms adduct with CO$_2$, see Figure 4.9.a and Figure 4.9.b). This is valid for both the D1-D2 experiments (Figure 4.10.a) and the D3-D4 experiments (Figure 4.10.b). Another result is that D1 and D3 curves were very close to each other. This indicates that the presence of MEA or MEA-CO$_2$ at the cathode has no effect when the anode flow rate is slow. However, the absorbance values of the D2 and D4 curves, where the anode flow rate is high, are different. The absorbance value in D4 was higher. Here, it can be said that the MEA-CO$_2$ complex at the cathode in the D4

experiment is responsible for this effect. A possible reason for this can be explained as follows. Cu ions form MEA-Cu complexes more readily in a MEA-only environment than in a MEA-CO_2 environment because they do not compete with CO_2. Therefore, Cu ions are more easily reduced to the electrode surface when MEA-CO_2 is present at the cathode because their probability of complexing with MEA decreases due to competition with CO_2. Thus, in the case of MEA-CO_2 at the cathode, the number of Cu ions reduced per unit time increases, and on the other hand, the number of Cl^- ions passing through the membrane to the anode side for charge balancing increases, and therefore the number of Cu ions dissolved at the anode increases. This causes an increase in the absorbance value at the anode.

(a)   **(b)**

Figure 4. 10. UV-Vis spectroscopy measurements of two sets of experiments with different anode flow rates, (a) D1; anode (1M MEA-CO_2+1M NaCl), cathode (1M MEA+1M NaCl+0.025M $CuCl_2$), anode flow rate=8.5 mL/min, D2; anode (1M MEA-CO_2+1M NaCl), cathode (1M MEA+1M NaCl+0.025M $CuCl_2$), anode flow rate=17 mL/min, (b) D3; anode (1M MEA-CO_2+1M NaCl), cathode (1M MEA-CO_2+1M NaCl+0.025M $CuCl_2$), anode flow rate=8.5 mL/min, D4; anode (1M MEA-CO_2+1M NaCl), cathode (1M MEA-CO_2+1M NaCl+0.025M $CuCl_2$), anode flow rate=17 mL/min.

Figure 4.11 shows the UV-Vis measurements of experiments D2-D4 and D6-D7 with different cathode solutions. In the D2 and D6 experiments, the cathode solutions did not contain CO_2, while in the D4 and D7 experiments the cathode solutions were saturated with CO_2. In addition, 0.025M $CuCl_2$ was used at the cathode in the D2-D4 experiments, while 0.25M $CuCl_2$ was used at the cathode in the D6-D7 experiments. In these four

experiments, although the anode fluid was the same, the absorbance values were different. The reason for this is the presence of Cl^- ion, which will ensure the ionic balance and pass from the cathode to the anode via the membrane. It is possible that the presence of $MEA-CO_2$ in Figure 4.11.a facilitated the passage of Cl^- ion to the anode compartment, as mentioned above. In Figure 4.11.b, it is seen that the effect of $MEA-CO_2$ in the cathode decreases as the amount of Cu ion increases.

Figure 4. 11. UV-Vis spectroscopy measurements of two sets of experiments with different cathode solutions, (a) D2; anode (1M $MEA-CO_2$+1M NaCl), cathode (1M MEA+1M NaCl+0.025M $CuCl_2$), anode flow rate=17 mL/min, D4; anode (1M $MEA-CO_2$+1M NaCl), cathode (1M $MEA-CO_2$+1M NaCl+0.025M $CuCl_2$), anode flow rate=17 mL/min, (b) D6; anode (1M $MEA-CO_2$+1M NaCl), cathode (1M MEA+1M NaCl+0.25M $CuCl_2$), anode flow rate=17 mL/min, D7; anode (1M $MEA-CO_2$+1M NaCl), cathode (1M $MEA-CO_2$+1M NaCl+0.25M $CuCl_2$), anode flow rate=17 mL/min.

Figure 4.12 shows the UV-Vis measurements of two different sets of experiments with different $CuCl_2$ concentrations at the cathode. In the interpretation of these measurements, Cl^- ions passing through membrane mentioned above are important. The absorbance values at the anode outlets of the experiments with high $CuCl_2$ concentration in the cathode solution were close to each other in the absence of CO_2 at the cathode. In the case of CO_2 at the cathode, it was observed that the absorbance value at the anode outlet was higher in the case with low $CuCl_2$ concentration. Apart from this, the evaluations made for Figure 4.11 are also valid for Figure 4.12.a and Figure 4.12.b. The

absorbance values in the anode fluids of the D4 and D7 experiments containing MEA-CO_2 in the cathode solution were higher than the others.
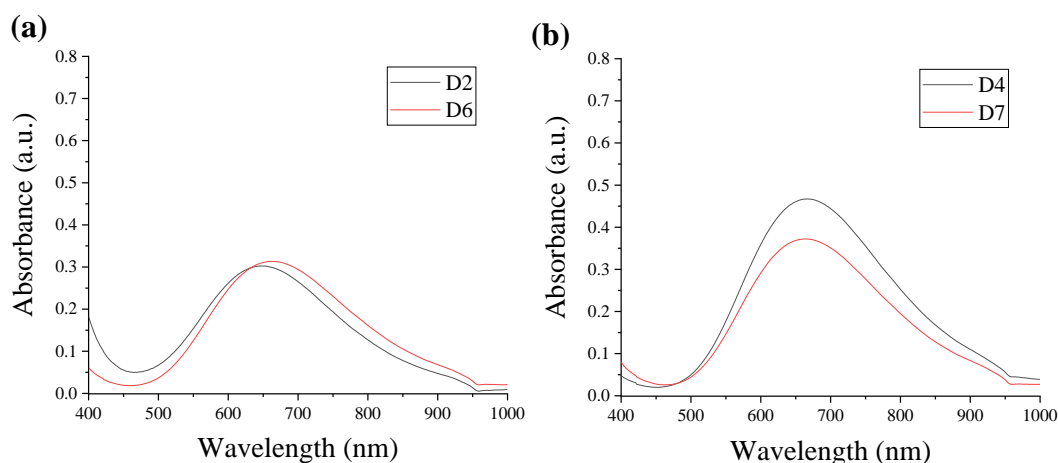
Figure 4. 12. UV-Vis spectroscopy measurements of two sets of experiments with different cathode $CuCl_2$ concentrations, (a) D2; anode (1M MEA-CO_2+1M NaCl), cathode (1M MEA+1M NaCl+0.025M $CuCl_2$), anode flow rate=17 mL/min, D6; anode (1M MEA-CO_2+1M NaCl), cathode (1M MEA+1M NaCl+0.25M $CuCl_2$), anode flow rate=17 mL/min, (b) D4; anode (1M MEA-CO_2+1M NaCl), cathode (1M MEA-CO_2+1M NaCl+0.025M $CuCl_2$), anode flow rate=17 mL/min, D7; anode (1M MEA-CO_2+1M NaCl), cathode (1M MEA-CO_2+1M NaCl+0.25M $CuCl_2$), anode flow rate=17 mL/min.

The last parameter checked is the concentration of the NaCl, which is called the supporting electrolyte and used to complete the electronic circuit. The membrane used in the cell is prepared in a form that Cl^- ions can pass through, so it is a very important parameter in terms of providing ionic balance and conductivity. Experiments were performed at two different NaCl concentrations (1M and 0.25M). Figure 4.13 shows two sets of experiments where the NaCl concentration is different. In experiments D2-D5 and D6-D8, shown in Figure 4.13.a and Figure 4.13.b, respectively, the anode and cathode solutions of D2 and D6 contain 1M NaCl, while D5 and D8 contain 0.25M NaCl. In the experiments analyzed according to the anode outputs, D2 and D6 containing NaCl with a concentration of 1M having higher absorbance values than D5 and D8 with a concentration of 0.25 M can be explained as follows. The ionic strength of the solution increases as the amount of supporting electrolyte increases, and more Cu ions can be dissolved, and thus, an increase in absorbance values occurs.
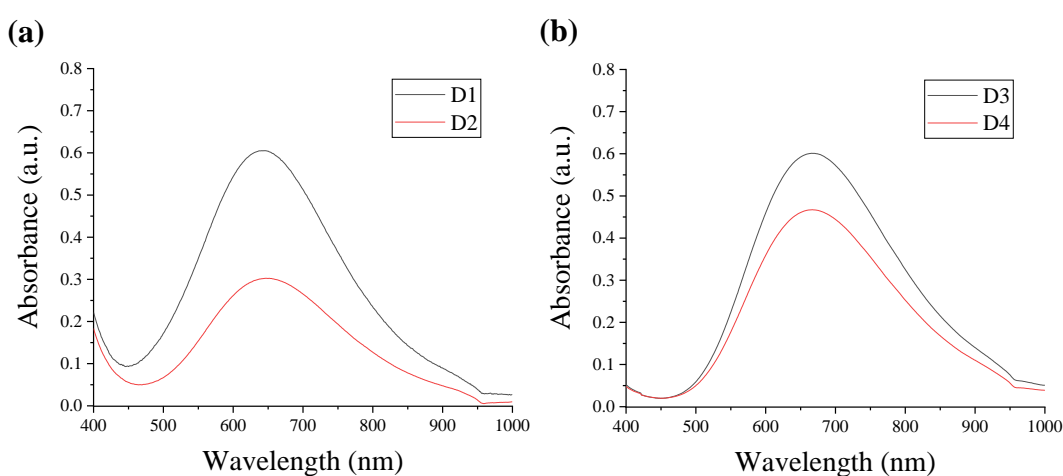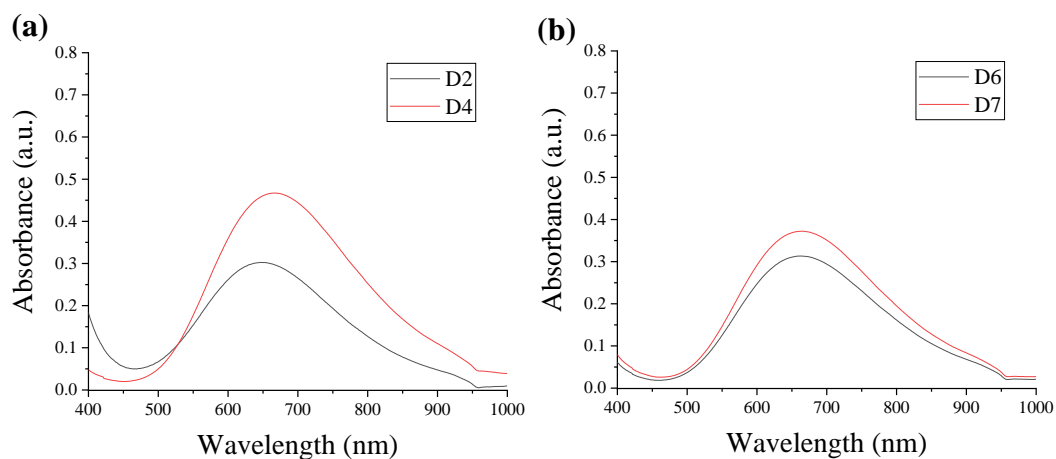
Figure 4. 13. UV-Vis spectroscopy measurements of two sets of experiments with different NaCl concentrations, (a) D2; anode (1M MEA-CO_2+1M NaCl), cathode (1M MEA+1M NaCl+0.025M $CuCl_2$), anode flow rate=17 mL/min, D5; anode (1M MEA-CO_2+0.25M NaCl), cathode (1M MEA+0.25M NaCl+0.025M $CuCl_2$), anode flow rate=17 mL/min, (b) D6; anode (1M MEA-CO_2+1M NaCl), cathode (1M MEA+1M NaCl+0.25M $CuCl_2$), anode flow rate=17 mL/min, D8; anode (1M MEA-CO_2+0.25M NaCl), cathode (1M MEA+0.25M NaCl+0.25M $CuCl_2$), anode flow rate=17 mL/min.

As mentioned at the beginning of the section, in order to understand the desorption behavior in the electrochemical cell, besides UV-Vis spectroscopy measurements, current-voltage measurements of the electrochemical cell were also performed. The current-voltage measurements made for the experiments listed in Table 4.2 are examined below.

Figure 4.14 is plotted for two different sets of experiments with all conditions being the same except for the anode flow rate. As can be seen in Figure 4.14, it can be seen that the voltage values read in the D1 and D3 experiments with a lower anode flow rate are slightly higher than in the D2 and D4 experiments with a high anode flow rate. The change in anode flow rate did not significantly change the voltage-current behavior. The voltage-current data is related to conductivity, and the ionic conductivity is mostly controlled by the supporting electrolyte, NaCl.

Figure 4. 14. Current-voltage measurements of two sets of experiments with different anode flow rates, (a) D1; anode (1M MEA-CO_2+1M NaCl), cathode (1M MEA+1M NaCl+0.025M $CuCl_2$), anode flow rate=8.5 mL/min, D2; anode (1M MEA-CO_2+1M NaCl), cathode (1M MEA+1M NaCl+0.025M $CuCl_2$), anode flow rate=17 mL/min, (b) D3; anode (1M MEA-CO_2+1M NaCl), cathode (1M MEA-CO_2+1M NaCl+0.025M $CuCl_2$), anode flow rate=8.5 mL/min, D4; anode (1M MEA-CO_2+1M NaCl), cathode (1M MEA-CO_2+1M NaCl+0.025M $CuCl_2$), anode flow rate=17 mL/min.

In Figure 4.15, voltage-current measurements made in experiments with different cathode solutions are given. While there was no CO_2 in the cathode solution in the D2 and D6 experiments, the cathode solution was saturated with CO_2 in the D4 and D7 experiments. Looking at Figure 4.15.a, when MEA-CO_2 is present at the cathode, at low $CuCl_2$ concentrations, the MEA-CO_2 complex facilitates the transition of the Cl^- ion to the anode side and provides the necessary charge balance more easily, as mentioned in the UV-Vis results above. Therefore, the voltage values in the D4 curve were measured less than the D2 curve. At high $CuCl_2$ concentrations (Figure 4.15.b), the presence or absence of MEA-CO_2 complex at the cathode does not seem to affect the voltage-current curves. This also coincides with the explanation of the UV-Vis measurement given in Figure 4.11.

Figure 4. 15. Current-voltage measurements of two sets of experiments with different cathode solutions, (a) D2; anode (1M MEA-CO_2+1M NaCl), cathode (1M MEA+1M NaCl+0.025M $CuCl_2$), anode flow rate=17 mL/min, D4; anode (1M MEA-CO_2+1M NaCl), cathode (1M MEA-CO_2+1M NaCl+0.025M $CuCl_2$), anode flow rate=17 mL/min, (b) D6; anode (1M MEA-CO_2+1M NaCl), cathode (1M MEA+1M NaCl+0.25M $CuCl_2$), anode flow rate=17 mL/min, D7; anode (1M MEA-CO_2+1M NaCl), cathode (1M MEA-CO_2+1M NaCl+0.25M $CuCl_2$), anode flow rate=17 mL/min.

The plots in Figure 4.16 belong to the experimental sets containing different NaCl concentrations. Experiments D2 and D6 contain 1M NaCl, while experiments D5 and D8 contain 0.25M NaCl. As expected, the presence of 1M NaCl in experiments D2 and D6 increases the ionic conductivity of the solution, and therefore the same current can be obtained at lower voltages.
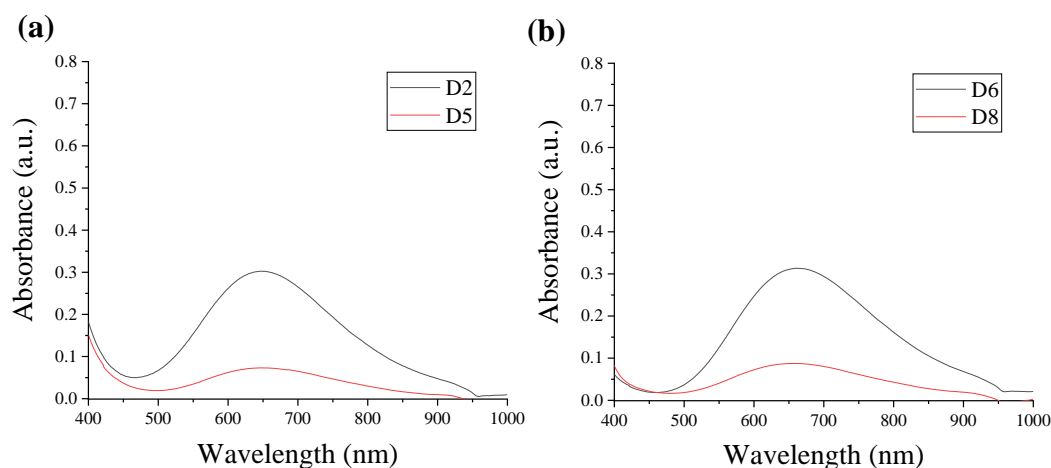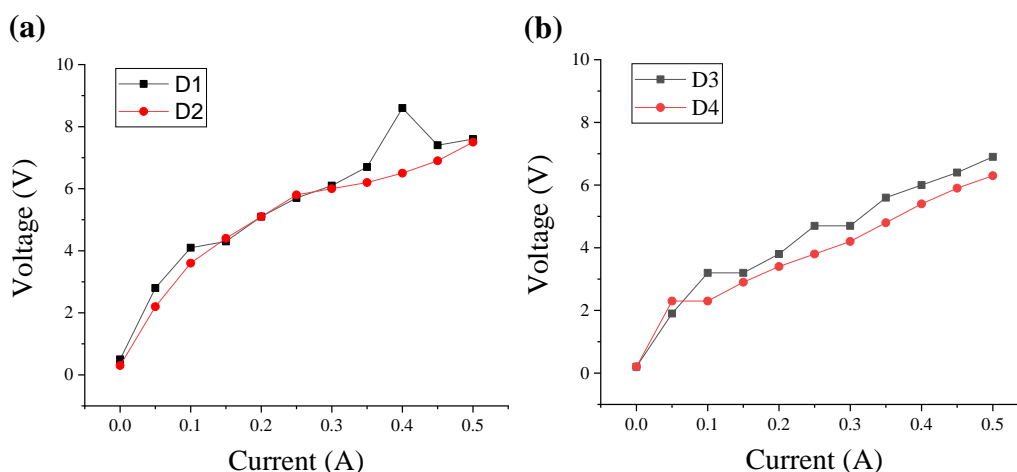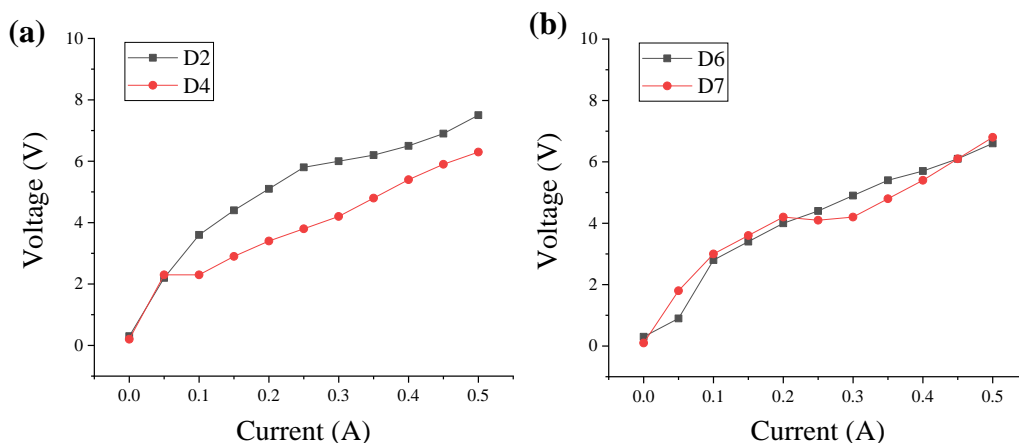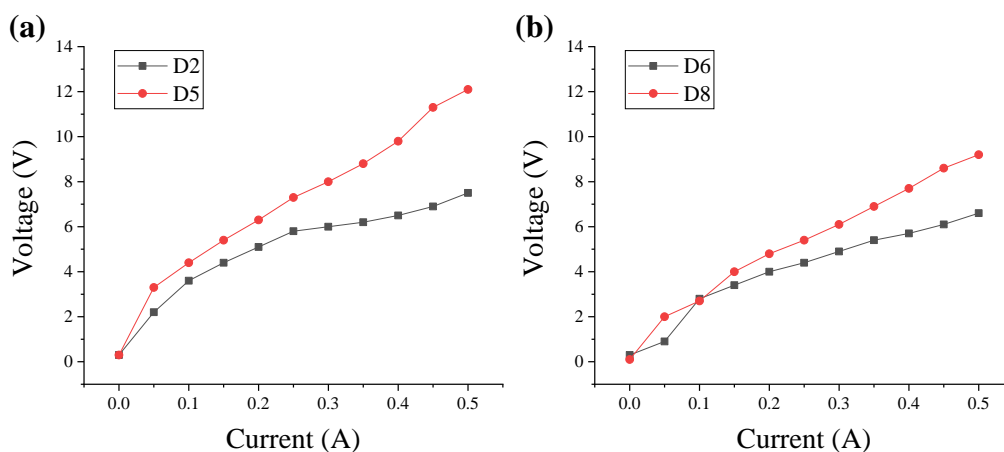

Figure 4. 16. Current-voltage measurements of two sets of experiments with different NaCl concentrations, (a) D2; anode (1M MEA-CO_2+1M NaCl), cathode (1M MEA+1M NaCl+0.025M $CuCl_2$), anode flow rate=17 mL/min, D5;

anode (1M MEA-CO$_2$+0.25M NaCl), cathode (1M MEA +0.25M NaCl+0.025M CuCl$_2$), anode flow rate=17 mL/min, (b) D6; anode (1M MEA-CO$_2$+1M NaCl), cathode (1M MEA+1M NaCl+0.25M CuCl$_2$), anode flow rate=17 mL/min, D8; anode (1M MEA-CO$_2$+0.25M NaCl), cathode (1M MEA+0.25M NaCl+0.25M CuCl$_2$), anode flow rate=17 mL/min.

4.5. Electrochemical Cell Characterization

For electrochemical cell characterization, two types of experiments were carried out, the details of which were described in Section 3.9: continuous cycle cell experiments and single-pass cell experiments. The purpose of the continuous cycle cell experiments is to examine the cumulative changes in the anode and cathode solutions after a certain period of time by rotating the anode and cathode solutions of the electrochemical cell in a closed circuit by means of pumps. In single-pass cell experiments, the aim is to examine the change in solutions once passed through the anode and cathode, as would occur in a real electrochemical CO$_2$ capture process. The results of these experiments are given below.

The results obtained from the experiments are given in Figure 4.17 and Figure 4.18. Figure 4.17 shows how the absorbance value changes at the anode and Figure 4.18 shows how the absorbance value changes at the cathode. As expected, the absorbance value increased over time as the copper concentration in the solution leaving the anode increased with time. On the contrary, at the cathode, the absorbance value decreased over time as copper ions accumulated on the surface of the copper plate. Considering all plots, it is seen that the absorbance change as a result of the reaction at the anode was higher than the change in absorbance as a result of the reaction at the cathode for both MEA and HPZ. This indicates that copper dissolution at the anode occurs faster than copper reduction at the cathode for both MEA and HPZ. When the two amine solutions are compared, it is found that the absorbance changes at the anode and cathode in 1M HPZ solution were higher than the changes in absorbance at the anode and cathode in 1M MEA solution. This shows that the solution containing 1M HPZ has a faster kinetics than the solution containing 1M MEA in terms of dissolution of copper at the anode and reduction of copper ions at the cathode.
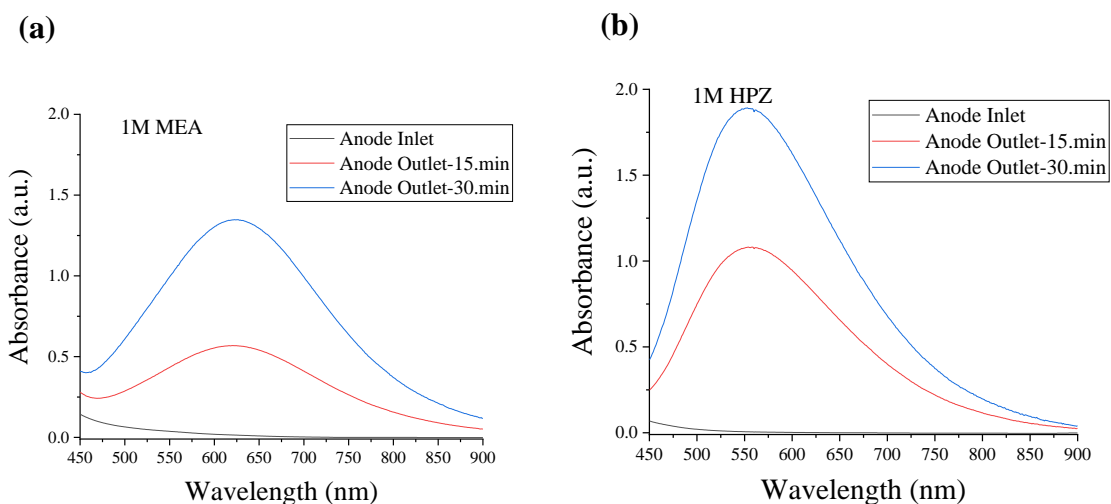
Figure 4. 17. UV-Vis spectroscopy measurements of anode samples in the continuous cycle electrochemical cell experiment, (a) 1M MEA, (b) 1M HPZ.
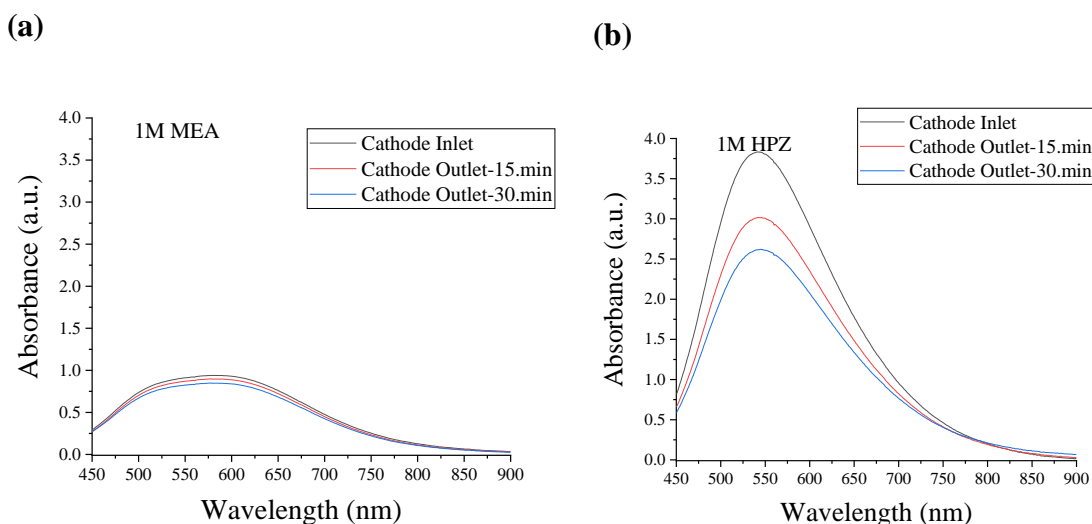
Figure 4. 18. UV-Vis spectroscopy measurements of cathode samples in continuous cycle electrochemical cell experiment, (a) 1M MEA, (b) 1M HPZ.

It has been seen from UV-Vis spectroscopy analyses that the electrochemical cell can perform copper dissolution at the anode and copper reduction at the cathode for continuously circulated solutions, although the kinetics of these electrochemical processes are different. However, in a real electrochemical CO_2 capture process, a solution will not be circulated continuously as done in this experiment, and each time a copper-free amine-CO_2 solution comes from the absorption column to the anode and an amine-Cu solution goes to the cathode to be regenerated. For this reason, single-pass cell experiments were carried out, the details of which were described in Section 3.9.

In this experiment, experiments were performed for 0.1M MEA-1A, 1M MEA-1A, 1M MEA-0.2A and 0.1M HPZ-1A (the xA after the dash means the experiment is carried out at x amperes of current). Solutions for the anode contain amine-CO_2 and 1M NaCl, and solutions for the cathode contain amine, 1M NaCl and 0.025M $CuCl_2$. Pump rates were set to be 17 mL/min in each experiment. In the UV-Vis spectroscopic analyses of this experiment; at the anode, the absorbance value of the solution sample taken at the anode inlet is expected to be 'zero', and the absorbance value of the samples taken at the anode outlet is expected to be higher than the input sample, and give a peak at the same absorbance value. At the cathode, it is expected that the sample taken at the cathode inlet will give a higher peak absorbance value than that of the cathode outlet samples, and all of the cathode outlet samples will have the same absorbance value. Faradaic efficiencies were calculated by using these absorbance values and calibration curves obtained with the UV-Vis spectroscopy measurements (Section 3.8). To provide a thorough explanation, 1M MEA-1A experiment and its results are described as an example below.

- For the anode compartment, a solution containing 1M MEA-CO_2 and 1M NaCl was prepared and a sample was taken from this solution (anode inlet sample). Likewise, a solution containing 1M MEA, 1M NaCl and 0.025M $CuCl_2$ was prepared for the cathode compartment and a sample was taken from this solution (cathode inlet sample). These solutions prepared for the anode and cathode were sent to the anode and cathode with the help of two pumps set at 17 mL/min. The power supply is set to be 1A. After the current value was fixed at 1A, the time was started and samples were taken from both compartments of cell at every 5 minutes. The UV-Vis spectroscopy measurements of the samples are shown in Figure 4.19. The absorbance values of the samples except the input samples were approximately the same in both anode and cathode samples. It is possible that those with different absorbance values are due to human error when diluting the samples to prepare them for UV-Vis spectroscopy measurement. As expected, looking at the anode, it is seen that the inlet sample did not give an absorbance peak, but the outlet samples had absorbance peaks very close to each other at a higher absorbance value compared to the inlet. While at the cathode, on the contrary, the inlet sample had an absorbance peak at a higher value than the outlet samples, and the outlet samples had absorbance peaks very close to each other. This shows that the

reaction in the anode compartment has a faster kinetics than the reaction in the cathode compartment.
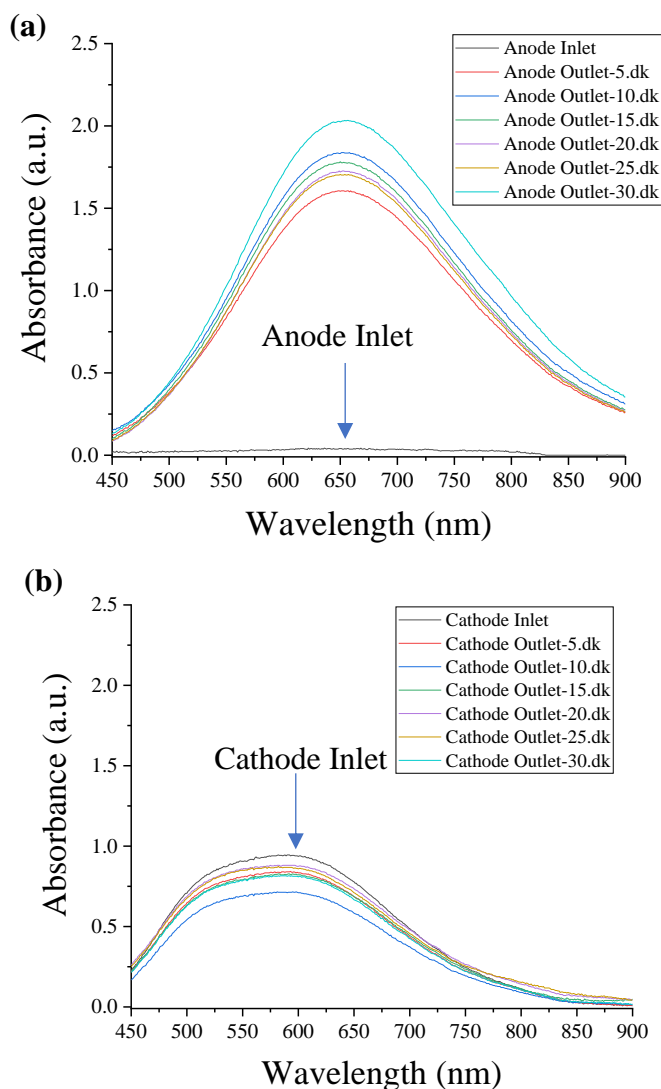
Figure 4. 19. UV-Vis spectroscopy measurements of samples taken for 1M MEA-1A, (a) anode, (b) cathode.

- Using UV-Vis spectroscopy measurements and previously obtained calibration equations, the Faradaic efficiency of the reactions was calculated with respect to copper ions. The absorbance value of each sample was read from the plots given in Figure 4.19, and these values were inserted into the equations of corresponding calibration curves, and the amount of Cu contained in the collected samples was calculated in molar (mol/L). Then, the volumes of the collected samples were calculated based on their density and mass. The calculated sample volume was divided by 17 mL/min, which is the rate at which the solution was sent to the system, and the time it took for the collected

83

sample to pass through the anode or cathode was calculated. Using Faraday's law given as Equation-3.51.b, the amount of Cu that should theoretically be dissolved or precipitated was found for each sample. The experimental amount was divided by the theoretically calculated amount and the Faradaic efficiency was calculated. The Faraday's law is given below as:

$$n_{Cu} = \frac{I.t}{n.F} \qquad \text{(Faraday's Law) (Equation-3.51.b)}$$

where n_{Cu} is the amount of dissolved or precipitated Cu in moles, I is the current in Amperes, t is the time in seconds, n is the amount of electrons required to oxidize or reduce one copper ion (dimensionless), and F represents the Faraday constant (96485 $A.s.mol^{-1}$).

For example, at the 25th minute at the anode;

- The value read in Figure 4.19.a is1.7019.
- Equation of the calibration curve of the 1M MEA for the anode (Figure 3.9) is y=58.892x.
- Given the y value is 1.7019, the x value, that is, the amount of Cu in the collected sample, is 0.02890 mol/L.
- The amount of Cu that should be theoretically present in the collected sample using Faraday's law is 0.01829 mol/L.
- Faraday efficiency is calculated as (0.02890/0.01829).100= 158.003%

The reason for the efficiency of the anode to be over 100% is that the reaction in the anode cell takes place even without any current supply. Photographs of an experiment conducted to prove this were given below. Copper electrodes was placed in the amine-containing solutions, and the photos were taken first at the end of 30 minutes and then at the end of one day. As seen in Figure 4.20, the solutions were clear at first, and the color turned blue after 30 minutes and the blue color was very dominant at the end of one day. Therefore, the reason why the Faraday efficiency at the anode is over 100% is interpreted as the copper dissolution reaction can take place without current in amine solutions.
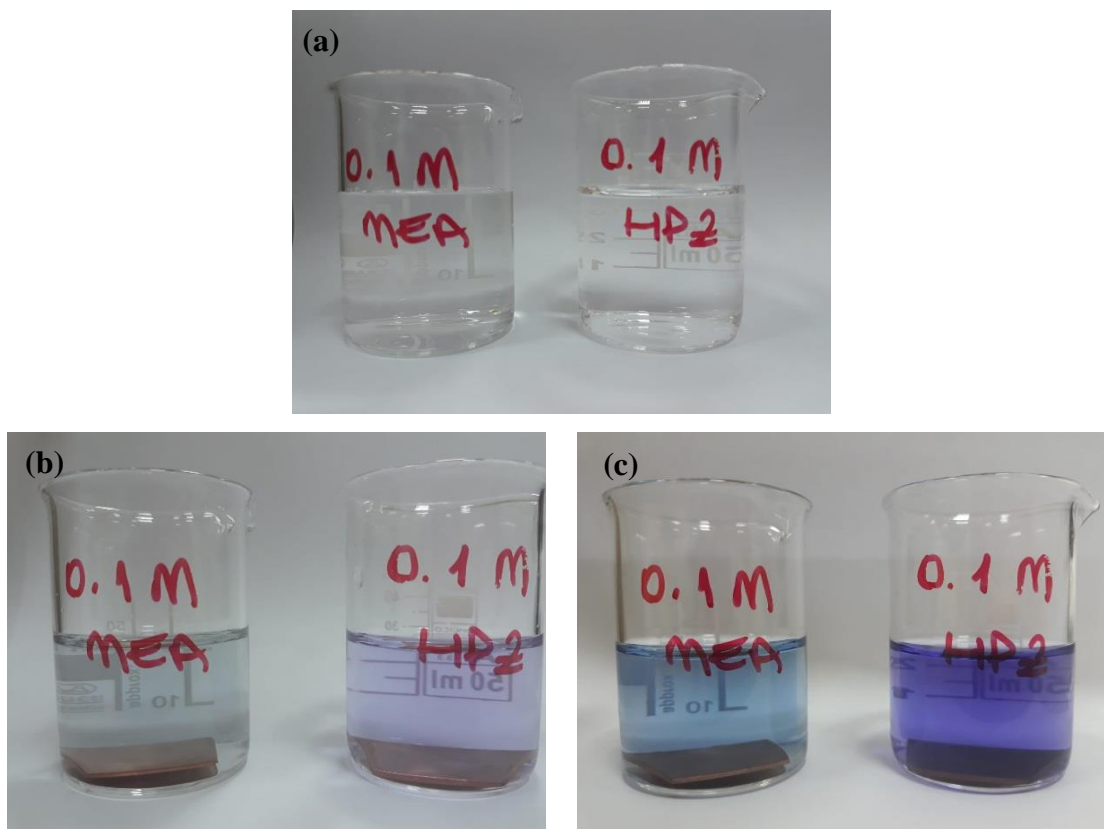
Figure 4. 20. Photos of copper electrodes in 0.1M MEA and 0.1M HPZ solutions, (a) at the beginning, (b) after 30 minutes, (c) after 1 day.

- The Faradaic efficiency calculation at the cathode was made differently compared to the anode. The reason for this is that the amount of Cu in the solution increases at the anode whereas the amount of Cu in the solution decreases at the cathode. In other words, the important thing at the cathode is how much Cu ions precipitate (i.e., leave the solution). However, since only the Cu amount in the solution was calculated by UV-Vis spectroscopy measurements, the experimentally calculated Cu amount was subtracted from the 0.025M Cu amount added to the solution during the solution preparation, and the precipitated Cu amount was found.

For example, at the 25th minute at the cathode;

- The value read in Figure 4.19.b is 0.868.
- Equation of the calibration curve of 1M MEA for the cathode (Figure 3.9) is y=38.008x.
- Given the y value is 0.868, the x value, that is, the amount of Cu in the collected sample is 0.02284 mol/L.

- The amount of Cu that should theoretically precipitate at the cathode using Faraday's law is 0.01681 mol/L.
- Faraday yield: $((0.025-0.02274)/0.01681).100 = 13.444\%$

These calculations are performed for 1M MEA at 0.2A and for 0.1M MEA, 0.1M HPZ and 1M MEA at 1A. A sample calculation is given in Appendix C. 0.1M HPZ is used instead of 1M HPZ. The reason for this is that 0.1M HPZ has a close CO_2 capture capacity (≈ 1.11 mol_{CO2}/mol_{amine}) to 1M HPZ (≈ 1.12 mol_{CO2}/mol_{amine}), and HPZ is an expensive chemical and therefore it is desired to be used more economically. The average Faradaic efficiency calculated from the samples collected at every 5 minutes from the anode and cathode compartments in single-pass cell experiments is given in Table 4.3. In the 0.1M MEA-1A and 0.1M HPZ-1A experiments, the Faradaic efficiency for the anode could not be calculated because copper precipitate was formed in these experiments. As mentioned in Appendix A, $CuCl_2$ salt added at a concentration with more than 0.0025M and 0.005M, forms a precipitate in 0.1M MEA and 0.1M HPZ solutions, respectively. Looking at Faradaic efficiencies for copper for other experiments, the most striking result is that efficiencies at the anode were higher than those at the cathode. The efficiencies at the cathode compartment were incomparably low compared to those at the anode in all experiments. This result shows that the reaction at the anode occurs easily, but the reaction at the cathode is harder to take place.

Table 4. 3. Average Faradaic efficiencies and standard deviations of Faradaic efficiencies calculated for the anode and cathode compartments using the samples collected for 30 minutes in single-pass experiments (standard deviation for the cathode efficiency is very high in the 1M MEA-0.2A experiment).

	Average Faradaic Efficiency			
	Anode	Standard Deviation	Cathode	Standard Deviation
0.1M MEA-1A	-	-	%23.41	%5.27
1M MEA-0.2A	%191.91	%8.41	-%3.33	%41.75
1M MEA-1A	%165.25	%13.56	%20.15	%9.43
0.1M HPZ-1A	-	-	%26.46	%5.27

This shows that under the experimental conditions investigated, Cu ions generation in the anode compartment and Cu reduction on the copper plate in the cathode

compartment of the electrochemical cell cannot take place at the same rate in a continuously operating electrochemical CO_2 capture system integrated with absorption process. In other words, in an electrochemical CO_2 capture process integrated with absorption, copper ions formed at the anode will accumulate continuously in the system and a complete copper regeneration will not be achieved at the cathode, and the system will not reach a steady-state in terms of copper ions. For this reason, experiments on integrating the electrochemical cell with absorption were not continued. This finding will be addressed as a point to be resolved in future projects.

4.6. CO_2 Release Rate Measurements in the Electrochemical Cell

In the studies explained in this section, it is aimed to measure the CO_2 release rates in the electrochemical cell and to calculate the required energy amounts. The amine used in an ideal electrochemical CO_2 capture process transforms into an amine-CO_2 complex by capturing CO_2 in the absorption column. The amine-CO_2 complex coming out of the absorption column is sent to the anode compartment of the electrochemical cell, where it is transformed into an amine-Cu complex with the dissolved Cu ions, thus releasing the CO_2 gas that was captured in the absorption. Then, the amine-Cu complex is sent to the cathode compartment where the Cu ions in the complex are reduced and deposited on the copper plate and thus amines are regenerated, so that the amine can absorb CO_2 again.

Details of the experiments for the measurement of CO_2 release rates were given in Section 3.11. This experiment was carried out at 0.5A current for 0.1M and 1M MEA and HPZ solutions. During the experiments, current-voltage values were recorded.

The CO_2 release rate measurement experiments performed at 0.5A for 1M MEA and described in detail in Section 3.11. The CO_2 release rates obtained in these experiments are shown in Figure 4.21. As seen in Figure 4.21, the highest release rate is obtained at 1M HPZ and the second highest release rate is obtained at 0.1M HPZ. Both HPZ concentrations provide higher CO_2 release flow rates than MEA. Therefore, it is understood that HPZ has a higher kinetic rate in the CO_2 release reaction than MEA.
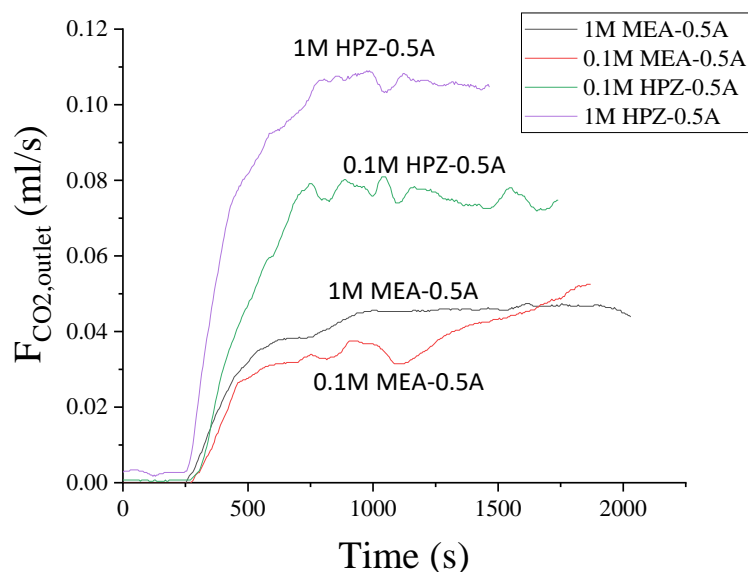
Figure 4. 21. CO_2 flow rate comparison for all experiments.

Current densities, Faradaic efficiencies calculated for CO_2 release, voltage values and the amount of energy required for 1 mol CO_2 release (kJ/mol_{CO2}) values are given for all experiments in Table 4.4. A sample calculation is also given in Appendix D. According to these data, the Faradaic efficiency of HPZ was higher than that of MEA at both concentrations (0.1M and 1M). Another result is that the voltage values required to keep the current constant for both concentrations (0.1M and 1M) were lower for MEA than HPZ. This may be due to the higher overpotential values required for HPZ reactions. Similarly, the energy requirement in HPZ was slightly higher than MEA for both concentrations. Another result is that the amount of voltage required to keep the current constant increased for both amines at low amine concentrations. Besides, Faradaic efficiency was higher at low current for 1M MEA. However, the amount of energy required for CO_2 release was higher at low current for 1M MEA. The energy required for CO_2 release at high amine concentration was almost the same for both amines, whereas HPZ had a higher energy requirement at low concentration. The results obtained here may indicate the complex character of the environment inside the cell.

Table 4. 4. Faradaic efficiency with respect to CO_2 release, voltage, power and energy/mol values required for CO_2 release in CO_2 release experiments. Cu electrode area is 5 cm^2 and the current density is 0.1 A/cm^2 in all experiments.

	Faradaic Efficiency	Voltage (V)	Power (W)	Required Energy (kJ/mol$_{CO2}$)
0.5A-1M MEA	%28.57	7.95±0.61	3.98	2354.83
0.5A-1M HPZ	%60.53	15.35±0.48	7.68	2445.91
0.5A-0.1M MEA	%23.61	10.94±1.59	5.47	3809.89
0.5A-0.1M HPZ	%44.22	26.71±0.84	13.35	5836.43

In Table 4.4, when the amount of energy required for the calculated CO_2 release is compared with the data published by T. Alan Hatton and his research group, it is seen that the energy amounts required for the CO_2 release calculated by us (2000-6000 kJ/mol$_{CO2}$) were quite high compared to the data in the literature (about 50 kJ/mol$_{CO2}$) (Wang et al., 2019 (1)). There are many reasons for this situation. One of the main reasons is that while flat copper plates were used as electrodes in our study, custom-made highly porous copper electrodes were used in Hatton's studies. These porous copper electrodes have very high specific surface areas (1000 m^2/m^3) and porosity values (90%) (Shaw, 2019). This specific surface area is at least 166 times greater than flat plates. The copper plates in our study were not porous structures. This prevents the effective use of the electrode surface by the fluids for the electrochemical reaction. Another related issue is that the fluid in the anode compartment of the cell exists in two phases as gas and liquid. In the case where flat plates are used instead of porous structures, the gas formed as the reaction product is much more likely to prevent contact of the reactant liquid with the electrode surface. In such a case, it is expected that the mass transfer in the electrochemical cell will be adversely affected and the mass transfer overpotential will considerably increase. A reason related to operational processes may be the high current densities used in our experiments (0.04-0.1 A/cm^2 = 400-1000 A/m^2). In a study by Wang and Hatton, it was observed that at high current densities, mass transfer limitations become dominant increasing energy consumption. It has been found that 32.5 kJ/mol$_{CO2}$ is consumed at a current density of 207 A/m^2, and a system with a current density of 310 A/m^2 leads to an energy consumption of 47.5 kJ/mol$_{CO2}$ (Wang &Hatton, 2020). It is seen

that the current densities used in the cell we designed were much higher than those in the literature. Another finding related to operational processes is the necessity of keeping the retention times at the anode and cathode at an optimal level in order to ensure that the reactions in the cell take place at optimal rates. In the light of the findings of this study, the fact that the retention times of the fluids in the anode and cathode were not optimized, considering that the reaction at the anode is fast and the reaction at the cathode is slow, may be a reason. For this purpose, reducing the cathode fluid velocity or using serpentine shaped flow channels may be an option to increase the retention time at the cathode (Wang et al., 2019 (1); Stern & Hatton, 2014).

CHAPTER 5

CONCLUSION AND RECOMMENDATIONS

The increasing CO_2 concentration in the atmosphere causing climate change through global warming is one of the most important problems of the 21st century. Approximately 40% of human-induced CO_2 emissions in the world come from fossil fuel based power plants. Typically, around 1 tonne of CO_2 is released in 1000 kWh of energy generation in coal-fired power plants. In terms of CO_2 capture options in coal-fired power plants, the post-combustion CO_2 capture option is the most suitable option due to industrial maturity and capability of retrofitting to existing power plants in operation. In the CO_2 capture process, which is conventionally used in the post-combustion CO_2 capture option, amine-based aqueous solutions selectively absorb CO_2 from the flue gas in an absorption column. Afterwards, the amine-water solution rich in CO_2 is heated in a stripping column to collect the CO_2 in concentrated form by separating it from the solution. Conventional CO_2 capture processes have not become widespread due to the high energy requirement in the stripping column, the expensive amine compounds used, and the thermal decomposition of amine compounds. In the literature, it is tried to develop CO_2 capture processes that are more energy efficient and that can use amine compounds less degradable with heat. Among these studies, electrochemical CO_2 capture processes stand out with the potential to work with less energy at low and constant temperatures.

In this project, the "electrochemical CO_2 capture" method, which has a high technical, economic and environmental potential for coal-fired power plants, has been studied. For this purpose, homopiperazine (HPZ) is proposed to be used as a promising amine which can be used in electrochemical CO_2 capture processes with a higher CO_2 capture capacity than conventional amines such as ethylenediamine (EDA) and monoethanolamine (MEA). Kinetic measurements were made for the CO_2 capture process and the rate equations were derived. Studies were carried out for the development of the electrochemical cell. A pilot process of the electrochemical CO_2 capture process was developed.

The findings and innovations obtained in the project are briefly summarized below:

- Homopiperazine (HPZ) compound, which has not been studied before in electrochemical processes in the project, has been found to have higher CO_2 capture capacity than monoethanolamine (MEA) compound and similar CO_2 absorption rate with MEA, through laboratory studies. It was also found that the CO_2 capture capacity of HPZ can be modulated by the copper ion concentration.

- Electrochemical CO_2 release rates of amine solutions were measured with the pilot setup and electrochemical cell developed in the project, and it was found that HPZ had a higher CO_2 release rate than MEA. The electrochemical CO_2 capture process is a challenging process from the traditional processes in the literature. Therefore, many difficulties have emerged in this project, which were encountered for the first time and needed to be solved. Despite all the difficulties encountered, the results obtained in this study revealed that HPZ has the potential to be used in electrochemical CO_2 capture processes.

- The usability of the UV-Vis spectroscopy technique, which can be applied to the inlet and outlet solutions of the anode and cathode parts of the cell, has been demonstrated as a technique to understand the reaction behavior in the electrochemical cell.

- Using the UV-Vis spectroscopy technique, it was found that the CO_2 release reactions at the anode were fast, while the amine regeneration reactions at the cathode were slow in the investigated amine solutions. This situation revealed that future studies should focus on the reactions taking place at the cathode.

- The mass balance equations of the absorption systems in laboratory and pilot setups were derived, and it was found that the derived equations provided correct results experimentally.

Recommendations for future projects are briefly summarized below:

- In electrochemical cells, mass transfer limitations can be tried to be eliminated by using special foamed metal electrodes with high porosity and surface area per volume values instead of flat plate electrodes. As another subject to be developed in the electrochemical cell, the design and optimization of flow channels that can increase the retention time of fluids in the cell without

creating mass transfer limitation can be studied. Another suggestion is to use suppressor molecules such as inhibitors to slow down the reaction at the anode to match the reaction rates in the anode and cathode for a balanced process in terms of reaction times in anode and cathode compartments.

- Experimental studies examining the speciation reactions of HPZ and the physical and chemical properties of the compounds in these reactions are very limited in the literature. More basic experimental studies are needed to be done in this area.

- Electrochemical CO_2 processes use an anionic exchange membrane (AEM) due to basic solutions involved. These membranes are produced by very few manufacturers abroad and are difficult to obtain. Studies can be carried out to develop AEM membranes suitable to the conditions in electrochemical CO_2 capture processes in our country.

- The electrochemical CO_2 capture process does not require hot steam as it does not require heating, and uses electrical energy directly in the electrochemical cell. In this sense, the electrochemical CO_2 capture process can theoretically be applied wherever electrical energy is available. For this reason, integration projects can be developed in our country, which is lucky in terms of renewable energy sources, where the energy required for electrochemical CO_2 capture processes is provided from renewable energy sources.

- The electrochemical CO_2 capture process can be made into portable CO_2 capture systems due to the modularity of the electrochemical systems. These portable systems can be piloted at the sites of various organizations and their long-term behavior can be studied.

REFERENCES

Arachchige, U. S. P. (2019). Carbon Dioxide Capture by Chemical Absorption: Energy Optimization and Analysis of Dynamic Viscosity of Solvents.

Asif, M., Suleman, M., Haq, I., & Jamal, S. A. (2018). Post-combustion CO_2 capture with chemical absorption and hybrid system: current status and challenges. Greenhouse Gases: Science and Technology, 8(6), 998-1031.

Blauwhoff, P. M. M., Versteeg, G. F., & Van Swaaij, W. P. M. (1983). A study on the reaction between CO_2 and alkanolamines in aqueous solutions. Chemical engineering science, 38(9), 1411-1429.

Boot-Handford, M. E., Abanades, J. C., Anthony, E. J., Blunt, M. J., Brandani, S., Mac Dowell, N., ... & Fennell, P. S. (2014). Carbon capture and storage update. Energy & Environmental Science, 7(1), 130-189.

Caplow, M. (1968). Kinetics of carbamate formation and breakdown. Journal of the American Chemical Society, 90(24), 6795-6803.

Chowdhury, F. A., Yamada, H., Higashii, T., Goto, K., & Onoda, M. (2013). CO_2 capture by tertiary amine absorbents: a performance comparison study. Industrial & engineering chemistry research, 52(24), 8323-8331.

Ciftja, A. F., Hartono, A., & Svendsen, H. F. (2014). Carbamate stability measurements in amine/CO_2/water systems with Nuclear Magnetic Resonance (NMR) spectroscopy. Energy Procedia, 63, 633-639.

D'Alessandro, D. M., Smit, B., & Long, J. R. (2010). Carbon dioxide capture: prospects for new materials. Angewandte Chemie International Edition, 49(35), 6058-6082.

Danckwerts, P. V. (1979). The reaction of CO_2 with ethanolamines. Chemical Engineering Science, 34(4), 443-446.

Dugas, R. E. (2009). Carbon dioxide absorption, desorption, and diffusion in aqueous piperazine and monoethanolamine. The University of Texas at Austin.

Eltayeb, A. E. (2015). Analysis and design of electrochemically-mediated carbon dioxide separation (Doctoral dissertation, Massachusetts Institute of Technology).

Hatton, T. A. (2021). Electrochemically-mediated amine regeneration in CO_2 scrubbing processes. Massachusetts Inst. of Technology (MIT), Cambridge, MA (United States).

Herzog, H., Meldon, J., & Hatton, A. (2009). Advanced post-combustion CO_2 capture. Clean Air Task Force, 1, 39.

Masson-Delmotte, V., Zhai, P., Pörtner, H. O., Roberts, D., Skea, J., Shukla, P. R., ... & Waterfield, T. (2018). Global warming of 1.5 C. An IPCC Special Report on the impacts of global warming of, 1(5).

Jorgensen, K. R., Cundari, T. R., & Wilson, A. K. (2012). Interaction energies of $CO_2 \cdot$ amine complexes: Effects of amine substituents. The Journal of Physical Chemistry A, 116(42), 10403-10411.

Kothandaraman, A. (2010). Carbon dioxide capture by chemical absorption: a solvent comparison study (Vol. 72, No. 01).

Lecomte, F., Broutin, P., Lebas, E., 2010. CO_2 Capture: Technologies to reduce greenhouse gas emissions. Editions Technip.

Leung, D. Y., Caramanna, G., & Maroto-Valer, M. M. (2014). An overview of current status of carbon dioxide capture and storage technologies. Renewable and Sustainable Energy Reviews, 39, 426-443.

Liu, W., King, D., Liu, J., Johnson, B., Wang, Y., Yang, Z. 2009. "Critical material and process issues for CO_2 separation from coal-powered plants", The Journal of The Minerals, Metals & Materials Society (TMS), 61(4), 36–44.

Lv, B., Guo, B., Zhou, Z., & Jing, G. (2015). Mechanisms of CO_2 capture into monoethanolamine solution with different CO_2 loading during the absorption/desorption processes. Environmental science & technology, 49(17), 10728-10735.

Mac Dowell, N., Samsatli, N. J., & Shah, N. (2013). Dynamic modelling and analysis of an amine-based post-combustion CO_2 capture absorption column. International Journal of Greenhouse Gas Control, 12, 247-258.

Madeddu, C., Errico, M., & Baratti, R. (2018). CO_2 Capture by Reactive Absorption-Stripping: Modeling, Analysis and Design. Springer.

Merkel, T. C., Lin, H., Wei, X., Baker, R. 2010. "Power Plant Post-Combustion Carbon Dioxide Capture: An Opportunity for Membranes", Journal of Membrane Science, 359 (1–2), 126–139.

Mikkelsen, M., Jorgensen, M., Krebs, F. C. 2010. "The teraton challenge. A review of fixation and transformation of carbon dioxide", Energy & Environmental Science 3, 43-81.

Pennline, H. W., Granite, E. J., Luebke, D. R., Kitchin, J. R., Landon, J., Weiland, L. M. 2010. "Separation of CO_2 from flue gas using electrochemical cells", Fuel 89, 1307-1314.

Puxty, G., Rowland, R., Allport, A., Yang, Q., Bown, M., Burns, R., ... & Attalla, M. (2009). Carbon dioxide postcombustion capture: a novel screening study of the carbon dioxide absorption performance of 76 amines. Environmental science & technology, 43(16), 6427-6433.

Rexed, I., Della Pietra, M., McPhail, S., Lindbergh, G., & Lagergren, C. (2015). Molten carbonate fuel cells for CO_2 separation and segregation by retrofitting existing plants–An analysis of feasible operating windows and first experimental findings. International Journal of Greenhouse Gas Control, 35, 120-130.

Rheinhardt, J. H., Singh, P., Tarakeshwar, P., & Buttry, D. A. (2017). Electrochemical capture and release of carbon dioxide. ACS Energy letters, 2(2), 454-461.

Shaw, R. A. (2019). Modeling and design for electrochemical carbon dioxide capture systems (Doctoral dissertation, Massachusetts Institute of Technology).

Sjöstrand, F., & Yazdi, R. (2009). Absorption of CO_2:-by Ammonia.

Stern, M. C., Simeon, F., Hammer, T., Landes, H., Herzog, H. J., & Hatton, T. A. (2011). Electrochemically mediated separation for carbon capture. Energy Procedia, 4, 860-867.

Stern, M. C. (2013). Electrochemically-mediated amine regeneration for carbon dioxide separations (Doctoral dissertation, Massachusetts Institute of Technology).

Stern, M. C., Simeon, F., Herzog, H., & Hatton, T. A. (2013). Post-combustion carbon dioxide capture using electrochemically mediated amine regeneration. Energy & Environmental Science, 6(8), 2505-2517.

Stern, M. C., & Hatton, T. A. (2014). Bench-scale demonstration of CO_2 capture with electrochemically-mediated amine regeneration. RSC Advances, 4(12), 5906-5914.

Yang, H., Xu, Z., Fan, M., Rajender, G., Slimane, R. B., Bland, A. E., Wright, I. 2008. "Progress in carbon dioxide separation and capture: A review", Journal of Environmental Sciences 20, 14-27.

Yousefzadeh, H., Güler, C., Erkey, C., & Uzunlar, E. (2022). CO_2 absorption into primary and secondary amine aqueous solutions with and without copper ions in a bubble column. Turkish Journal of Chemistry, 46(4), 999-1010.

Wang, M., Lawal, A., Stephenson, P., Sidders, J., & Ramshaw, C. (2011). Post-combustion CO_2 capture with chemical absorption: A state-of-the-art review. Chemical engineering research and design, 89(9), 1609-1624.

Wang, M., Rahimi, M., Kumar, A., Hariharan, S., Choi, W., & Hatton, T. A. (2019). Flue gas CO_2 capture via electrochemically mediated amine regeneration: System design and performance. Applied Energy, 255, 113879.

Wang, M., Hariharan, S., Shaw, R. A., & Hatton, T. A. (2019). Energetics of electrochemically mediated amine regeneration process for flue gas CO_2 capture. International Journal of Greenhouse Gas Control, 82, 48-58.

Wang, M., & Hatton, T. A. (2020). Flue gas CO_2 capture via electrochemically mediated amine regeneration: desorption unit design and analysis. Industrial & Engineering Chemistry Research, 59(21), 10120-10129.

web1, https://mrgeogwagg.wordpress.com/2015/06/24/greenhouse-effect-and-anthropogenic-warming/. Greenhouse Effect and Anthropogenic Warming. Retrieved 21.08.2022, 2022.

web2, https://climate.nasa.gov/vital-signs/carbon-dioxide/. Global Climate Change. Retrieved 20.08.2022, 2022.

web3, https://webbook.nist.gov/chemistry/fluid/. Nist Chemistry WebBook. Retrieved 21.07.2022, 2022.

web4, https://avys.omu.edu.tr/storage/app/public/icbudak/109094/3_ELEKTRONIK_G ECISLER.pdf). Elektronik Geçişler. Retrieved 05.05.2022, 2022.

web5, https://acikders.ankara.edu.tr/pluginfile.php/51384/mod_resource/content/0/UV %20Spektroskopisi.pdf). Enstrümental Analiz Yöntemleri. Retrieved 05.05.2022, 2022.

web6, https://avys.omu.edu.tr/storage/app/public/hasanc/120960/3-Ultraviyole%20(morotesi)%20g%C3%B6r%20spektroskopisi.pptx). UV-Görünür Bölge Spektroskopisi. Retrieved 06.05.2022, 2022.

Wu, X., Yu, Y., Qin, Z., & Zhang, Z. (2014). The advances of post-combustion CO_2 capture with chemical solvents: review and guidelines. Energy Procedia, 63, 1339-1346.

APPENDIX A.

CuCl$_2$ SOLUBILITY OF SOLUTIONS

Information about the CuCl$_2$ solubility of the amine solutions was obtained qualitatively while the calibration curves of the solutions were calculated. Solutions were prepared by dissolving 0.025M, 0.05M, 0.075M, 0.1M, 0.125M and 0.15M CuCl$_2$ in 1M MEA and 1M HPZ; 0.005M, 0.01M, 0.015M and 0.02M CuCl$_2$ in 0.1M MEA; 0.005M, 0.01M, 0.015M, 0.02M and 0.025M CuCl$_2$ in 0.1M HPZ; 0.025M, 0.05M, 0.075M, 0.1M and 0.125M CuCl$_2$ in 1M MEA-CO$_2$; 0.025M, 0.05M, 0.075M and 0.1M CuCl$_2$ in 1M HPZ-CO$_2$; 0.000625M, 0.00125M, 0.0025M and 0.005M CuCl$_2$ in 0.1M MEA-CO$_2$ and 0.1M HPZ-CO$_2$. However, it was determined that precipitate formed in 1M MEA-CO$_2$ using 0.1M and 0.125M CuCl$_2$, in 0.1M MEA-CO$_2$ using 0.005M CuCl$_2$, and in 0.1M HPZ-CO$_2$ solutions using more than 0.005M CuCl$_2$. UV-Vis spectroscopy measurements of the precipitated solutions were not performed. UV-Vis spectroscopy measurements were made in clear solutions without precipitation. When the amine type and amount are examined, it is understood that HPZ has higher Cu solubility than MEA, pure amines have higher Cu solubility than solutions containing amine-CO$_2$ complexes, and concentrated amine solutions have higher Cu solubility than dilute amine solutions. In line with this study, the Cu solubility ranking was obtained as follows:

1M HPZ>1M HPZ-CO$_2$>1M MEA>1M MEA-CO$_2$>0.1M HPZ>0.1M HPZ-CO$_2$>0.1M MEA>0.1M MEA-CO$_2$

APPENDIX B.

CALIBRATION CURVES OF AMINE AND
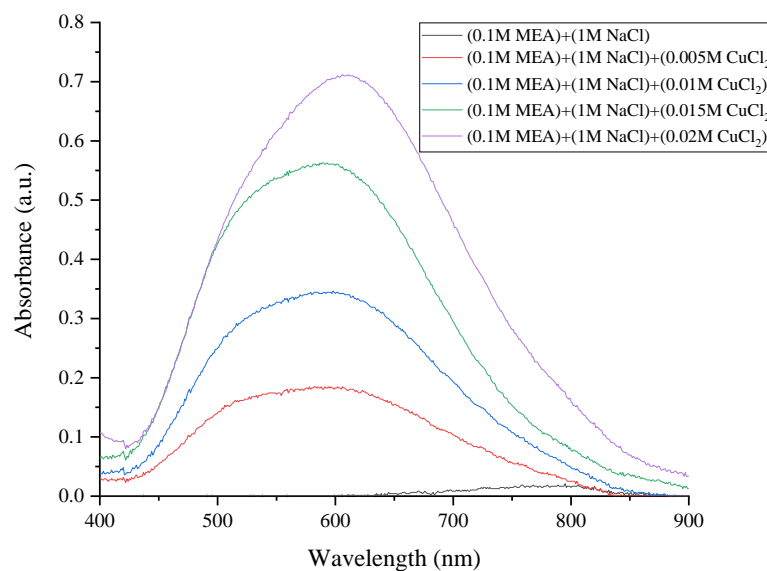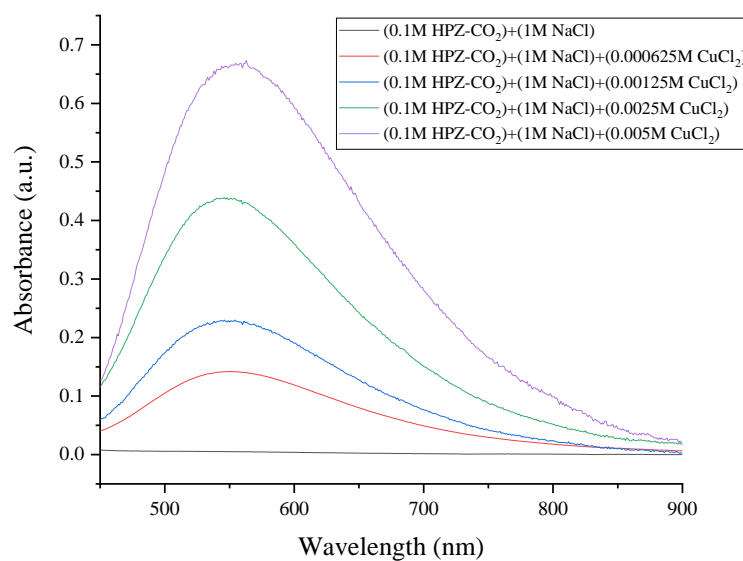
AMINE-CO₂ SOLUTIONS

0.1M MEA

- Anode:
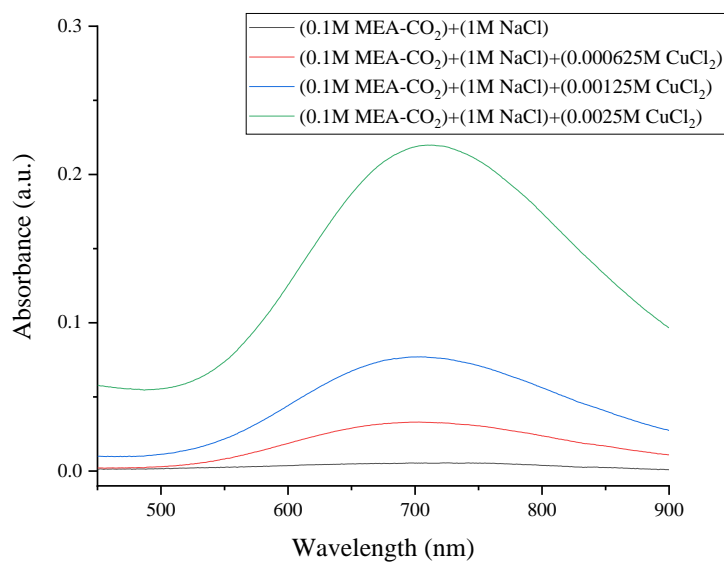
Figure B.1. UV-Vis Spectroscopy measurements of anode solutions for 0.1M MEA.

Table B.1. Maximum absorbance values for Figure B.1.

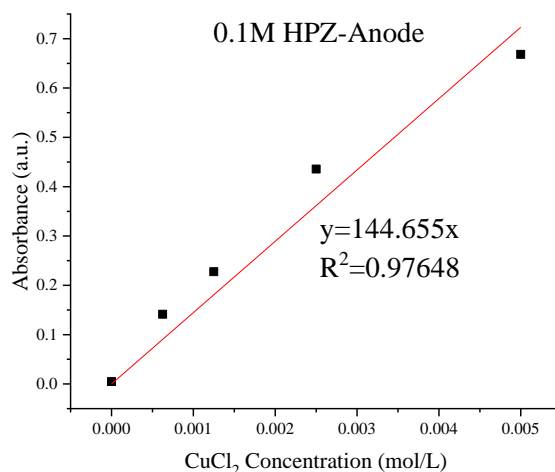| The wavelength of the peak	712 nm
CuCl₂ Concentration (mol/L)	Absorbance (a.u.)
0	0.0053
0.000625	0.0328
0.00125	0.0766
0.0025	0.2197
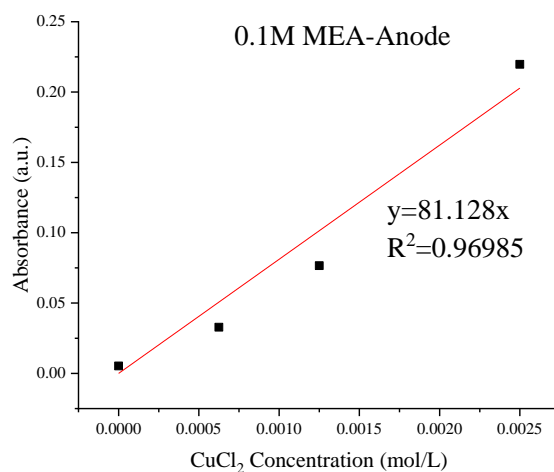
Figure B.2. Calibration curve of anode solution for 0.1M MEA.

- Cathode:

Figure B.3. UV-Vis Spectroscopy measurements of cathode solutions for 0.1M MEA.

Table B.2. Maximum absorbance values for Figure B.2.

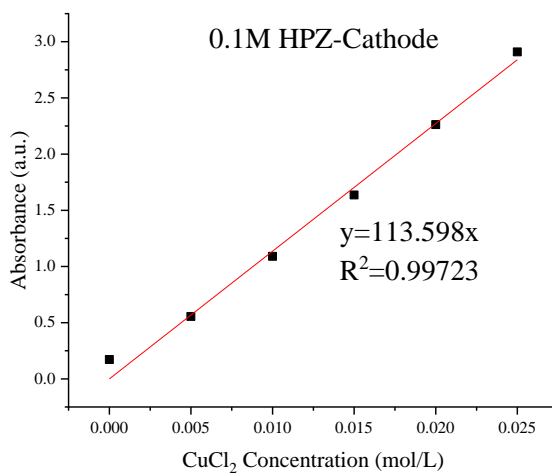| The wavelength of the peak	605 nm
$CuCl_2$ Concentration (mol/L)	Absorbance (a.u.)
0	0.0021
0.005	0.1806
0.01	0.3423
0.015	0.5544
0.02	0.7098
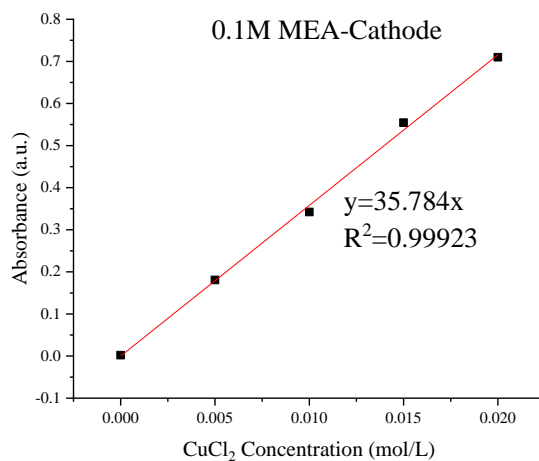
Figure B.4. Calibration curve of cathode solution for 0.1M MEA
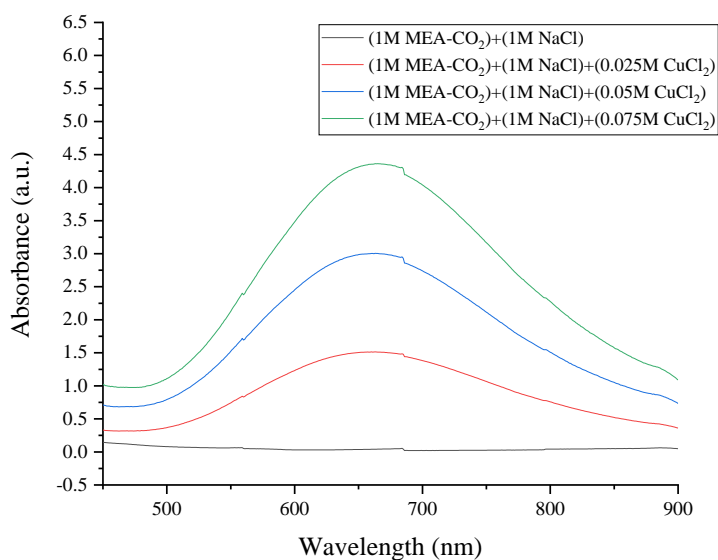
0.1M HPZ

- Anode:

Figure B.5. UV-Vis Spectroscopy measurements of anode solutions for 0.1M HPZ.

Table B.3. Maximum absorbance values for Figure B.5.

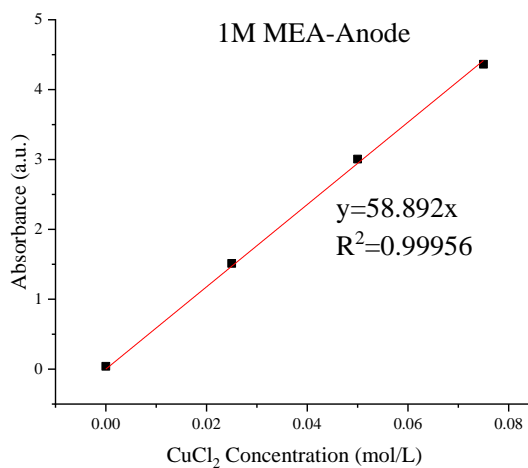| The wavelength of the peak	555 nm
CuCl$_2$ Concentration (mol/L)	Absorbance (a.u.)
0.000000	0.0049
0.000625	0.1414
0.001250	0.2277
0.002500	0.4356
0.005000	0.6682

Figure B.6. Calibration curve of anode solution for 0.1M HPZ.

- Cathode:
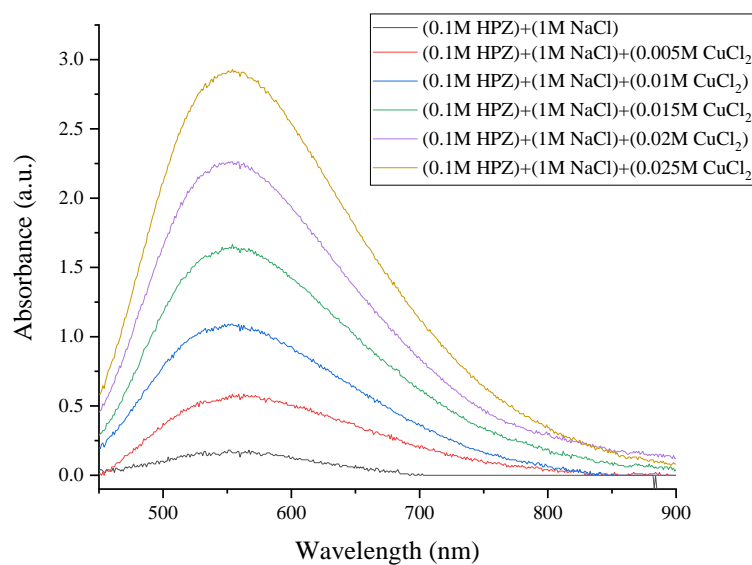
Figure B.7. UV-Vis Spectroscopy measurements of cathode solutions for 0.1M HPZ.

Table B.4. Maximum absorbance values for Figure B.7.

The wavelength of the peak	553 nm
CuCl$_2$ Concentration (mol/L)	Absorbance (a.u.)
0.000	0.1717
0.005	0.5555
0.010	1.0908
0.015	1.6362
0.020	2.2624
0.025	2.9088

Figure B.8. Calibration curve of cathode solution for 0.1M HPZ.

1M MEA

- Anode:

Figure B.9. UV-Vis Spectroscopy measurements of anode solutions for 1M MEA.

Table B.5. Maximum absorbance values for Figure B.9.

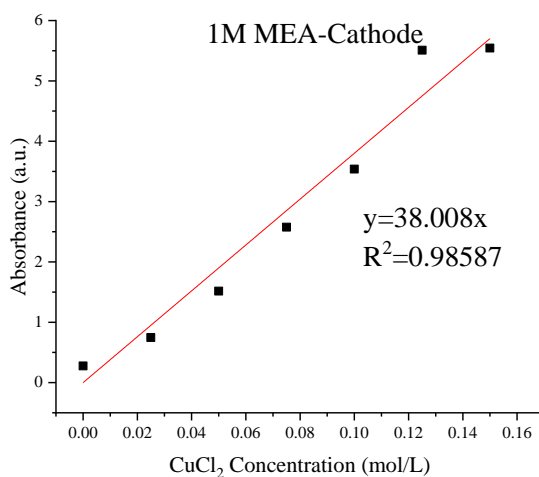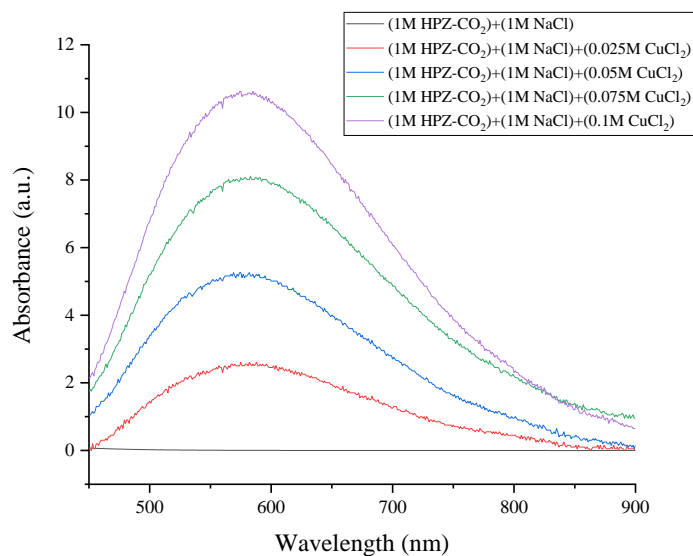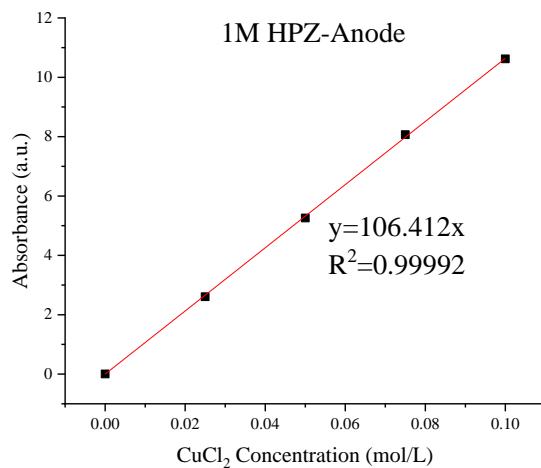| The wavelength of the peak	663 nm
CuCl$_2$ Concentration (mol/L)	Absorbance (a.u.)
0.000	0.0408
0.025	1.5136
0.050	3.0051
0.075	4.3628

Figure B.10. Calibration curve of anode solution for 1M MEA.

- Cathode:
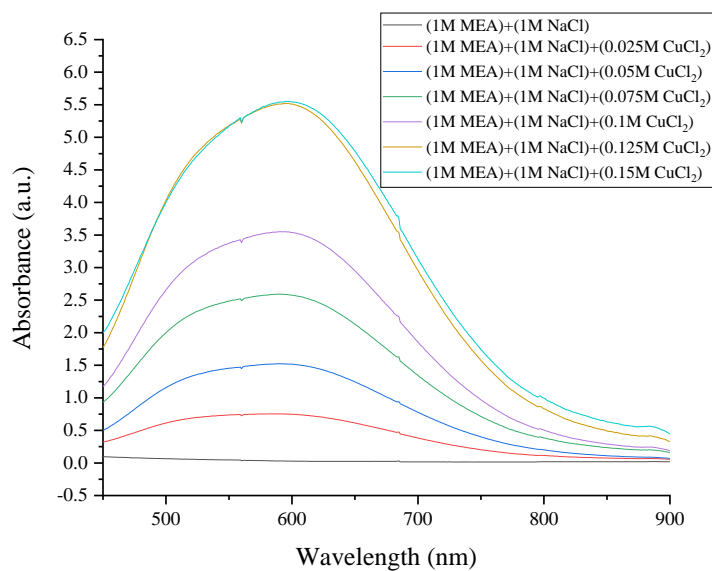
Figure B.11. UV-Vis Spectroscopy measurements of cathode solutions for 1M MEA.

Table B.6. Maximum absorbance values for Figure B.11.

The wavelength of the peak	600 nm
$CuCl_2$ Concentration (mol/L)	Absorbance (a.u.)
0.000	0.276
0.025	0.7469
0.050	1.5169
0.075	2.5767
0.100	3.5386
0.125	5.5087
0.150	5.5432

Figure B.12. Calibration curve of cathode solution for 1M MEA.
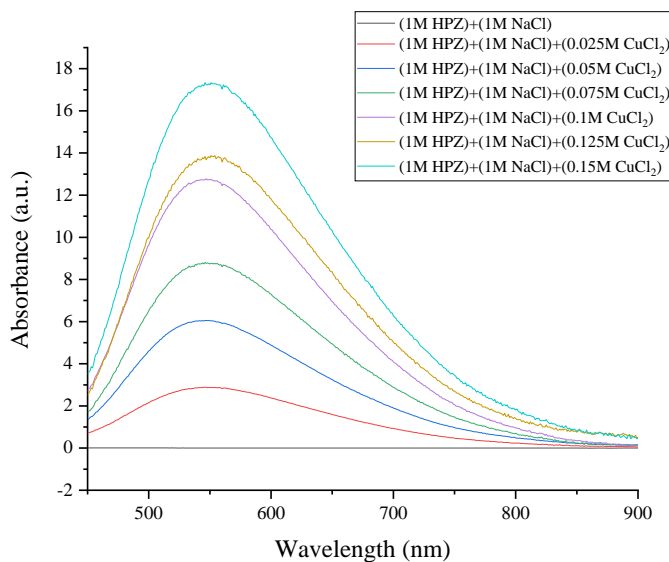
1M HPZ

- Anode:

Figure B.13. UV-Vis Spectroscopy measurements of anode solutions for 1M HPZ.

Table B.7. Maximum absorbance values for Figure B.13.

The wavelength of the peak	575 nm
CuCl$_2$ Concentration (mol/L)	Absorbance (a.u.)
0.000	0.0047
0.025	2.6052
0.050	5.2605
0.075	8.0661
0.100	10.6212

Figure B.14. Calibration curve of anode solution for 1M HPZ.

- Cathode:

Figure B.15. UV-Vis Spectroscopy measurements of cathode solutions for 1M HPZ.

Table B.8. Maximum absorbance values for Figure B.15.

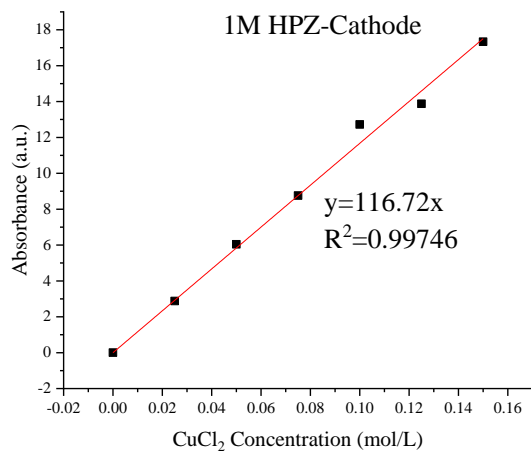| The wavelength of the peak	551 nm
CuCl$_2$ Concentration (mol/L)	Absorbance (a.u.)
0.000	0.005
0.025	2.8785
0.050	6.0398
0.075	8.7599
0.100	12.7257
0.125	13.8777
0.150	17.3346

Figure B.16. Calibration curve of cathode solution for 1M HPZ.

APPENDIX C.

SINGLE-PASS ELECTROCHEMICAL CELL

EXPERIMENTS SAMPLE CALCULATIONS

1 mole e^- = 96485 C

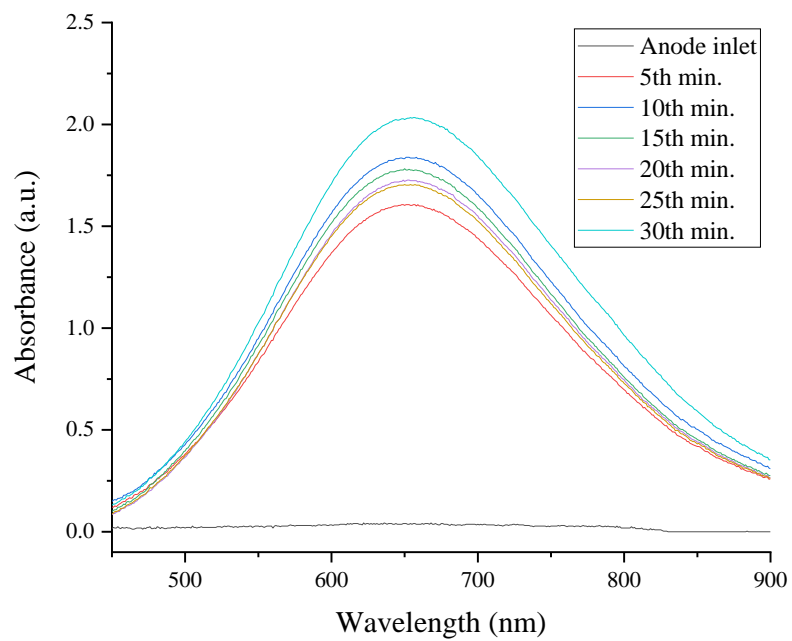1 mole of MEA-CO_2 dissolves 2 moles of e^- and 1 mole of Cu.

- 1M MEA-1A

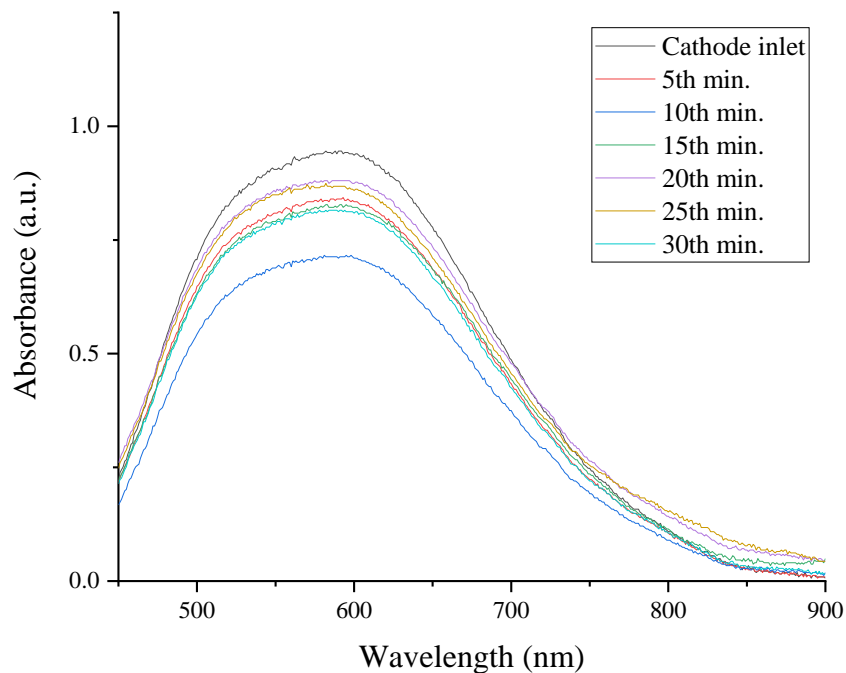Figure C.4. UV-Vis spectroscopy for anode solutions of 1M MEA-1A

Figure C.5. UV-Vis spectroscopy for cathode solutions of 1M MEA-1A

MEA Concentration (mol/L)	1					
Current [(A),(C/s)]	1					
Empty sample tube (small tube) (g)	10.77					
Empty sample tube (big tube) (g)	28.87					
Solution density (g/mL)	1					
ANODE						
Flow rate (mL/min)	17					
Total mass of sample and tube (g)	19.32	19.35	15.64	18.22	16.55	18.66
Volume of sample (mL)	8.55	8.59	4.88	7.46	5.78	7.89
Time (min.)	**5**	**10**	**15**	**20**	**25**	**30**
Max. absorbance From Figure C.4	1.62	1.84	1.78	1.73	1.70	2.03
Conc. calculated from Figure B.10 (mol/L)	0.03	0.03	0.03	0.03	0.03	0.04
Conc. calculated from Faraday Law (mol/L)	0.02	0.02	0.02	0.02	0.02	0.02
Faradaic efficiency (%)	149.08	170.38	164.91	160.31	158.00	188.79
CATHODE						
Flow rate (mL/min)	18.5					
Total mass of sample and tube (g)	21.62	14.31	15.38	15.95	37.59	38.49
Volume of sample (mL)	10.85	3.54	4.61	5.18	8.72	9.63
Time (min.)	**5**	**10**	**15**	**20**	**25**	**30**
Max. absorbance value read from Figure C.5	0.82	0.71	0.83	0.88	0.87	0.82
Conc. calculated from Figure B.12 (mol/L)	0.02	0.02	0.02	0.02	0.02	0.02
Conc. calculated from Faraday Law (mol/L)	0.02	0.02	0.02	0.02	0.02	0.02
Faradaic efficiency (%)	20.15	37.62	19.18	10.93	13.44	20.15

APPENDIX D.

SAMPLE CALCULATION OF RELEASED CO_2
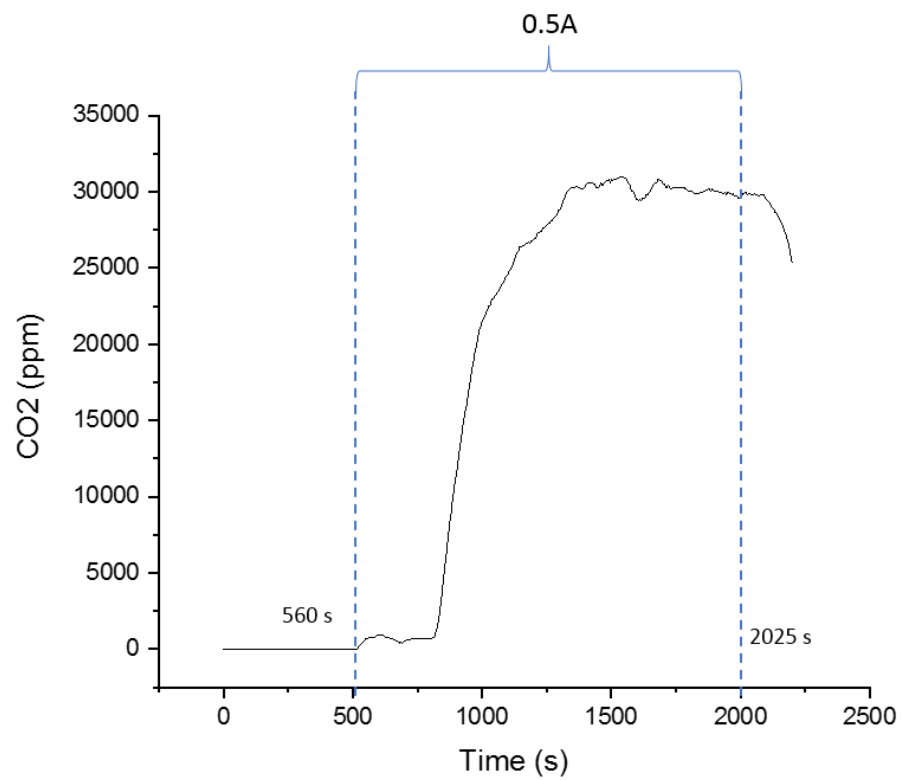
FLOW RATE AT THE ANODE

- 0.5A-1M HPZ

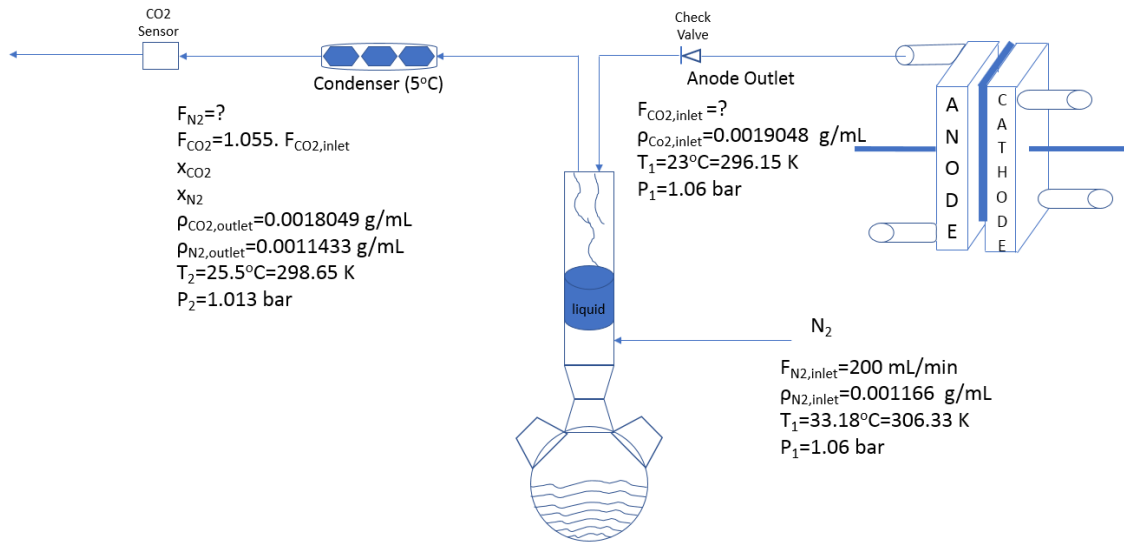Figure D.5. CO_2 concentration obtained from CO_2 sensor.

Figure D.6. Experimental setup and parameters for 1M HPZ-0.5A.

From Equation 3.48 in Table 3.2:

$F_{N2,outlet} = (F_{N2,inlet} \cdot P_{1,N2} \cdot T_2)/(P_2 \cdot T_{1,N2})$

$F_{N2,outlet} = [(200mL/min).(1/60s).(1.06bar).(298.65K)]/[(1.013bar).(306.33K)]$

$F_{N2,outlet} = 3.400$ mL/s

Relationship between $F_{CO2,inlet}$ and $F_{CO2,outlet}$ from Equations-3.41, 3.42 and 3.43 in Table 3.2:

$F_{CO2,outlet} = (F_{CO2,inlet} \cdot P_{1,CO2} \cdot T_2)/(P_2 \cdot T_{1,CO2})$

$F_{CO2,outlet} = (1.055).(F_{CO2,inlet})$

From Equation-3.50 in Table 3.2, the $F_{CO2,inlet}$ values are calculated and calculated $F_{CO2,inlet}$ values are multiplied by 1.055 and the following $F_{CO2,outlet}$ graph is obtained:
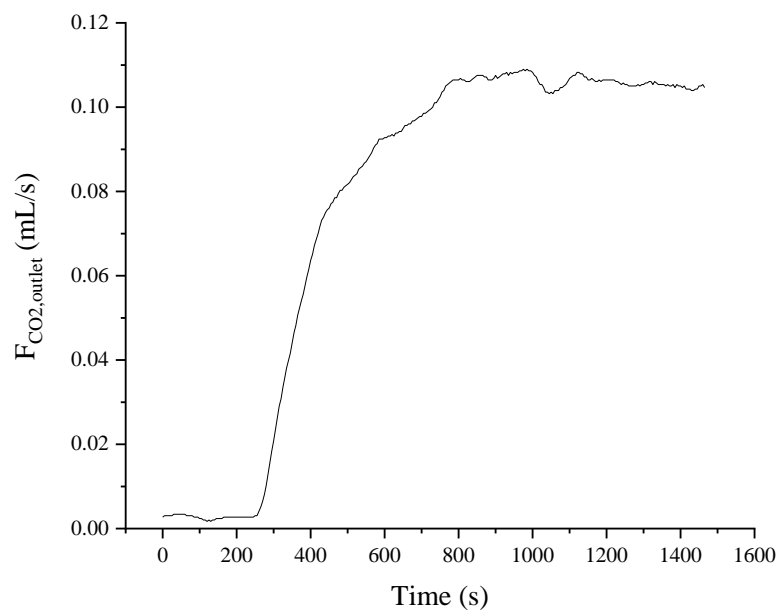
Figure D.7. $F_{CO2,outlet}$ vs. time plot for 1M HPZ-0.5A.

The outlet value of n_{CO2} was calculated as 0.0046 mol and it is the amount of CO_2 released at the anode experimentally.
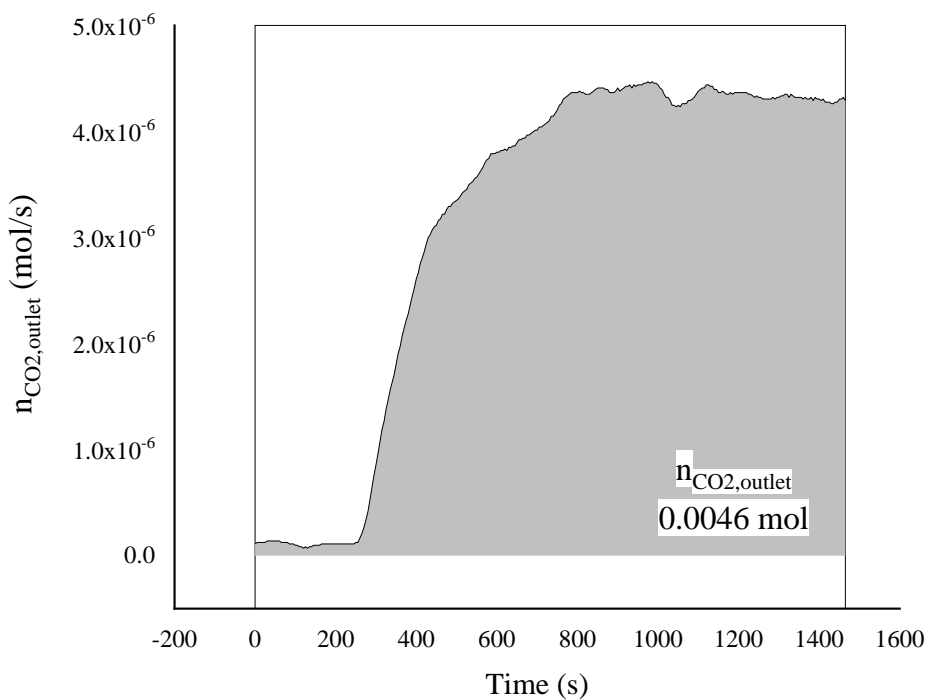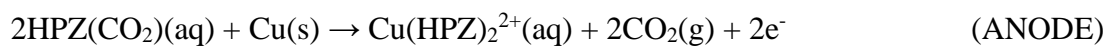

Figure D.8. $n_{CO2,outlet}$ value for 1M HPZ-0.5A.

n=1; the amount of e⁻ per CO_2 is taken;

$$2HPZ(CO_2)(aq) + Cu(s) \rightarrow Cu(HPZ)_2^{2+}(aq) + 2CO_2(g) + 2e^- \qquad \text{(ANODE)}$$

$$n_{CO2} = \frac{I.\,t}{n.\,F} \qquad\qquad \text{(Faraday's Law) (Equation-3.51.a)}$$

$$n_{CO2} = \frac{I.\,t}{n.\,F} = \frac{(0.5A).\,(1465s)}{1.\,(96485A.\frac{s}{mol})}$$

$$= 0.0076 \text{ mol (amount of } CO_2 \text{ that should theoretically be released)}$$

$$\text{Faradaic efficiency\%} = \frac{\text{Experimentally released amount of } CO_2}{\text{amount of } CO_2 \text{ that should theoretically be released}} \times 100$$

$$\text{Faradaic efficiency\%} = \frac{0.0046 \text{ mol}}{0.0076 \text{ mol}} \times 100 = \%60.53$$

Table D.2. Voltage, power and required energy values for 1M HPZ-0.5A.

Current (A)	0.5
Voltage (V)	15.35
Power (W)	7.68
Required Energy (kJ/mol$_{CO2}$)	2445.91